The Dissertation Committee for Sungmin Ock
certifies that this is the approved version of the following dissertation:

Design of Linear Transmitters for Wireless Applications

Committee:

Ranjit Gharpurey, Supervisor

Jacob Abraham

Adnan Aziz

Michael Orshansky

Jacques Rudell

Design of Linear Transmitters for Wireless Applications

by

Sungmin Ock, B.S.; M.S.

DISSERTATION

Presented to the Faculty of the Graduate School of

The University of Texas at Austin

in Partial Fulfillment

of the Requirements

for the Degree of

DOCTOR OF PHILOSOPHY

THE UNIVERSITY OF TEXAS AT AUSTIN

May 2016

To my beloved family

Acknowledgments

I would like to express my gratitude to numerous people who have helped me complete my journey to the Ph.D. First and foremost, I would like to thank my advisor, Prof. Ranjit Gharpurey, for his invaluable support and guidance over the years. Without his sincere encouragement and inspiring enthusiasm, this day could not have been reached.

I would also like to thank Prof. Jacob Abraham, Prof. Adnan Aziz, Prof. Michael Orshansky, and Prof. Jacques Rudell, for serving as dissertation committee members in spite of their busy schedules, and for providing insightful technical advice.

I am fortunate to be a part of Prof. Gharpurey's group, and I am grateful to my colleagues of this group for their support on my design and for interesting discussions. These include Diptendu Ghosh, Hyejeong Song, Jaegan Ko, Wei-Gi Ho, Jingxue Lu, Jonathan Hung, Kunhee Han, Travis Forbes and Vineet Singh.

I am very thankful to Melanie Gulick for her kind assistance with graduate advising, and Andrew Kieschnick for his technical support with CERC computer systems.

Outside of school, I would like to extend my gratitude to Sridhar Ramaswamy, Krishnaswamy Nagaraj, Reza Sharifi, Bryan Bloodworth, Pankaj

Pandey, Arup Polley, Rajarshi Mukhopadhyay, Eunyoung Seok and Swaminathan Sankaran of Texas Instruments Incorporated, and Marzio Pedrali-Noy, Eric Huang, Amar Rudravaram, Zushu Yan, Tongyu Song and Joonhoi Hur of Qualcomm for their technical expertise and great teamwork.

This Ph. D. would not have been possible without the patient love and encouragement of my family. My special gratitude goes to my wife, Hyunlee and my son, Subin, who have always stood by me through the years.

IC fabrication support through the MOSIS Educational Program is gratefully acknowledged.

Design of Linear Transmitters for Wireless Applications

Sungmin Ock, Ph.D.
The University of Texas at Austin, 2016

Supervisor: Ranjit Gharpurey

Wireless standards for high data-rate communications typically employ complex modulation schemes that have large peak-to-average power ratios (PAPR), along with a significant bandwidth requirement. Transmitters for such applications often employ off-chip power amplifiers (PAs), that are typically operated in back-off, such that the peak output power is less than the output 1-dB compression point (P1dB), in order to minimize distortion. In mobile systems, architectures that can enhance the linearity of the transmit chain are highly attractive since these can reduce the PA's back-off requirement, which helps to enhance efficiency.

In this dissertation, linearization techniques for mobile transmitters are explored. A Cartesian feedback-feedforward transmitter is proposed for linearity enhancement. The transmit path in the architecture is placed in a Cartesian feedback loop. The feedback error signal is applied to a Cartesian feedforward path for further linearity improvement. Linearity of the feedback-feedforward system is analyzed by using a Volterra series representation. System simulations using two-tone signals and modulated signals are also presented and are

used to verify the linearity enhancement provided by the proposed architecture.

A prototype transmitter IC that employs the Cartesian feedback-feedforward approach is implemented in a 0.13 μm CMOS process. Design considerations for critical transmitter circuits are discussed. A proof-of-concept Cartesian feedback-feedforward architecture that includes the prototype IC and external components is demonstrated. The implementation allows for a 8.7 dB improvement in the adjacent channel leakage ratio (ACLR), compared to an open-loop transmitter, for an output power of 16.6 dBm at 2.4 GHz while employing a 16-QAM LTE signal with 1.4 MHz bandwidth.

The linearity of the Cartesian feedback-feedforward system is found to depend primarily on the loop gain of the Cartesian feedback and the linearity of the Cartesian feedforward path, which introduces a trade-off with power consumption. To enhance the linearity of the Cartesian feedback-feedforward transmitter even further within the Cartesian feedback loop, two modified Cartesian feedback-feedforward architectures are explored. System simulations show that both modified configurations can help to enhance linearity compared to the above Cartesian feedback-feedforward transmitter.

Table of Contents

List of Tables

List of Figures

Chapter 1

Introduction

In the last two decades, the proliferation of mobile devices has changed human lifestyles extensively. In 2000 the number of worldwide mobile phone subscriptions was only 0.7 billion. In 2014, however, the total number was close to 7 billion [11]. The growth of the mobile device market has occurred in conjunction with progress in wireless communication systems. The mobile phones used in the late 1990s mainly supported cellular communication technologies such as GSM and IS-95 CDMA, which had data rates in the range from 9.5 kbps to 115 kbps, respectively. The peak download data rate of LTE by contrast is 100 Mbps. Additionally in recent smart phones, a variety of wireless protocols such as LTE, WLAN, Bluetooth, and NFC are employed simultaneously.

The demand for higher data rates for communication has made transmitter design increasingly challenging. High data rate wireless systems use broadband standards with high-order modulation for spectral efficiency. The transmitter needs to accommodate large bandwidth, high output power, and non-constant envelope modulation simultaneously. Typically, when a non-constant envelope modulation signal is employed, it has a substantial peak-to-

average power ratio (PAPR) such that the peak power is significantly higher than average power. Table 1.1 shows the characteristics of uplink signals used in recent wireless standards, and most of uplink signals shown in Table 1.1 have large PAPR. When a modulation signal with high PAPR is used, the system requires stringent linearity performance of the transmit chain, since it is required to deliver a signal with high peak power.

Table 1.1: Uplink signal comparison of wireless standards [1]

Standard	Output Power (dBm)	Channel BW (MHz)	PAPR (dB)	Modulation
GSM	35	0.2	0	GMSK
IS-95	28	0.2	5.5-12	O-QPSK
UMTS	27	5	3.5-7	HPSK
802.11 A/G	14-20	20	8-10	OFDM
LTE	22-25	20	2-4	SC-FDMA

In addition, with CMOS scaling, the digital computing capability required to support high data rate baseband signals, and digital power dissipation has continued to improve. However, as the supply voltage has decreased due to CMOS scaling, the total achievable linearity of the transmitters has declined accordingly owing to the reduced voltage headroom. Therefore, advanced linearization techniques for transmitters for mobile wireless systems are highly desirable for high data rate communication.

1.1 Transmitters for Mobile Wireless Systems

Fig. 1.1 shows a conventional transmit chain composed of baseband digital signal processing (DSP), digital to analog converters (DACs), low pass

filter (LPFs), variable gain amplifiers (VGAs), I/Q up-conversion mixers, local oscillator (LO) generator, driver amplifier, and the power amplifier (PA). The baseband DSP generates the digitally modulated I/Q data. It is converted to an analog baseband signal by the DACs. The analog baseband signal is properly filtered and scaled when it passes through the LPFs and VGAs. Next, it is up-converted by the LO signal to RF in the I/Q mixers. The output signal at the I/Q up-conversion mixers is typically very small. It must be amplified by a driver amplifier and a power amplifier, to meet the output power level required at the antenna.

At the current level of development of CMOS technology, most of the design blocks can be integrated on to one transmitter IC, but for high data rate communications, an off-chip PA is often used to meet the linearity and reliability requirements. In addition, in spite of significant progress, CMOS PAs have been mainly been applied for low power systems and PAs based on compound semiconductor technology such as InGaP/GaAs HBTs, are still very popular for high performance systems

To achieve the linearity specification of the full transmit chain, the linearity of the PA is critical. Due to the aforementioned high PAPR, the PA is typically operated in back-off, such that the maximum average power is much less than the output 1-dB compression point (P1dB), which significantly degrades its power efficiency.

However, it would be highly desirable for a transmitter architecture to enhance the total linearity of the transmit chain using the same PA. Fig. 1.2

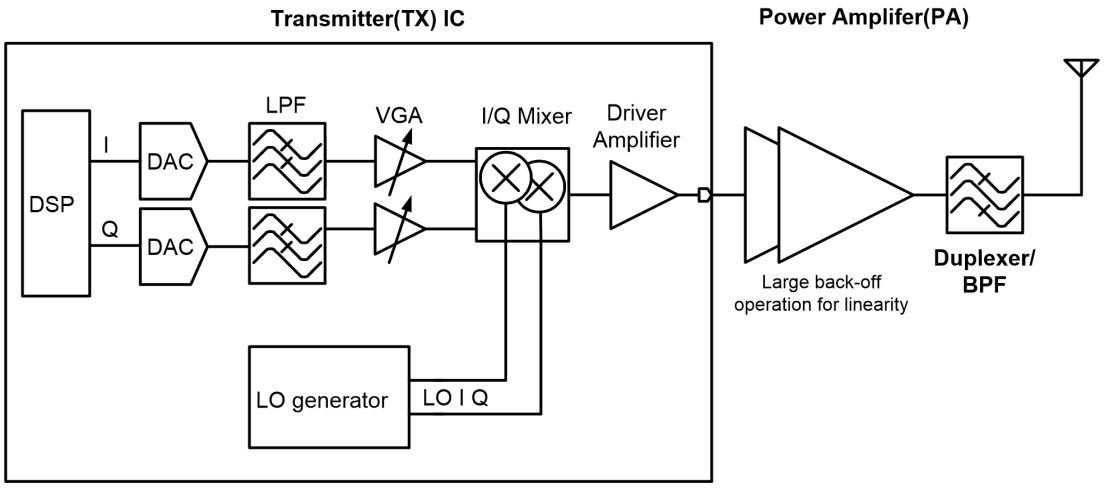

Figure 1.1: Conventional transmit chain

shows a conceptual illustration of such a design. Once the distortion product at the PA output is sensed, a suitable linearization technique implemented in the transmitter improves the overall linearity using the sensed distortion information. If the linearity requirement of the PA is relieved by the highly linear transmitter architecture, it could reduce the PA back-off, as well as the power dissipation, accordingly. In addition, due to the relaxed linearity requirement, CMOS PAs would be more feasible, even for high data rate and high power transmitters, which should lower implementation cost.

This dissertation proposes and demonstrates an architecture for enhancing transmitter linearity.

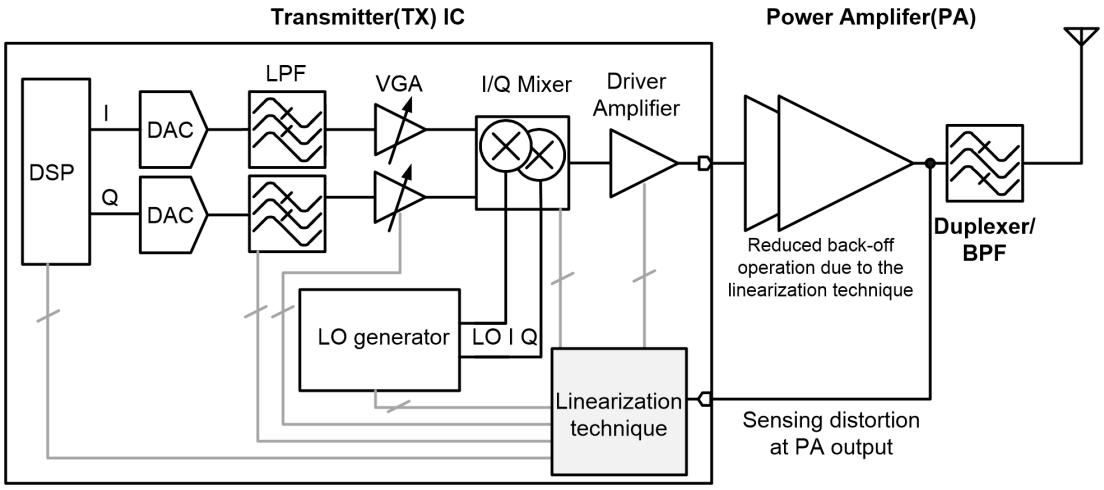

Figure 1.2: Transmitter with linearization

1.2 Organization

The dissertation is organized as follows. Chapter 2 is a brief review of key characteristics related to the linearity of transmitters and a survey of prior transmitter architectures for high linearity, such as feedforward, digital predistortion, and several feedback techniques. In Chapter 3, a Cartesian feedback-feedforward transmitter is proposed that enhances the overall linearity. The proposed architecture is analyzed using a linear additive model and Volterra series. Results from system simulations using two-tone signals and modulated signals are provided. In Chapter 4, a prototype transmitter IC implemented using 0.13 μm CMOS technology, is introduced. Its architecture and key design blocks are discussed. The measurement set-up used to demonstrate the Cartesian feedback-feedforward architecture, is described, and the measurement results are also presented. In Chapter 5, the linearity

limitations of the Cartesian feedback-feedforward architecture are discussed and two modified Cartesian feedback-feedforward transmitters are introduced for further linearity improvement. In Chapter 6, a review of the dissertation, conclusions, and directions for future research are presented.

Chapter 2

Linearity and Transmitter Architectures

2.1 Introduction

The role of the transmitter is to provide the modulated signal with the required power level and bandwidth to the antenna, without signal distortion or addition of noise. The signal distortion primarily depends on the linearity of the transmitter chain and must satisfy the system requirement. As described in Chapter 1, the linearity of a conventional transmitter is governed by the front-end PA. The linearity performance of a PA can be enhanced by increasing the back-off, however this can lead to unacceptable increase in power dissipation. Therefore, transmitter architectures that can enhance linearity without requiring greater linearity in the PA are desirable for mobile applications.

Before the proposed technique is presented, a short review is provided of state-of-the-art transmitter architectures for linearity enhancement. First, the main aspects and characteristics of transmitter linearity are introduced in Section 2.2. This is useful for providing an understanding of the nonlinear processes in conventional transmitters, and the analysis and measurement results presented in later chapters.

In Section 2.3, key transmitter architectures for achieving high linear-

ity are investigated, including feedforward, digital predistortion (DPD), and a variety of approaches based on feedback. Linearity and stability of the feedback system are explored further because the transmitter topology proposed in Chapter 3 is based on Cartesian feedback. It should be noted that the transmitters discussed are assumed to employ a linear PA, because linear PAs have been extensively utilized for high data rate communications. Therefore, several well-known transmitter architectures based on switching PAs are not discussed in this section, such as envelope elimination and restoration (EE&R) [12, 13], polar transmitters [14, 15], and linear amplification using non-linear components (LINC) [16–18].

2.2 Transmitter Linearity Metrics

2.2.1 1dB Compression Point (P1dB)

The transfer function of a memoryless nonlinear amplifier can be written as a power series, as shown in Fig. 2.1. In the transfer function, the coefficient a_1 represents the small signal gain. Higher-order coefficients such as a_2 and a_3 generate various nonlinear products. When a sinusoidal signal, $x = Acos\omega t$, is applied to the input, the output, taking into consideration only the first three terms of the transfer characteristic, can be expressed as

$$y = \frac{a_2 A^2}{2} + \left(a_1 A + \frac{3a_3 A^3}{4}\right) cos\omega t + \frac{a_2 A^2}{2} cos2\omega t + \frac{a_3 A^3}{4} cos3\omega t \cdots \quad (2.1)$$

The output is composed of a DC term, the fundamental term, and high-

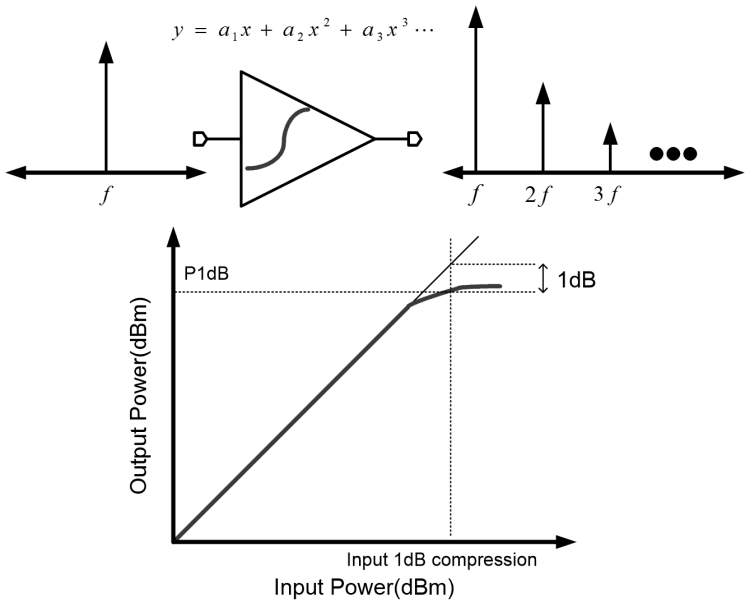

Figure 2.1: Single tone distortion and P1dB

order harmonic terms. In narrowband RF systems, the fundamental term is retained but the other harmonic terms can be filtered out of the output. If a_1 and a_3 have opposite polarity, as the input amplitude A is increased, the fundamental term is reduced by the non-linear product $3a_3A^3/4$, which reduces the effective small-signal gain of the amplifier. Fig. 2.1 also shows a plot that depicts the gain compression as the input power is increased. The output power at which the gain is decreased from the small signal gain by 1dB, is defined as the 1dB compression point (P1dB). The input amplitude at which the gain is reduced by 1 dB is given by

$$A_{1dB} \approx 0.332\sqrt{\frac{4}{3}\left|\frac{a_1}{a_3}\right|} \tag{2.2}$$

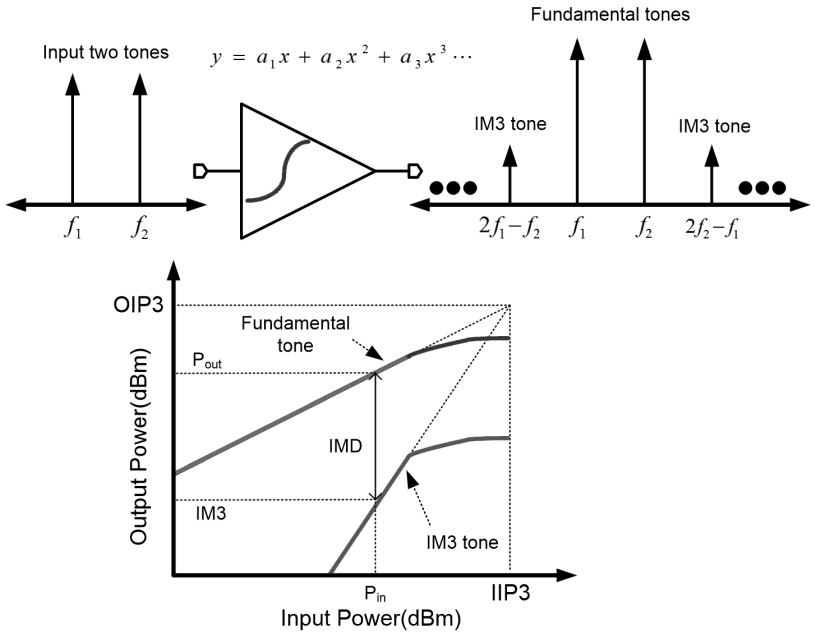

Figure 2.2: Two-tone distortion and IIP3

2.2.2 Third-Order Input-Referred Intercept Point (IIP3)

When two sinusoidal input signals with the same amplitude are applied to the above non-linear circuit, such that the total input is given by $x = Acos\omega_1 t + Acos\omega_2 t$, the output can consists of numerous harmonic terms and intermodulation terms simultaneously. When ω_1 and ω_2 are close, 3^{rd} order intermodulation terms at $2\omega_1 - \omega_2$ and $2\omega_2 - \omega_1$, known as IM3, will be in the vicinity of fundamental terms at ω_1 and ω_2 which is critical for both the transmitter and the receiver. Fig. 2.2 shows intermodulation distortion caused by two-tone signals. In order to estimate the linearity of the narrowband RF system with two-tone signals, fundamental tones at ω_1 and ω_2 and IM3 products at $2\omega_1 - \omega_2$ and $2\omega_2 - \omega_1$ are considered, and the output is written

as

$$\begin{aligned} y &\approx \left(a_1 A + \frac{9a_3 A^3}{4}\right) cos\omega_1 t + \left(a_1 A + \frac{9a_3 A^3}{4}\right) cos\omega_2 t \\ &\quad + \frac{a_3 A^3}{4} cos\left(2\omega_1 - \omega_2\right) t + \frac{a_3 A^3}{4} cos\left(2\omega_2 - \omega_1\right) t \end{aligned} \tag{2.3}$$

From Eq. (2.3), the input amplitude A is assumed to be too small to compress the fundamental tone, that is $3a_3A^3/4$ is much smaller than a_1A. Then, when the input amplitude A is increased, the fundamental and IM3 tones are increased with the slope of 20 dB/decade and 60 dB/decade, respectively. Fig. 2.2 also shows the plot of fundamental tone and IM3 tone on a dB scale. If there is no compression, the fundamental and IM3 tones will intersect at a certain input power defined as the input intercept point (IIP3). When the input-level equals IIP3, the fundamental tone and IM3 tone should be the same, which means that $a_1 A_{IIP3} = 3a_3 A_{IIP3}^3/4$. Therefore, the input amplitude at IIP3, A_{IIP3} is given by

$$A_{IIP3} = \sqrt{\frac{4}{3}\left|\frac{a_1}{a_3}\right|} \tag{2.4}$$

When the power of a fundamental tone, P_{out}(dBm) and the power of a 3^{rd} order intermodulation tone, IM3(dBm) are measured for an input power level, P_{in}(dBm), the IIP3 can be estimated as

$$IIP3(dBm) = P_{in}(dBm) + \frac{IMD(dB)}{2} \tag{2.5}$$

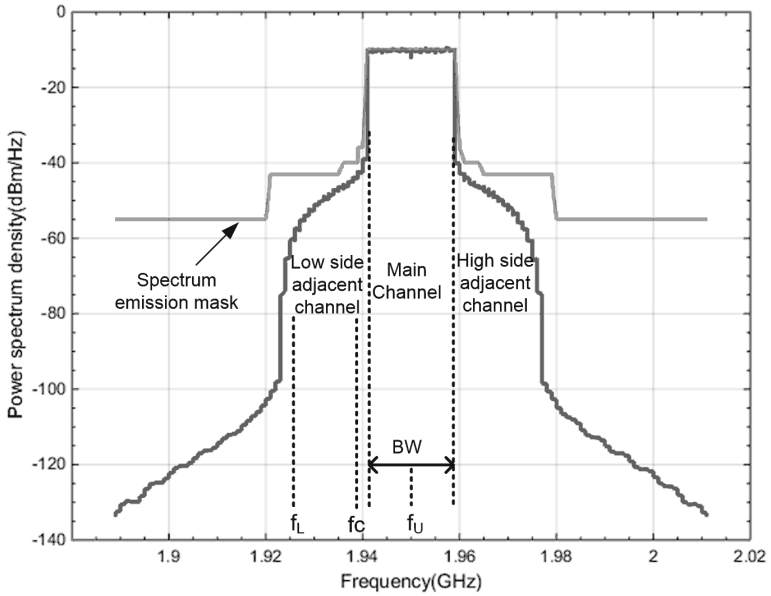

Figure 2.3: Spectrum of digitally modulated signal and spectrum emission mask

where,

$$IMD(dB) = P_{out}(dBm) - IM3(dBm)$$

Second order nonlinearities, cause a DC offset, which is also critical for direct-upconversion based transmitter architectures. When baseband I/Q signals are up-converted by a transmitter mixer, the nonlinearity generates a substantial LO tone at the output, which not only deteriorates the transmitted signal but can also saturate the power amplifier due to large inband interference.

2.2.3 Spectrum Emission Mask and Adjacent Channel Leakage Ratio (ACLR)

When the transmitter provides a band-limited, modulated signal, nonlinearity and noise of the transmitter generate a spectral leakage that can appear on adjacent frequency bands relative to the desired output spectrum, which is known as adjacent channel leakage. Adjacent channel leakage can corrupt other communication signals. Therefore, wireless standards define a spectrum emission mask to limit the amount of spectral leakage on nearby frequency bands.

Fig. 2.3 shows the spectrum of a digitally modulated signal with a 20 MHz channel bandwidth and its spectrum emission mask. The spectrum shows substantial leakage on both adjacent channels, which are quantified by the adjacent channel leakage ratio (ACLR) [19]. Based on Fig. 2.3, low side ACLR is defined as

$$ACLR = \frac{\int_{f_L}^{f_U} PSDdf}{\int_{f_c-0.5\cdot BW}^{f_c+0.5\cdot BW} PSDdf} \tag{2.6}$$

2.2.4 Error Vector Magnitude (EVM)

Error vector magnitude (EVM) is another metric to quantify the quality of digitally modulated signals. Fig. 2.4 shows a typical 16-QAM constellation at the output of a transmitter. The constellation plot shows a cloud of points around each assigned position, which represents amplitude and phase errors of the transmitted signal. EVM is defined as

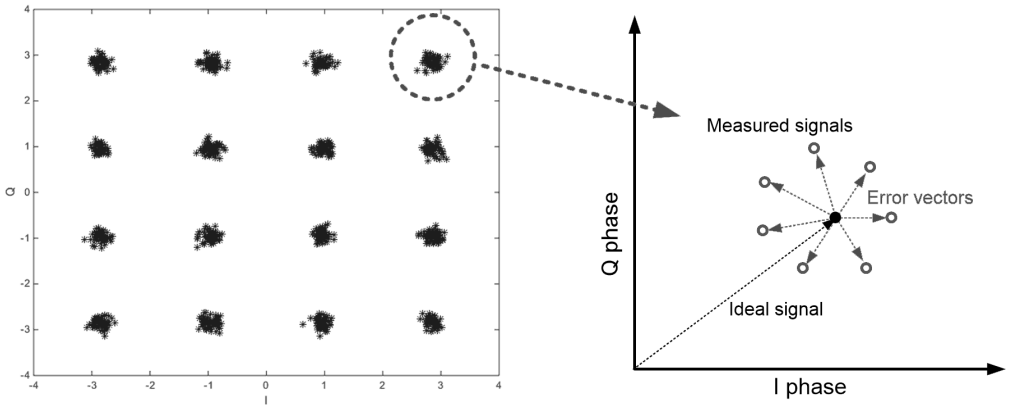

Figure 2.4: 16-QAM constellation and EVM illustration

$$EVM = \sqrt{\frac{1}{N}\sum_{k=1}^{N}\left(\left|\frac{e_k}{s_k}\right|\right)^2} \tag{2.7}$$

In Eq. (2.7), N is the number of data samples, and e_k and s_k are an error vector and a signal vector at the k^{th} sample, respectively.

While ACLR is mainly determined by nonlinear distortion, EVM characterizes total errors generated by nonlinear distortion, thermal noise, LO phase noise, and I/Q mismatch. Therefore, EVM can characterize the signal-to-noise ratio (SNR) of the transmitted signal. A typical nonlinear mechanism was discussed in Section 2.2.1 and 2.2.2, but Fig. 2.5 shows another mechanism involving I/Q impairment and the resulting spurious LO signal which can degrade EVM [9]. If baseband I/Q amplifiers have DC errors, or quadrature LO signals have phase errors, I/Q paths would have substantial mismatch. In this case, I/Q imbalance induces inband noise due to the deterioration of

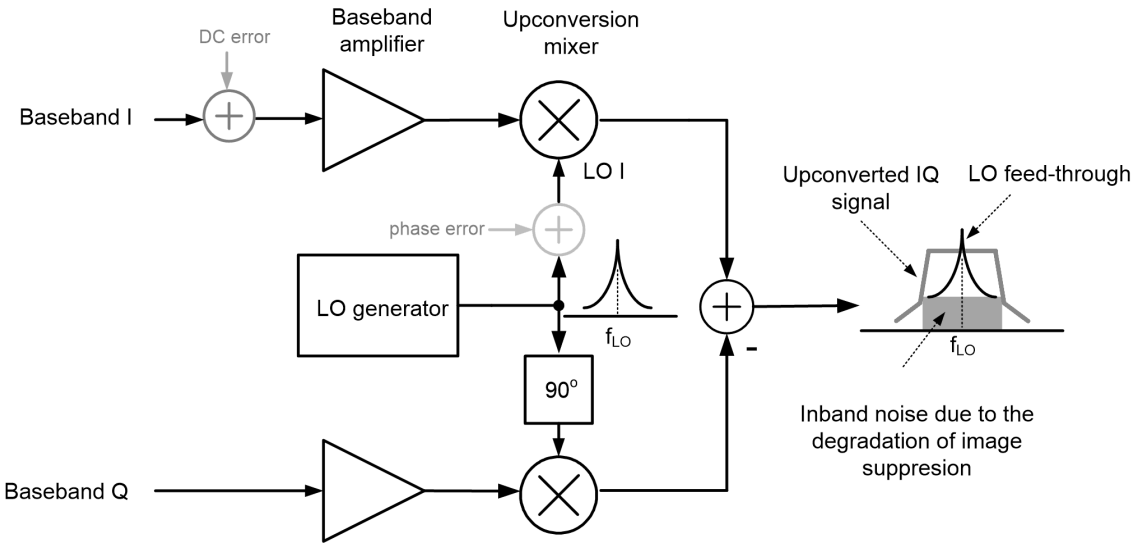

Figure 2.5: EVM degradation due to I/Q mismatch

image suppression, as well as LO feed-through. This can be a major source of interference in the signal band.

2.2.5 Modulation and PAPR

High order modulation would be preferred in high data rate communication systems, because spectral efficiency is proportional to $log_2 M$ where M is the number of bits per symbol. However, in the case that quadrature amplitude modulation (QAM) and amplitude-shift keying (ASK) are employed, PAPR of the modulated signal is increased by M, which requires correspondingly higher linearity of the transmitter.

Orthogonal frequency-division multiplexing (OFDM) modulation is also widely used to mitigate multipath fading for high data rate systems, but

the use of numerous sub-carriers in OFDM can also sharply increase PAPR. When OFDM has N sub-carriers using M-QAM, and all sub-carriers are assumed to use the same symbol with the highest energy simultaneously [19], the worst-case PAPR of an OFDM signal can be derived as

$$PAPR_{worst} \approx 2N \times 3 \left(\frac{\sqrt{M}-1}{\sqrt{M}+1} \right) \tag{2.8}$$

For example, when OFDM has 64 sub-carriers using 64-QAM, the worst PAPR would be around 24.7 dB. In practice, the sub-carriers of OFDM signals are statistically distributed and the PAPR should be estimated by using accumulated statistical data for all sub-carriers. The complementary cumulative distribution function (CCDF) is used extensively to measure the probability distribution of PAPR. Fig. 2.6 shows the CCDF of an OFDM signal with 64 sub-carriers using 64-QAM. The OFDM signal has the maximum PAPR of 9.8dB, which is still large, but significantly smaller than 24.7dB.

It should be mentioned that various coding techniques have been developed to reduce the PAPR, such as clipping, interleaving and windowing. Moreover, while an LTE system uses OFDMA in the downlink, for the uplink path of the mobile system, the LTE standard uses single carrier (SC) frequency-division multiple access (FDMA) to reduce PAPR. This would usually be smaller than the PAPR of a WLAN system.

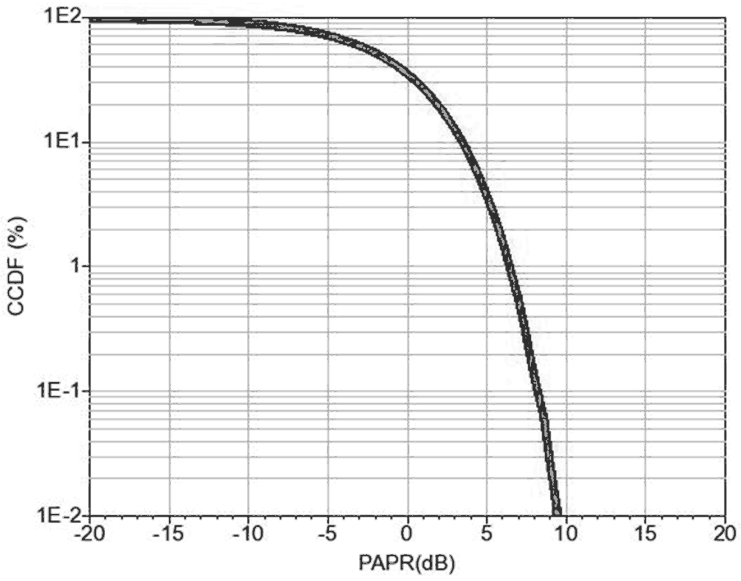

Figure 2.6: CCDF of OFDM signal with 64 sub-carriers using 64-QAM

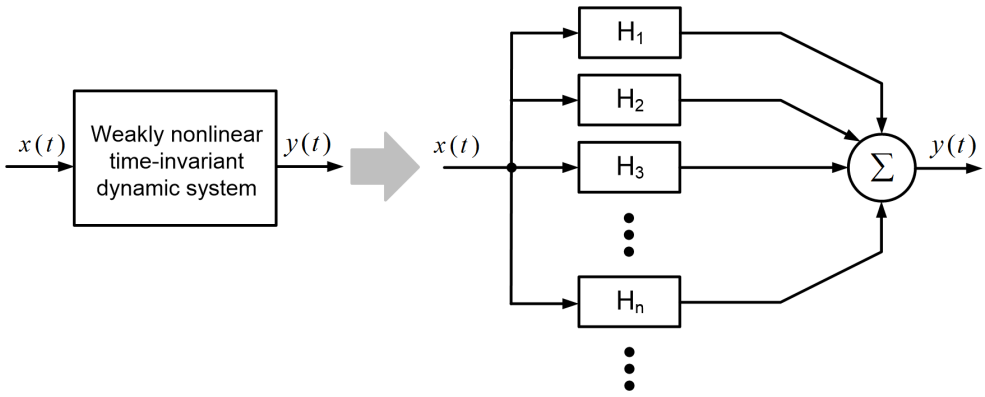

Figure 2.7: Volterra series illustration

2.2.6 Volterra Series

Conventional memoryless time-invariant nonlinear systems are described by a power series as shown in Sections 2.2.1 and 2.2.2. However, when a nonlinear system has memory, leading to frequency dependence due to time delay or energy storage, a Volterra series is a useful analytical tool especially for weakly nonlinear time-invariant dynamic systems [20, 21]. Here, weak nonlinearity means that the input signal is sufficiently small such that the nonlinearity can be represented by a finite series of relevant terms [22, 23].

Fig. 2.7 illustrates a Volterra series representation of a weakly nonlinear dynamic system. The nonlinear output of $y(t)$ is represented by the sum of responses of individual Volterra operators H_1, H_2 etc. Then, the Volterra series is expressed as

$$y(t) = H_1[x(t)] + H_2[x(t)] + H_3[x(t)] \cdots \tag{2.9}$$

where

$$\begin{aligned} H_n[x(t)] &= \int \cdots \int_{-\infty}^{+\infty} h_n(\tau_1, \tau_2, \cdots, \tau_n) \\ &\times \; x(t-\tau_1)\, x(t-\tau_2) \cdots x(t-\tau_n)\, d\tau_1 d\tau_2 \cdots d\tau_n \end{aligned}$$

,

In Eq. (2.9), $h_n(\tau_1, \tau_2, \cdots, \tau_n)$ is called the n^{th}-order Volterra kernel, which is equivalent to an n-dimensional impulse response. Therefore, the op-

eration $H_n[x(t)]$ represents the n-dimensional convolution integral of the input with an n-dimensional impulse response.

When the Volterra series is described in the Laplace domain, it can be also written as

$$\begin{aligned} Y = {} & H_1(s_1) \circ X(s_1) + H_2(s_1, s_2) \circ X(s_1) \circ X(s_2) \\ & + H_3(s_1, s_2, s_3) \circ X(s_1) \circ X(s_2) \circ X(s_3) \cdots \end{aligned} \tag{2.10}$$

where

$$\begin{aligned} H_n(s_1, s_2, \cdots, s_n) = \int \cdots \int_{-\infty}^{+\infty} & h_n(\tau_1, \tau_2, \cdots, \tau_n) \\ & \times e^{-(s_1\tau_1 + s_2\tau_2 + \cdots + s_n\tau_n)} d\tau_1 d\tau_2 \cdots d\tau_n \end{aligned}$$

In Eq. (2.10), $H_n(s_1, s_2, \cdots, s_n)$ is an n^{th}-order Volterra kernel in the Laplace domain with $s = j\omega$ and solving the output of the nonlinear system is the equivalent of finding the Volterra kernels.

It can be extremely complicated to solve a Volterra series of a general nonlinear dynamic system. However, if the system can be decomposed to linear dynamic blocks and nonlinear memoryless blocks, the Volterra kernels can be more easily calculated. Fig. 2.8 describes an exemplary nonlinear dynamic system [24, 25]. In Fig. 2.8, the nonlinear dynamic system consists

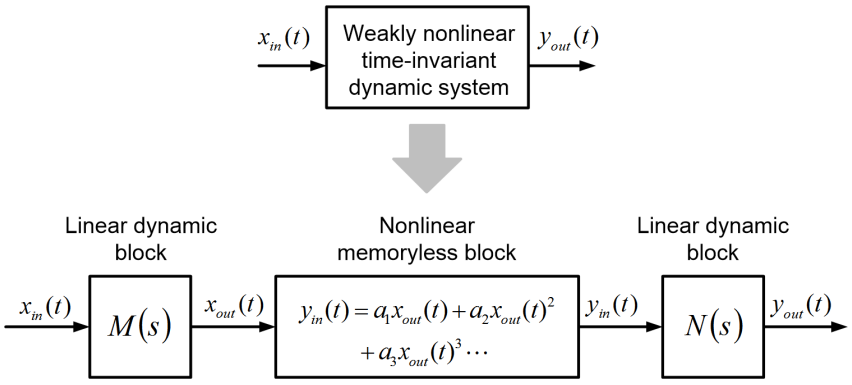

Figure 2.8: Typical weakly nonlinear time-invariant dynamic system

of the input linear dynamic block of $M(s)$, the nonlinear memoryless block of $y_{in} = a_1 x_{out} + a_2 x_{out}^2 + a_3 x_{out}^3 \cdots$, and the output linear dynamic block of $N(s)$. For example, for the RF amplifier, $M(s)$ and $N(s)$ can be assumed to be the input and output matching networks, respectively, and the nonlinear memoryless block represents the nonlinear current of an active device in the amplifier.

Then, the first three Volterra kernels of Y_{out} in Fig. 2.8 are given by

$$\begin{aligned} H_1(s_1) &= a_1 M(s_1) N(s_1) \\ H_2(s_1, s_2) &= a_2 M(s_1) M(s_2) N(s_1 + s_2) \\ H_3(s_1, s_2, s_3) &= a_3 M(s_1) M(s_2) M(s_3) N(s_1 + s_2 + s_3) \end{aligned} \tag{2.11}$$

Based on Eq. (2.11), the system linearity can be evaluated. For example, if two-tone signals with the amplitude of A and narrow frequency spacing

are employed, this means $s_1 = s_3 = j\omega_1$, $s_2 = -j\omega_2$, and $\omega_1 \approx \omega_2 = \omega$. Then, the $IIP3$ is given by

$$A_{IIP3} = \sqrt{\frac{4}{3}\left|\frac{H_1}{H_3}\right|} \approx \sqrt{\frac{4}{3}\left|\frac{a_1}{a_3 M\,(j\omega)^2}\right|} \tag{2.12}$$

2.3 Transmitter Architectures for Linearization

2.3.1 Feedforward Architecture

Feedforward is a classical technique for linearization, invented by H.S. Black [26]. Fig. 2.9 shows a feedforward architecture and an illustration of how to cancel IM3 terms at the output when two-tone signals are applied. First, a time delayed version of the input signal is subtracted from the attenuated output of the main amplifier to provide an error signal. This mainly contains the distortion terms of the main amplifier. The error signal is adjusted by the error amplifier and the phase shifter, and is used to cancel the distortion term of the main amplifier, in the combined output.

Feedforward is unconditionally stable and is useful for linearizing broadband signals. However, the main power amplifier usually suffers from large variation in nonlinearity as a function of signal strength, process, and temperature. Gain and phase of the error amplifier in the feedforward path could also vary similarly, which increases the cancellation error in the combined output. Therefore, in order to match the two paths, the design would need a complex analog/digital calibration loop to monitor the variation of both signal paths

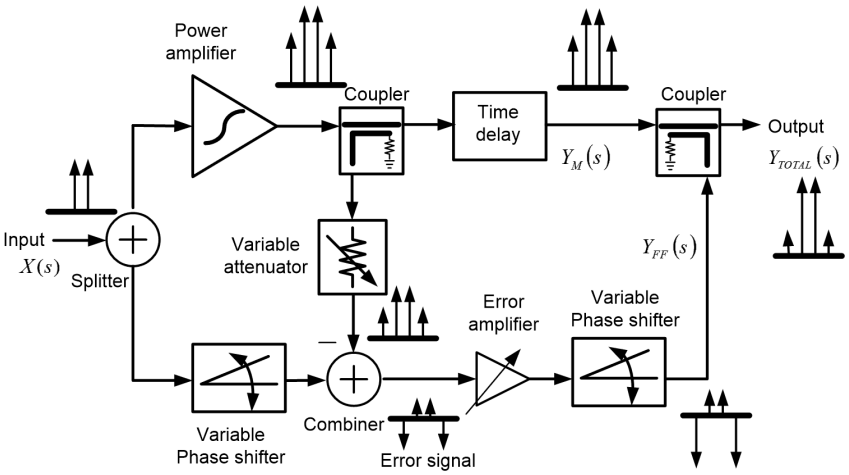

Figure 2.9: Feedforward architecture for PA [2]

and to adjust the gain and phase of the feedforward path adaptively. In addition, the architecture also requires several discrete passive components, like couplers and power splitters, which make reduction of size and cost difficult. Therefore, while the feedforward approach has been widely employed in base stations, it would be very challenging to utilize in mobile systems.

2.3.2 Digital Predistortion (DPD)

DPD is a digital compensation scheme to linearize the overall transmit path by using baseband DSP [27, 28]. In theory, DPD systems are well-suited for broadband linearization. Fig. 2.10 represents conventional DPD architecture. It is composed of the main transmitter path including the PA, the feedback loop, and the digital predistortion generator inside the DSP. The feedback loop senses the PA output and converts it to the digital domain after down-conversion. The DPD generator estimates the DPD coefficients

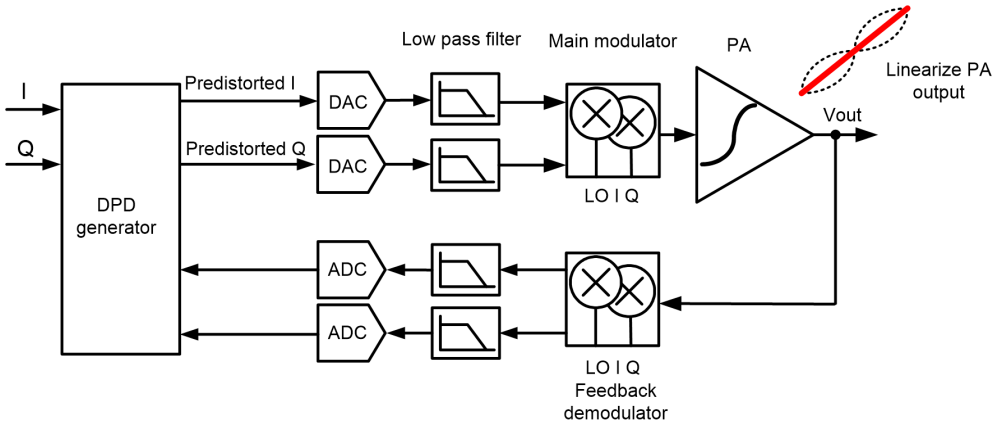

Figure 2.10: DPD system for linearizing PA [3]

using the feedback signal. The estimated DPD coefficients are subsequently multiplied by the original I/Q signals to generate DPD I/Q signals, which are then applied to the main DACs.

The output of the power amplifier needs to be monitored by the system to control the DPD signal adaptively. This typically requires a high level of digital computation for fast tracking and calibration, especially for broadband signals. To satisfy system requirements, prior DPDs for mobile systems mainly used a look up table (LUT) to generate DPD signals after a calibration period. This approach did not support real-time adaptive adjustment for PA variation. However, as the computing power of digital signal processors (DSP) has improved with CMOS process scaling, DPD is becoming viable for mobile systems. Real-time adaptation of DPD has been demonstrated for broad band applications in [3, 22, 29].

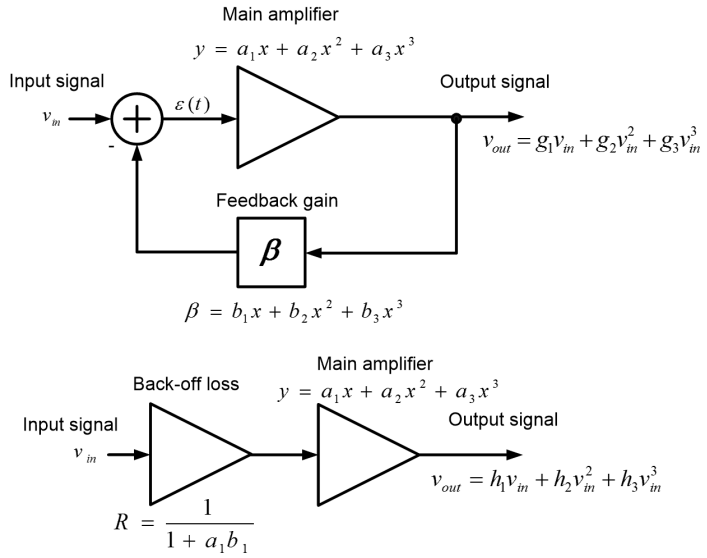

Figure 2.11: Linearity comparison of feedback amplifier and open-loop amplifier

2.3.3 Feedback Transmitter

Feedback is another major approach for linearizing systems, and was also invented by H.S. Black [26, 30]. A variety of transmitter architectures are based on a basic negative feedback approach.

2.3.3.1 Linearity Improvement Through Feedback

It is well known that negative feedback can improve the linearity of an amplifier. Consider an amplifier within a feedback loop that has the same gain as an open-loop amplifier. Fig. 2.11 shows the feedback loop and the corresponding open-loop amplifier. The feedback loop and the open-loop use the same amplifier but an ideal back-off is added in front of the open-loop amplifier, to match gains of the feedback and the open-loop cases. In the

feedback loop, the main amplifier and the feedback gain are represented as $y = a_1x + a_2x^2 + a_3x^3$ and $\beta = b_1x + b_2x^2 + b_3x^3$, respectively. The open-loop has the same amplifier used in the feedback loop and the back-off loss is represented as $R = 1/(1 + a_1b_1)$. The nonlinear equation of the feedback loop, $v_{out} = g_1v_{in} + g_2v_{in}^2 + g_3v_{in}^3$, can be derived from

$$\begin{aligned} v_{out} = g_1v_{in} + g_2v_{in}^2 + g_3v_{in}^3 &= a_1\left(v_{in} - \left(b_1v_{out} + b_2v_{out}^2 + b_3v_{out}^3\right)\right) \\ &\quad + a_2\left(v_{in} - \left(b_1v_{out} + b_2v_{out}^2 + b_3v_{out}^3\right)\right)^2 \\ &\quad + a_3\left(v_{in} - \left(b_1v_{out} + b_2v_{out}^2 + b_3v_{out}^3\right)\right)^3 \end{aligned} \tag{2.13}$$

Assuming fully differential implementation for the amplifier and the feedback path, 2^{nd} order distortion terms can be ignored ($a_2 = b_2 = g_2 = h_2 = 0$). Then, nonlinear coefficients of the closed loop, g_1 and g_3 are expressed as

$$\begin{aligned} g_1 &= \frac{a_1}{1 + a_1b_1} \\ g_3 &= \frac{a_3 - a_1^4b_3}{(1 + a_1b_1)^4} \end{aligned} \tag{2.14}$$

Nonlinear coefficients of the open-loop amplifier, h_1 and h_3 are simply written as

$$\begin{aligned} h_1 &= \frac{a_1}{1 + a_1b_1} \\ h_3 &= \frac{a_3}{(1 + a_1b_1)^3} \end{aligned} \tag{2.15}$$

As expected, g_1 and h_1 are the same, but g_3/h_3 is given by

$$\frac{g_3}{h_3} = \frac{\frac{a_3 - a_1^4 b_3}{(1+a_1 b_1)^4}}{\frac{a_3}{(1+a_1 b_1)^3}} = \frac{1 - a_1^4 \left(\frac{b_3}{a_3}\right)}{1 + a_1 b_1} \tag{2.16}$$

If the feedback path has sufficiently small 3$^{\text{rd}}$ order distortion to ensure that $a_1^4 b_3/a_3 \ll 1$, then

$$\frac{g_3}{h_3} \approx \frac{1}{1 + a_1 b_1} \tag{2.17}$$

Thus the IM3 terms of the feedback loop are attenuated by the loop gain $(1 + a_1 b_1) \approx a_1 b_1$, compared to the IM3 terms of the open-loop. The feedback path should be highly linear to get the result of Eq. (2.17). Otherwise, distortion terms of the feedback gain can substantially degrade the linearity of the feedback loop. Typically, the feedback path is implemented by passive circuits that have very good linearity. In a Cartesian feedback architecture however, the baseband buffer following the down-conversion mixer may deteriorate the linearity of the feedback path. For this reason, it must be designed carefully.

In addition, when $b_3 = a_3/a_1^4$, g_3 will be zero, which means that the 3$^{\text{rd}}$ order distortion term of the main amplifier is canceled by the 3$^{\text{rd}}$ order distortion of the feedback path. The condition ($b_3 = a_3/a_1^4$) can be employed for achieving high linearity. However, it would actually be very challenging to meet this condition in practice, because of substantial variation of a_1 and a_3.

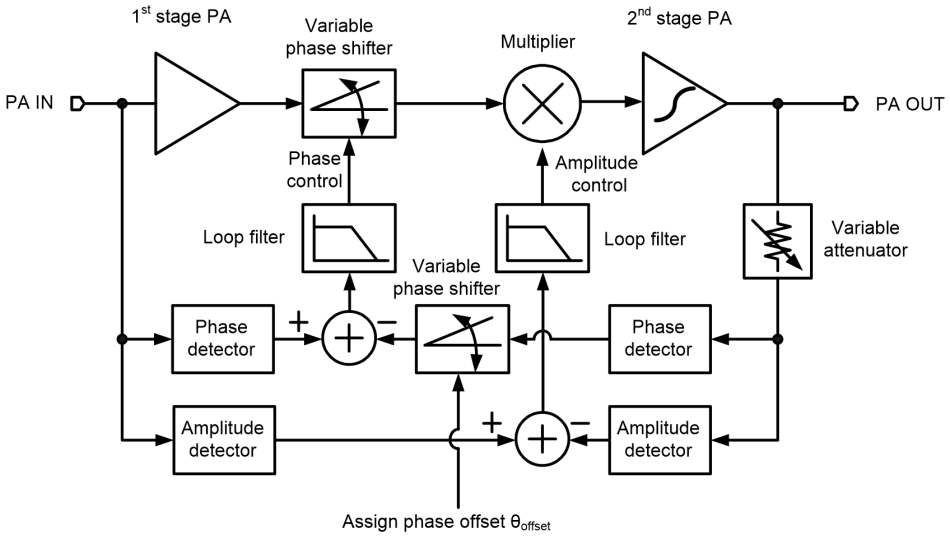

Figure 2.12: RF feedback using separate amplitude and phase loops for PA [4]

2.3.3.2 RF Feedback

A simple approach to employing a feedback loop to linearize a PA, involves the use of RF feedback. With RF feedback, the PA output signal is directly fed back to the RF input through a coupler or an attenuator. However, it would be difficult to achieve high forward gain of RF feedback due to loop stability requirements and the large power consumption of RF gain blocks. This makes it difficult to implement RF feedback.

Recently, a linearization technique based on RF feedback was proposed, and its block diagram is shown in Fig. 2.12. Unlike conventional RF feedback, this approach includes two separate indirect feedback loops for an envelope and phase. From the PA output, the envelope and phase are extracted by a phase detector and an amplitude detector. Once they are compared to the

envelope and phase of the PA input signal, these two error signals are used to control the phase and amplitude, respectively, in the forward path. This achieves an equivalent RF feedback.

Typically, separate envelope and phase signals would have larger bandwidth than the resulting composite signal. This makes it difficult to implement separate envelope and phase feedback loops. However, the proposed RF feedback approach demonstrated moderate ACLR improvement without supporting the full signal bandwidth. This is because most of the power of the envelope and phase signals is found around DC and this power can be detected and regulated by the loop [4].

2.3.3.3 RF Feedback-Feedforward

The RF feedback-feedforward architecture was proposed by Faulkner [31]. Fig. 2.13 shows the conceptual block diagram. The idea is to combine conventional RF feedback with RF feedforward. The error signal of the feedback loop can be the input of the feedforward path that achieves additional improvement in the linearity. The proposed transmitter introduced in Chapter 3 is based on this architecture.

Within the forward path, down-conversion and up-conversion mixers are added to control the loop phase. This also allows for the use of the baseband amplifier and loop filter indicated by G in Fig. 2.13, that provides both the high forward gain and the proper loop bandwidth. With RF feedback, due to the limited loop gain, the amount of error signal is not small. Thus, if

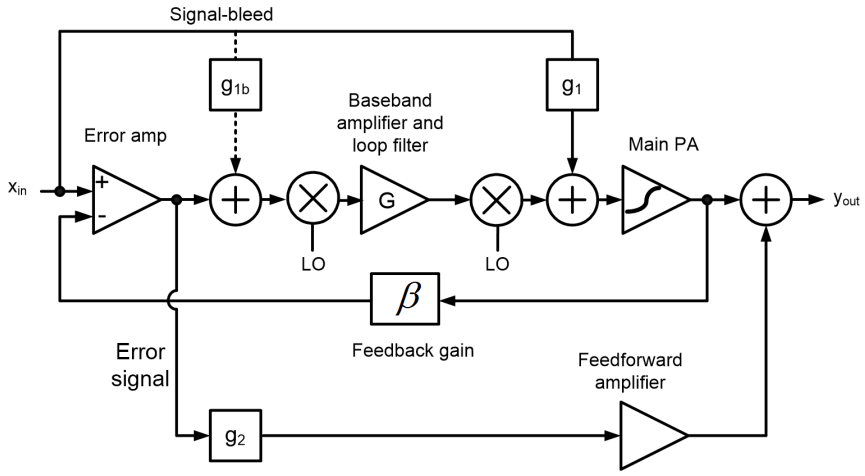

Figure 2.13: RF feedback-feedforward architecture for PA

additional gain paths represented as g_{1b} and g_1 provide the proper amount of signal in the loop instead, the error signal could be significantly reduced [32]. This could relieve the linearity requirement on both the error amplifier and the feedforward amplifier. This idea will be discussed more in Chapter 5.

2.3.3.4 Introduction to Cartesian Feedback

A Cartesian feedback transmitter is a modification of traditional feedback [33, 34]. It uses two decoupled feedback loops operating on the I and Q paths. Fig. 2.14 shows the Cartesian feedback architecture. Compared to a conventional transmitter, Cartesian feedback adds a down-conversion feedback path to the RF path. This path does not require high power consumption as it can use primarily passive circuits. However, potentially large group delay, multiple poles and zeros distributed along the feedback path and RF matching network, and AM-to-PM conversion in the PA can deteriorate the loop

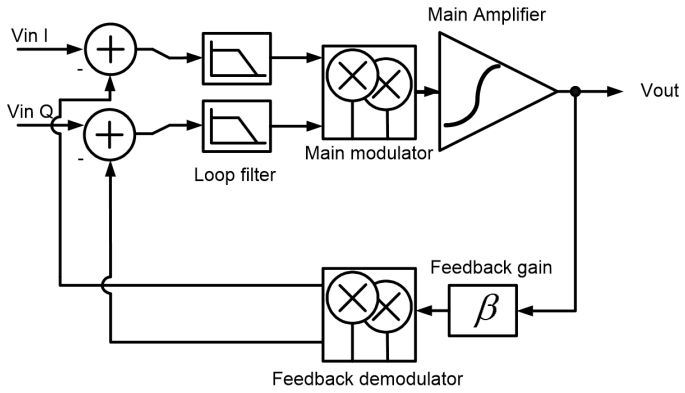

Figure 2.14: Cartesian feedback transmitter

stability. Ensuring loop stability limits the loop bandwidth and makes it challenging to use Cartesian feedback in a broadband system [5, 35]. Therefore, it has been used for narrow band systems such as TETRA which has a channel bandwidth of about 25KHz, or for linearizing fully integrated transmitter ICs that include the PA, and thus avoid a large onboard feedback delay [36, 37].

To understand the impact of time delay in a Cartesian loop, Fig. 2.15 shows the open loop path of the Cartesian feedback architecture [5]. In Fig. 2.15, the I and Q channel inputs are up-converted by a quadrature up-conversion mixer. The PA and feedback gain are represented by A and β, respectively. The time delay τ is added between the PA and the feedback gain. LO signals of down-conversion mixer in the feedback are assumed to have an adjustable phase ϕ. Then, the PA output is shown as

$$P_{out}(t) = AI_{in}(t)\, sin\omega_{LO}t + AQ_{in}(t)\, cos\omega_{LO}t \tag{2.18}$$

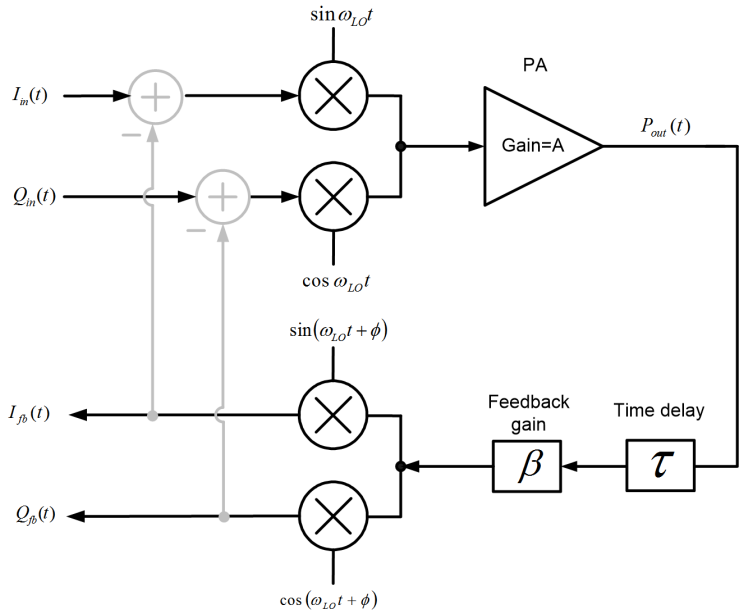

Figure 2.15: Open loop analysis of the Cartesian feedback transmitter [5]

If the $2\omega_{LO}$ terms are assumed to be rejected by filtering, the I channel and Q channel feedback outputs are given by

$$\begin{aligned} I_{fb}(t) &= \frac{A\beta}{2}\left[I_{in}(t-\tau)\,cos\,(\omega_{LO}\tau+\phi)+Q_{in}(t-\tau)\,sin\,(\omega_{LO}\tau+\phi)\right] \\ Q_{fb}(t) &= \frac{A\beta}{2}\left[-I_{in}(t-\tau)\,sin\,(\omega_{LO}\tau+\phi)+Q_{in}(t-\tau)\,cos\,(\omega_{LO}\tau+\phi)\right] \end{aligned} \tag{2.19}$$

If $sin\,(\omega_{LO}\tau+\phi)\neq 0$, $I_{fb}(t)$ does not only contain $I_{in}(t-\tau)$ but also $Q_{in}(t-\tau)$. Here, $Q_{fb}(t)$ also consists of both $I_{in}(t-\tau)$ and $Q_{in}(t-\tau)$ simultaneously. Therefore, the I and Q paths are not isolated and the loop stability of the Cartesian feedback can be degraded by the phase of $\omega_{LO}\tau+\phi$ [38]. For

example, if $\omega_{LO}\tau + \phi = \pi/2$, $I_{fb}(t)$ and $I_{fb}(t)$ are given by

$$\begin{aligned} I_{fb}(t) &= \frac{A\beta}{2} Q_{in}(t-\tau) \\ Q_{fb}(t) &= -\frac{A\beta}{2} I_{in}(t-\tau) \end{aligned} \tag{2.20}$$

Here, $I_{fb}(t)$ and $Q_{fb}(t)$ only have signals from the opposite channels and this would be the worst possible condition for stability [38].

Additionally, when $I_{fb}(t)$ and $Q_{fb}(t)$ have the correct signal as well as the other channel simultaneously, the other channel signal can be regarded as input noise at the up-conversion mixer. Then, even if the I and Q paths are assumed to have no mismatch errors, the opposite channel signal will not be suppressed by the up-conversion mixer. This condition leads to large inband noise as shown in 2.2.4.

Therefore, in order to ensure loop stability and I/Q image suppression, the LO phase of the down-conversion mixer ϕ, needs to be controlled to make $\phi = 2n\pi - \omega_{LO}\tau$. The I/Q feedback outputs can then be simplified to

$$\begin{aligned} I_{fb}(t) &= \frac{A\beta}{2} I_{in}(t-\tau) \\ Q_{fb}(t) &= \frac{A\beta}{2} Q_{in}(t-\tau) \end{aligned} \tag{2.21}$$

Now $I_{fb}(t)$ and $Q_{fb}(t)$ only contain correct signals and the Cartesian feedback can be interpreted as two independent feedback loops with a time delay of τ. In a Cartesian feedback loop with an off-chip PA, the time delay τ can be large. This causes a significant phase lag that can severely degrade loop stability. For example, if τ is 2 ns and the unity gain bandwidth is 100 MHz, the delay generates the phase lag of $2\,ns \times 100\,MHz \times 360^{o} = 72^{o}$ at the unity gain frequency.

If the loop bandwidth is small, the loop filter can easily provide a good phase margin for the feedback. Also, the effective phase lag caused by the delay might not be critical because the unity gain frequency can be small. However, to increase the loop bandwidth, the loop filter would need a wide pass band simultaneous with sufficient phase margin. Even though several loop filter topologies have been attempted for Cartesian feedback, such as high order filters or those employing properly placed zeros [39, 40], it is still challenging to achieve large loop bandwidth with Cartesian feedback.

The group delay of Cartesian feedback has not been discussed in this section, but a large group delay variation of a Cartesian loop could be problematic, primarily when high order envelope modulation is employed. Thus, while deciding the type and order of the loop filter, the overall group delay variation should be taken into consideration.

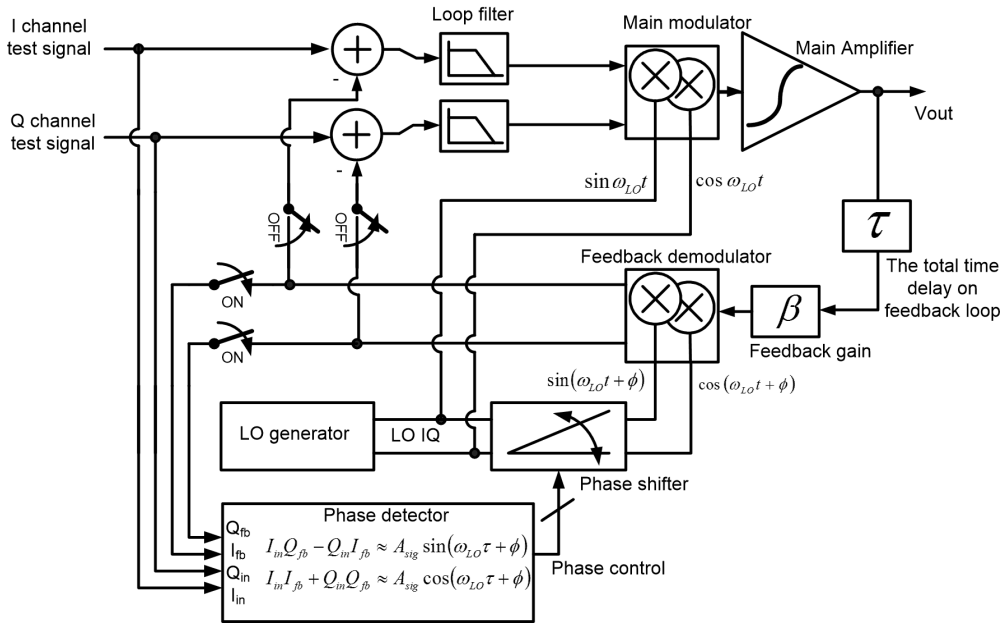

Figure 2.16: LO phase alignment of Cartesian feedback [6]

2.3.3.5 Techniques for Cartesian Feedback

In a Cartesian feedback loop with large delay, the LO phase should be correctly aligned so as to not couple the I/Q signals. Also, to achieve the required loop bandwidth, Cartesian feedback would need suitable schemes to compensate for stability degradation arising from the delay. Fig. 2.16 represents a typical architecture for LO phase alignment in Cartesian feedback [6, 38]. First, the switches to the combiners are set to off which disconnects the feedback loop. Other switches to phase detectors are turned on, which provides the correct LO phase adjustment. When the test signals are applied to I/Q inputs, $I_{in}(t)$, $Q_{in}(t)$, $I_{fb}(t)$ and $Q_{fb}(t)$ will be presented to the phase detector. If the I/Q test signals are assumed to be very low frequency mod-

ulation signals, such that $I_{in}(t-\tau) \approx I_{in}(t)$ and $Q_{in}(t-\tau) \approx Q_{in}(t)$, Eq. (2.22) and (2.23) can be easily derived by using Eq. (2.19).

$$\begin{aligned} I_{in}(t) Q_{fb}(t) - Q_{in}(t) I_{fb}(t) &= -\frac{A\beta}{2} I_{in}(t)^2 sin(\omega_{LO}\tau + \phi) \\ &\quad + \frac{A\beta}{2} I_{in}(t) Q_{in}(t) cos(\omega_{LO}\tau + \phi) \\ &\quad - \frac{A\beta}{2} Q_{in}(t) I_{in}(t) cos(\omega_{LO}\tau + \phi) \\ &\quad - \frac{A\beta}{2} Q_{in}(t)^2 sin(\omega_{LO}\tau + \phi) \\ &= -\frac{A\beta}{2} \left(I_{in}(t)^2 + Q_{in}(t)^2 \right) sin(\omega_{LO}\tau + \phi) \end{aligned} \tag{2.22}$$

$$\begin{aligned} I_{in}(t) I_{fb}(t) + Q_{in}(t) Q_{fb}(t) &= \frac{A\beta}{2} I_{in}(t)^2 cos(\omega_{LO}\tau + \phi) \\ &\quad + \frac{A\beta}{2} I_{in}(t) Q_{in}(t) sin(\omega_{LO}\tau + \phi) \\ &\quad - \frac{A\beta}{2} Q_{in}(t) I_{in}(t) sin(\omega_{LO}\tau + \phi) \\ &\quad \frac{A\beta}{2} Q_{in}(t)^2 cos(\omega_{LO}\tau + \phi) \\ &= \frac{A\beta}{2} \left(I_{in}(t)^2 + Q_{in}(t)^2 \right) cos(\omega_{LO}\tau + \phi) \end{aligned} \tag{2.23}$$

It should be noted that $I_{in}(t)^2 + Q_{in}(t)^2$ is the square of the magnitude of the I/Q test signals. Based on Eq. (2.22) and (2.23), when the LO phase

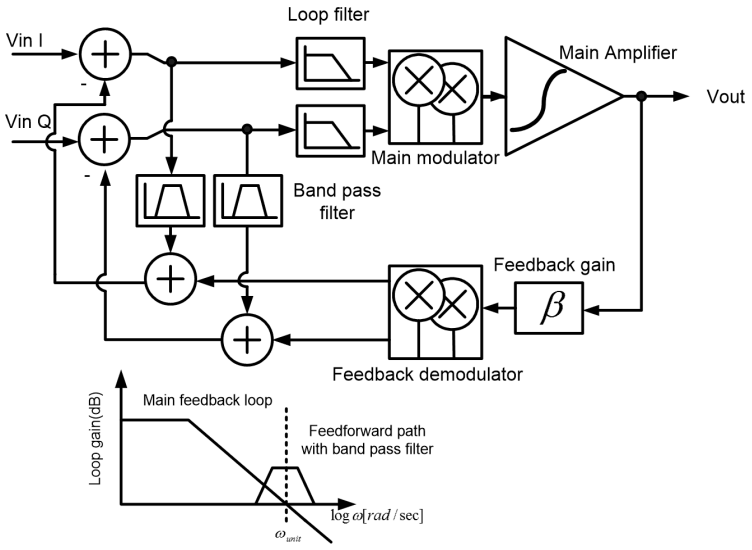

Figure 2.17: Stability enhancement technique using feedforward path and band pass filter [5]

of the down-conversion mixer ϕ is adjusted, the optimal LO phase to make both $sin\,(\omega_{LO}\tau + \phi) = 0$ and $cos\,(\omega_{LO}\tau + \phi) = 1$ can be selected, and it will be saved in memory for the Cartesian loop. In addition, a conventional phase detector can be implemented using analog multipliers and a subtractor. The DC offsets of the analog multipliers might generate significant errors in the phase detection and the offset should be minimized by matched layout and additional calibration, if necessary. In [38], chopper stabilization was proposed to implement analog multiplication without offsets.

Even when the LO phase is perfectly aligned, the time delay in the feedback loop is still critical for stability. As mentioned, there have been several prior ideas focused on the loop filter design, but Fig. 2.17 shows another stability improvement technique. As shown in Fig. 2.17, the error

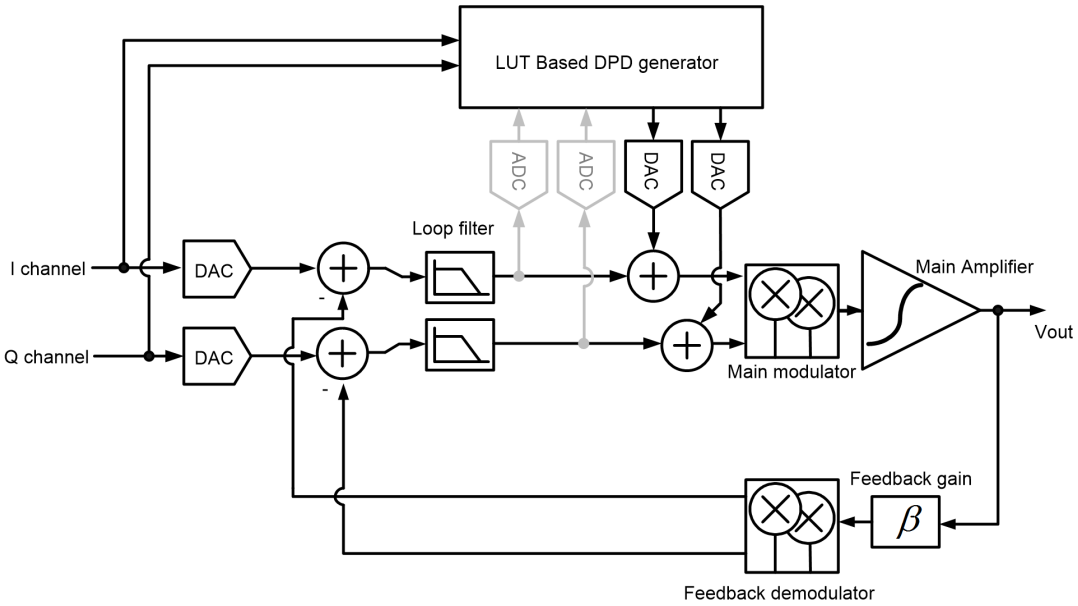

Figure 2.18: Cartesian feedback with DPD feedforward [7]

signal in the baseband is re-applied to the demodulator output through a band pass filter, which serves as a local feedforward. The center frequency of the band pass filter is located around the unity gain frequency of the main loop. The band pass feedforward path provides an additional zero and pole on both sides of the unity gain frequency, which helps to enhance the phase margin.

Cartesian feedback can also be combined with various digital techniques to improve the PA linearity [7, 41]. Fig. 2.18 shows an example which combines Cartesian feedback with DPD. It consists of a conventional Cartesian loop, a look-up table (LUT) based DPD generator, additional ADCs and DACs. When the Cartesian loop is initially ON for training the DPD generator, sig-

nals at the loop filter outputs are applied to the DPD generator through the ADCs. Using the given data and original I/Q data, the DPD generator updates the LUT to enable it to generate the proper I/Q signals with distortion terms. Once the update is finished, the ADCs turn off and the DPD generator provides additional I/Q signals through the DACs, which helps to improve the total linearity. Basically, the additional signal applied to the feedback appears similar to the linear signal-bleed shown in Fig. 2.13, but the DPD signal also has predefined distortion terms.

2.4 Conclusion

In this chapter, fundamental characteristics and metrics for describing transmitter linearity were introduced. The metrics discussed included P1dB, IIP3, ACLR, EVM and PAPR. While P1dB and IIP3 are basic metrics that are used to represent block level nonlinearity, ACLR and EVM can be used to demonstrate the linearity of transmitters and receivers. PAPR is a critical factor for determining the maximum linearity needed for the transmitter output. Volterra series representation of weakly nonlinear systems with memory was described. This is employed for the analysis of the proposed architecture in Chapter 3.

Various previously reported architectures for high linearity transmitters were explored. With feedforward, two transmit paths generating the same amount of distortion products with opposite polarities, are combined in parallel. This approach has mostly been used in base stations to linearize

high power signals with wide bandwidth. However, it is challenging to apply feedforward to mobile systems directly, because many passive components are required in the feedforward path. Moreover, a complicated compensation scheme is required to address the substantial variation of the PA over time [7].

For DPD, the distortion product of the front-end PA is compensated by the intended pre-distortion term created from the baseband digital stage, after correct estimation of the nonlinearity of the PA. Typically, this requires large computing power in the digital domain to calculate the distortion products and to provide a suitable DPD signal that is effective even with large PA variations. As high performance DSPs become more practical for mobile devices due to rapid development of CMOS technology, DPD could become a feasible solution for linearization of the transmitter chain in mobile systems.

As described above, a feedback loop can attenuate nonlinear products generated by the forward path, in proportion to the loop gain. For wireless transmitters, RF feedback and Cartesian feedback have been explored but due to limited loop bandwidth and loop stability constraint, most feedback architectures have been applied to narrow-band systems.

Chapter 3

Cartesian Feedback-Feedforward Transmitter

3.1 Introduction

For Cartesian feedback to be a practicable technique for improving the linearity of off-chip linear PAs [33] in low-cost systems, the baseband signal processing requirement should be relatively simple. In broadband systems, ensuring loop stability limits the loop bandwidth and makes it challenging to use Cartesian feedback [5]. Several techniques to improve the loop bandwidth and stability of Cartesian feedback have been proposed. Automatic LO phase alignment and calibration for Cartesian feedback are reported in [6, 38]. In [5], the loop gain and phase near the unity gain frequency of Cartesian feedback can be enhanced by the feedforward path with the use of a bandpass filter. In [7], a digital look-up table (LUT) and DACs are used to generate predistorted signals similar to DPD.

In this chapter[1], a Cartesian feedback-feedforward transmitter is proposed for improving the linearity of the transmit path that includes an off-chip PA [42]. While previously reported techniques for Cartesian feedback mainly

[1]This chapter includes material from the publication : Sungmin Ock, Jaegan Ko and Ranjit Gharpurey, "A Cartesian Feedback Feedforward Transmitter", *IEEE International Symposium on Circuits and Systems*, pp. 209 - 212, 2011, © 2011 IEEE.

focus on improving the loop stability and bandwidth in order to suppress the distortion of broadband signals, the proposed architecture can achieve additional linearity improvement by combining a conventional Cartesian feedback loop with feedforward, while satisfying the requirement for a low-complexity implementation.

Section 3.2 introduces the Cartesian feedback-feedforward transmitter. System analysis and simulation results are presented in Section 3.3. A feedback-feedforward model is described to describe the basic idea. The architecture is further explored using a Volterra-series analysis. The impact of time delays in the feedback and feedforward paths is also discussed. System simulation results using two-tone signals and modulated signals are provided in Section 3.4. Section 3.5 presents conclusions.

3.2 Cartesian Feedback-Feedforward Transmitter

Fig. 3.1 shows the architecture of the Cartesian feedback-feedforward transmitter. It consists of a traditional Cartesian feedback transmitter and an auxiliary transmit path that consists of an I/Q modulator and an auxiliary driver amplifier. Fundamentally, it is based on the RF feedback-feedforward structure proposed in [31]. However, the proposed approach employs a Cartesian architecture that uses separate I/Q signal paths with up- and down-conversion. As Fig. 3.1 shows, the feedforward path uses as its input the baseband error signal of the Cartesian feedback loop.

In this approach, linearization is achieved using two mechanisms.

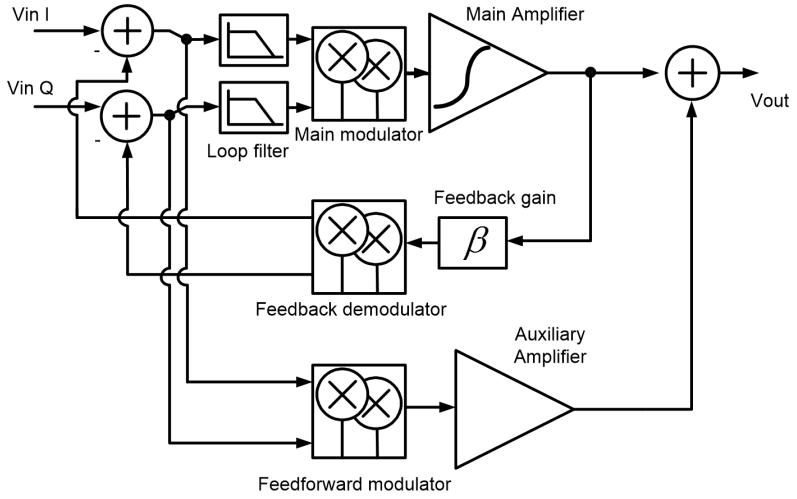

Figure 3.1: Cartesian feedback-feedforward transmitter

Cartesian feedback is used to improve the linearity of the main amplifier by employing the loop gain. Then, by combining the feedforward path output with the output of the Cartesian feedback transmitter, the residual distortion product arising from the main PA is reduced by cancellation resulting from the distortion product that the feedforward path delivers. By combining feedback and feedforward in this manner, the proposed architecture achieves a greater improvement in linearity for a given loop bandwidth than Cartesian feedback by itself.

3.3 Analysis of Cartesian Feedback-Feedforward Transmitter

3.3.1 Feedback-Feedforward without Frequency-Translation

To understand the proposed idea intuitively, we use a simple feedback-feedforward model shown in Fig. 3.2 that does not involve frequency-translation.

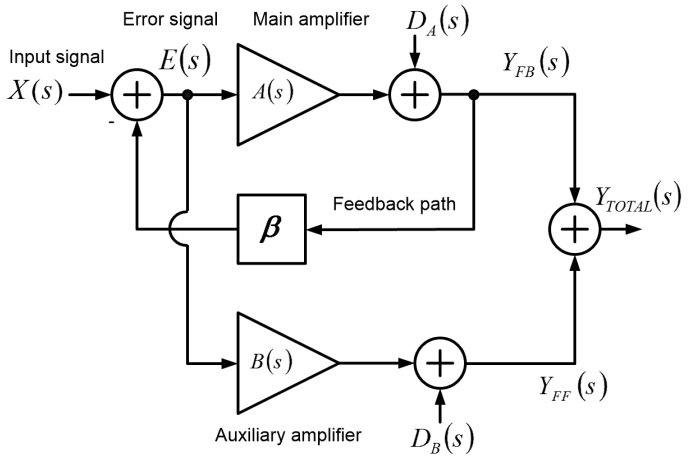

Figure 3.2: Feedback-feedforward model

In Fig. 3.2, $A(s)$ represents the transfer function of the main amplifier and $B(s)$ denotes the transfer function of the auxiliary feedforward path. The distortion products arising from the main and auxiliary amplifiers can be represented as additive errors $D_A(s)$ and $D_B(s)$ respectively. Here, β symbolizes the feedback gain which for simplicity is assumed to be perfectly linear and memoryless.

The feedback output $Y_{FB}(s)$ and the error signal $E(s)$ are given by

$$Y_{FB}(s) = \frac{A(s)}{1 + A(s)\beta} X(s) + \frac{1}{1 + A(s)\beta} D_A(s) \tag{3.1}$$

$$E(s) = \frac{1}{1 + A(s)\beta} X(s) - \frac{\beta}{1 + A(s)\beta} D_A(s) \tag{3.2}$$

As can be expected in a negative feedback system, the distortion output of the main amplifier $D_A(s)$ is suppressed by the loop gain. When the error signal provided by Eq. (3.2) is used as the input of the auxiliary amplifier, with $B(s)$ of $1/\beta$, the output of the auxiliary amplifier $Y_{FF}(s)$ is given by

$$Y_{FF}(s) = \frac{1/\beta}{1 + A(s)\beta} X(s) - \frac{1}{1 + A(s)\beta} D_A(s) + D_B(s) \tag{3.3}$$

By combining the feedback output from Eq. (3.1) and the feedforward output from Eq. (3.3), the resultant signal can be expressed as

$$Y_{TOTAL}(s) = \frac{A(s) + 1/\beta}{1 + A(s)\beta} X(s) + D_B(s) \tag{3.4}$$

We observe that the distortion output of the main amplifier $D_A(s)$ is canceled above and that the distortion output of the auxiliary amplifier $D_B(s)$ is the only remaining component in the total output. The auxiliary amplifier has a gain of $1/\beta$ that can be made significantly lower than that of the main amplifier $A(s)$. In this case, we can expect that the distortion output of the auxiliary amplifier $D_B(s)$ will be much smaller than the distortion of the main

amplifier $D_A(s)$. Thus the overall linearity can be significantly improved by the feedforward path without changing the feedback network.

3.3.2 Analysis using Two-Tone Signals and Volterra Series

Fig. 3.3 shows the detailed feedback-feedforward network. The network includes a nonlinear polynomial model of the main amplifier, the loop filter, delay of the main path, and the feedback paths, as well as a nonlinear model of the feedforward path. The main amplifier is assumed to have a memoryless nonlinearity given by $ax_{in} + a_2x_{in}^2 + a_3x_{in}^3 \cdots$. The auxiliary amplifier in the feedforward path is also modeled by $bx_{in} + b_2x_{in}^2 + b_3x_{in}^3 \cdots$, similar to the main amplifier (Fig. 3.3).

Cartesian feedback loops can employ different types of loop filters to ensure the stability of the feedback loop. In this analysis, a simple one-pole loop filter $L(s)$ with a 3dB frequency of ω_c is included in the main forward path. A time delay of τ_1 with a frequency response of $e^{-s\tau_1}$ is also included in the forward path. This delay is assumed to be static for this linearity analysis but in reality it can vary with output power due to phenomena such as AM-to-PM conversion, which can be observed if the non-linearity has memory. The feedback path has a gain of β and a time delay of τ_2. Unlike the forward time delay of τ_1, the time delay of the feedback path is primarily a static delay, and arises due to passive components such as the PCB traces.

For simplicity, the two amplifiers are assumed to have identical linear gains, i.e., $a_1 = b_1$ and their 2^{nd} order distortion terms are assumed to be

negligible ($a_2 = b_2 = 0$), which would be the case for a fully differential system. An attenuator with a gain of R is added to adjust the gain of the feedforward path. A phase shifter $P(s)$ that provides a delay of τ_{ff}, is also employed in the feedforward path to align its phase. When the output signals of the feedback and the feedforward paths are combined, a coupler can be used to minimize the signal loss of the main feedback path and to provide isolation between the feedback and feedforward outputs. The coupler is modeled by an ideal summation device with a coupling loss of C, and the insertion loss of the coupler is ignored for simplicity. Thus, while the output signal of the main feedback network is assumed to be delivered to the final output without loss, the output signal of the feedforward path is transferred to the final combined output with a coupling loss of C.

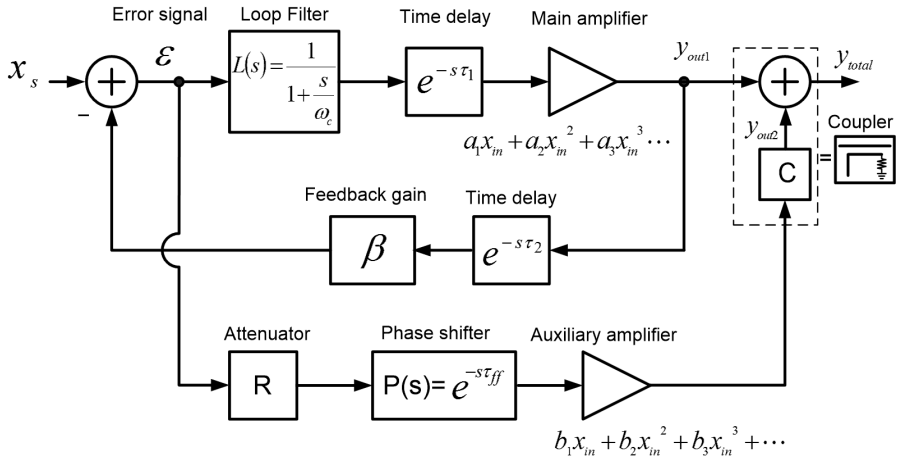

Figure 3.3: Amplifier-based feedback-feedforward model

Volterra series representation is widely utilized for analyzing weakly nonlinear systems [20, 21]. By applying a Volterra series analysis to the feed-

back network in the frequency domain [25, 42, 43], the output of the main feedback network, Y_{out1}, can be written as

$$\begin{aligned} Y_{out1} = {} & A_1(s_1) \circ X_s(s_1) + A_2(s_1, s_2) \circ X_s(s_1) \circ X_s(s_2) \\ & + A_3(s_1, s_2, s_3) \circ X_s(s_1) \circ X_s(s_2) \circ X_s(s_3) \cdots \end{aligned} \tag{3.5}$$

where,

$$\begin{aligned} A_1(s_1) &= \frac{a_1 e^{-s_1\tau_1} L(s_1)}{T(s_1)} \\ A_2(s_1, s_2) &= 0 \\ A_3(s_1, s_2, s_3) &= \frac{a_1 e^{-(s_1+s_2+s_3)\tau_1} L(s_1) L(s_2) L(s_3)}{T(s_1) T(s_2) T(s_3) T(s_1+s_2+s_3)} \\ T(s) &= 1 + a_1 \beta e^{-s(\tau_1+\tau_2)} L(s) \end{aligned}$$

For a two-tone test, assuming narrow frequency separation, the 3rd order intermodulation distortion ($IM3$) of the feedback network can be shown to be given by

$$IM_3 = \frac{3}{4} X_s^2 \left| \frac{A_3}{A_1} \right| \approx \frac{3}{4} X_s^2 \left| \frac{a_3}{a_1} \right| \frac{|L(j\omega)|^2}{|T(j\omega)|^3} \tag{3.6}$$

where $s_1 = s_3 = j\omega_1$, $s_2 = -j\omega_2$ and $\omega_1 \approx \omega_2 = \omega$.

The output of the feedforward path, Y_{out2}, is expressed by

$$Y_{out2} = B(s_1) \circ X_s(s_1) + B_2(s_1, s_2) \circ X_s(s_1) \circ X_s(s_2) + B_3(s_1, s_2, s_3) \circ X_s(s_1) \circ X_s(s_2) \circ X_s(s_3) \cdots \tag{3.7}$$

where,

$$\begin{aligned} B_1(s_1) &= b_1 \times R \times C \times P(s_1) E(s_1) \\ B_2(s_1, s_2) &= 0 \\ B_3(s_1, s_2, s_3) &= -b_1 \times R \times C \times \beta e^{-(s_1+s_2+s_3)\tau_2} \times P(s_1, s_2, s_3) \\ &\quad \times A_{f3}(s_1, s_2, s_3) + b_3 R^3 C P(s_1) P(s_2) P(s_3) \\ &\quad \times E(s_1) E(s_2) E(s_3) \\ E(s) &= \left(1 - \beta e^{-s\tau_2} A_1(s)\right) = \frac{1}{T(s)} \end{aligned}$$

For $P(s) = e^{-s\tau_{ff}}$, the total output Y_{total} is given by

$$Y_{total} = D(s_1) \circ X_s(s_1) + D_2(s_1, s_2) \circ X_s(s_1) \circ X_s(s_2) + D_3(s_1, s_2, s_3) \circ X_s(s_1) \circ X_s(s_2) \circ X_s(s_3) \cdots \tag{3.8}$$

where,

$$
\begin{aligned}
D_1(s_1) &= A_1(s_1) + B_1(s_1) \\
D_2(s_1, s_2) &= 0 \\
D_3(s_1, s_2, s_3) &= \left[1 - b_1 RC\beta e^{-(s_1+s_2+s_3)\left(\tau_2+\tau_{ff}\right)}\right] \\
&\quad \times A_3(s_1, s_2, s_3) + b_3 R^3 C e^{-(s_1+s_2+s_3)\tau_{ff}} \\
&\quad \times E(s_1) E(s_2) E(s_3)
\end{aligned}
$$

When the attenuator has a gain of $R = 1/(b_1\beta C) = 1/(a_1\beta C)$ and the phase shifter has a time delay that satisfies $(2\omega_1 - \omega_2)(\tau_2 + \tau_{ff}) = 2\pi N$; $N = 0, 1, 2, \cdots$, then the 3rd order distortion term that the main amplifier generates in $D_3(s_1, s_2, s_3)$ is canceled and $D_3(s_1, s_2, s_3)$ can be re-written as

$$
D_3(s_1, s_2, s_3) = \frac{b_3 e^{-(s_1+s_2+s_3)\tau_{ff}}}{a_1^3 \beta^3 C^2 T(s_1) T(s_2) T(s_3)} \tag{3.9}
$$

If the loop gain is assumed to be sufficiently large that $T(s) \approx a\beta e^{-s(\tau_1+\tau_2)} L(s)$, the $IM3$ of the feedback-feedforward network is given by

$$
IM3 = \frac{3}{4} X_s^2 \left|\frac{D_3}{D_1}\right| \approx \frac{3}{4} X_s^2 \left|\frac{b_3}{a_1}\right| \frac{1}{|T(j\omega)|^3 (a_1\beta C)^2} \tag{3.10}
$$

Therefore, using Eq. (3.6) and (3.10), the $IM3$ ratio of the feedback and the feedback-feedforward network can be expressed by

$$\frac{IM3|_{Feedback-Feedforward}}{IM3|_{Feedback}} = \frac{\frac{3}{4}X_s^2\left|\frac{b_3}{a_1}\right|\frac{1}{|T(j\omega)|^3(a_1\beta C)^2}}{\frac{3}{4}X_s^2\left|\frac{a_3}{a_1}\right|\frac{|L(j\omega)|^2}{|T(j\omega)|^3}}$$

$$\approx \left|\frac{b_3}{a_3}\right|\frac{1}{|T(j\omega)|^2 C^2} \quad (3.11)$$

As shown in Eq. (3.11), compared to the feedback system by itself, the feedback-feedforward system can improve linearity further, by a factor that is inversely dependent on the magnitude of the loop gain of the feedback network, and the coupling loss, and linearly proportional to the ratio of the nonlinearity of the auxiliary and main path amplifiers. The total gain of the feedforward path, $1/(\beta C)$, is mainly determined by the feedback network and the coupler, which are typically implemented using passive components. The phase shifter in the feedforward path would have similar characteristics.

When the two-tone frequencies are known, the time delay of the phase shifter is decided by the time delay of the feedback path τ_2 that might be mostly static unlike the time delay τ_1 in the main forward path. While a conventional feedforward technique requires stringent matching of the feedforward path and the main path that could have substantial time-dependent variation due to the main PA, the proposed technique needs matching of the feedforward path and passive networks that typically exhibit a small and predictable variation. To minimize the power consumption of the feedforward path, the auxiliary amplifier can be designed with lower linearity than the main amplifier. Thus b_3 will be larger than a_3 in practice.

Fig. 3.4 shows the achievable IM3 ratio for various loop gains and ratios of $|b_3| / |a_3|$. Using Eq. (3.11), for an assumed coupling loss of 10 dB which means C = 0.316, $|b_3| / |a_3| = 4$, which implies that the auxiliary amplifier has 6 dB lower OIP3 than the main amplifier, and a loop gain of 26 dB, the feedback-feedforward system can still achieve additional 20 dB $IM3$ improvement compared to the feedback system by itself.

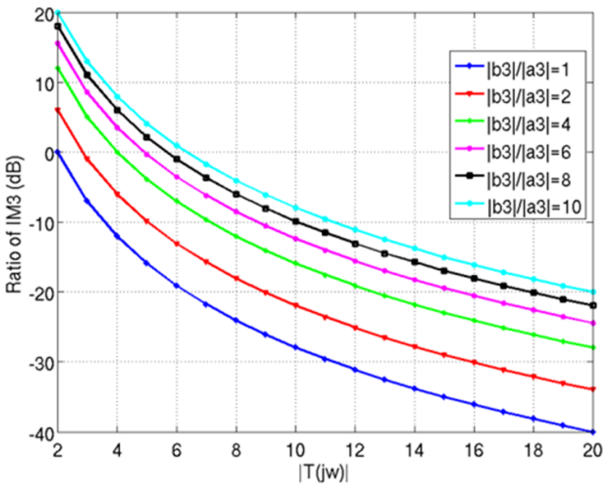

Figure 3.4: Dependence of IM3 ratio of feedback and feedback-feedforward systems on loop gain and the $|b_3| / |a_3|$ ratio

3.3.3 Further Discussion of Multi-Tone signals

When multi-tone signals are applied to the feedback-feedforward system, closed-loop linearity analysis based on Volterra series is excessively complicated. As such, in Section 3.4 we will rely on system simulations to demonstrate the utility of this approach. However, some key inferences can be drawn based on the above two-tone analysis. Based on the previous analy-

sis, when the time delay of the phase shifter in the feedforward path satisfies $(2\omega_1 - \omega_2)(\tau_2 + \tau_{ff}) = 2\pi N;\ N = 0, 1, 2, \cdots$, the feedforward path can cancel the distortion product of the main amplifier. It can be observed that the required time delay of the phase shifter $P(s)$, τ_{ff}, is not only decided by the time delay of the feedback path τ_2 but also decided by the frequency separation of the two-tones. Therefore, if multi-tone signals are employed in the system, each distortion signal generated by various combinations of two-tone signals would require a different time delay for cancellation. This implies a phase error of the feedforward path that is proportional to the signal and adjacent channel bandwidth.

If the time delay in the phase shifter has a negative value like $\tau_{ff} = -\tau_2$, a correct phase alignment would be available regardless of the two-tone frequencies. This is clearly impossible because of causality. However by employing a phase shifter between the feedback output and the output combiner, it is possible to achieve an equivalent phase relation.

Fig. 3.5 shows the modified feedback-feedforward model. In Fig. 3.5, a phase shifter is not added in the feedforward path but added after the feedback output. Now, the modified 3$^{\text{rd}}$ order Volterra Kernel of $Y_{total}(s)$ is given by

$$\begin{aligned} D(s_1, s_2, s_3) = &\left[e^{-(s_1+s_2+s_3)\tau_{fb}} - b_1 RC\beta e^{-(s_1+s_2+s_3)\tau_2}\right] \\ &\times A_3(s_1, s_2, s_3) + b_3 R^3 C E(s_1) E(s_2) E(s_3) \end{aligned} \tag{3.12}$$

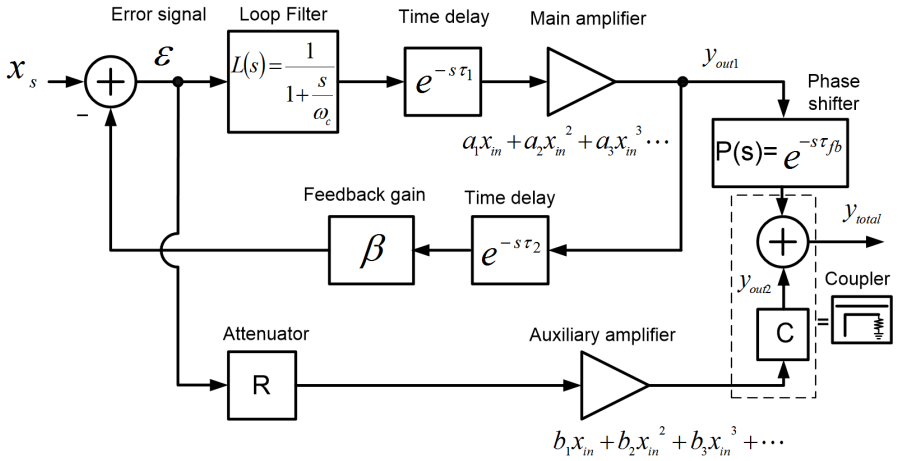

Figure 3.5: Modified feedback-feedforward model

When $R = 1/(b_1 R\beta)$ and $\tau_{fb} = \tau_2$, the distortion output of the main amplifier can be canceled correctly. Considering the signal strength of the PA output, it would be difficult to implement the active RF phase shifter after PA. However, a passive phase shifter using a transmission line on the PCB might be feasible, even though it would require substantial board area at RF bands. An LC network could also be used to provide the required delay if the bandwidth is relatively narrow, e.g., less than 5%. An integrated transmission line might be also possible, but would likely involved greater losses if used alone.

3.4 Architectural Simulation

3.4.1 Two-Tone Test

First, the concept of combined feedback-feedforward is explored using a feedback-feedforward amplifier without the use of up-and down-conversion

mixers. Fig. 3.6 shows the block diagram of the feedback-feedforward amplifier. The total amplification in the main path is assumed to be 80 dB with an OIP3 of 35 dBm. It is noted that if a Cartesian feedback-feedforward system was employed, the baseband stage would have contributed to the overall gain, which for the case of this model is assumed to be 65 dB. The total gain of the feedfoward path is 40 dB. This also assumes an equivalent baseband gain of 65 dB, and an auxiliary amplifier of 15 dB gain, with an OIP3 of 29 dBm. An attenuator of -34 dB (R) and a coupler with 6 dB loss (C) is assumed in the auxiliary path. The feedback path is assumed to have a loss of 40 dB. Therefore, the loop gain is 100 (40 dB), which equals the net linear gain of the feedforward path (80-34-6 dB). In this simulation, all blocks are operated at 1 GHz and for simplicity, the time delay of the feedback path is assumed to be canceled by the phase adjustment. Initially the feedforward path is assumed to have no phase and gain error, but those errors are examined in the following simulation.

Fig. 3.7 shows the output spectrum of an open-loop amplifier, a feedback amplifier and a feedback-feedforward amplifier. The feedback amplifier achieves about 38.8 dB IM3 improvement, which is nearly equal to the loop gain of 40 dB. The feedback-feedforward amplifier demonstrates an additional 55.9 dB improvement in IM3 compared to the feedback amplifier. This enhancement is consistent with Eq. (3.11).

Fig. 3.8 shows the impact of gain and phase errors in the feedforward path on IM3, relative to the Cartesian feedback loop. It can be observed that a

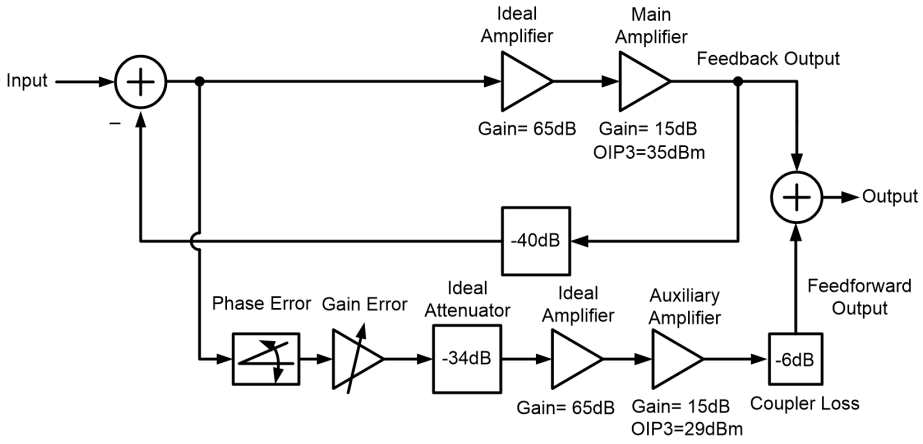

Figure 3.6: Block diagram of the feedback-feedforward transmitter for two-tone simulation

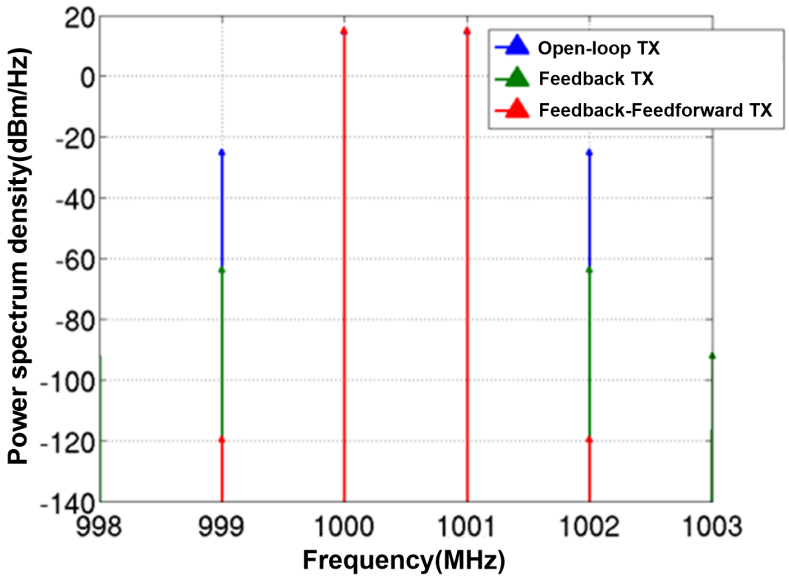

Figure 3.7: Output spectrum of open-loop transmitter, feedback transmitter, and feedback-feedforward transmitter

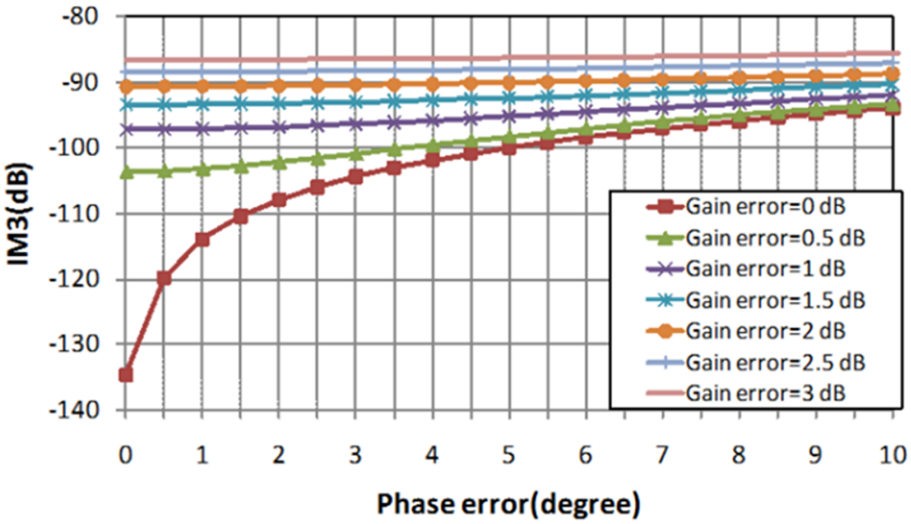

Figure 3.8: Impact of gain and phase errors in feedforward path on overall IM3

small gain error between the main path and the feedforward path could degrade the total linearity. It should be noted however, that the gain of the feedforward path is set by the attenuation in the feedback path (since $b_1RC = 1/\beta$ in Fig. 3.6). In a practical implementation, β is typically achieved through the use of passive elements, for example using resistive dividers with resistors of fixed ratio. Therefore, even though the matching requirement between the feedback path and the feedforward path is stringent, variation of the feedback path is not expected to be significant. This implies that a one-time calibration may be sufficient to align the phase and the gain of the feedforward path.

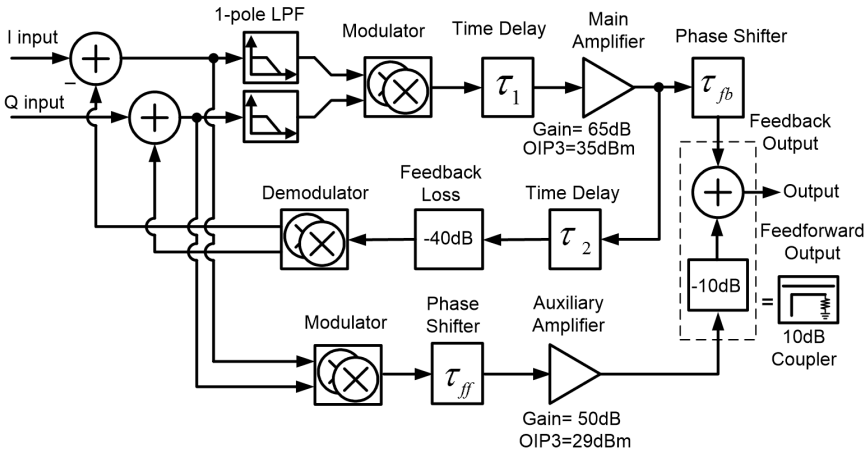

Figure 3.9: Block diagram of the Cartesian feedback-feedforward transmitter for system simulation.

3.4.2 Simulation Employing A WLAN 802.11b Signal

In this section, the results for system level simulation using modulation signal are reported. The system simulation is used to mainly explore the impact of the time delay in the feedback loop on the feedforward cancellation of the Cartesian feedback-feedforward transmitter.

Fig. 3.9 shows the block diagram of the Cartesian feedback-feedforward transmitter. Either a phase shifter (τ_{fb}) or a phase shifter (τ_{ff}) could be used for the phase adjustment between the feedback output and the feedforward output. The simulation uses a WLAN 802.11b signal with a data rate of 11 Mbps and QPSK modulation in CCK mode, as in [42]. A 1-pole low-pass loop filter with 3 dB frequency of 33 MHz (3× the signal bandwidth of 11 MHz) is employed. The main forward path and the feedforward path have separate ideal modulators that are used to combine I/Q signals. An ideal demodulator

is also used in the feedback path.

The main amplifier has an assumed gain of 65 dB and an OIP3 of 35 dBm. The feedback path has a loss of 40 dB. To combine the feedback signal and the feedforward signal, a 10 dB coupler is assumed at the output. The total feedforward gain including the coupling loss of 10 dB in the coupler should be the reciprocal value of the total feedback gain (40 dB). Thus the auxiliary amplifier needs a gain of 50 dB (40 dB +10 dB). The OIP3 of the auxiliary amplifier is assumed to be 6 dB lower than the OIP3 of the main amplifier. A time delay (τ_1) and a time delay (τ_2) can exist in the main forward path and the feedback path respectively. However, in the simulation, only a time delay (τ_2) was considered with $\tau_1 = 0$. This is the case because the time delay (τ_1) can be absorbed within the time delay (τ_2) in the linearity analysis of Cartesian feedback loop and the time delay (τ_2) can represent the total time delay of the feedback loop.

The phase adjustment of the feedback output and feedforward output is only related to a time delay (τ_2). Fig. 3.9 also shows two phase shifters that are represented by τ_{fb} and τ_{ff}. These phase shifters are used to adjust the time delay of the main feedback signal and the feedforward signal, respectively. These two signals are used in the feedforward cancellation to compensate the effect of τ_2.

Fig. 3.10 shows the output spectrum of open-loop transmitter, Cartesian feedback transmitter, and Cartesian feedback-feedforward transmitter with no time delay ($\tau_1 = \tau_2 = \tau_{fb} = \tau_{ff} = 0$ in Fig. 3.9). The center of the

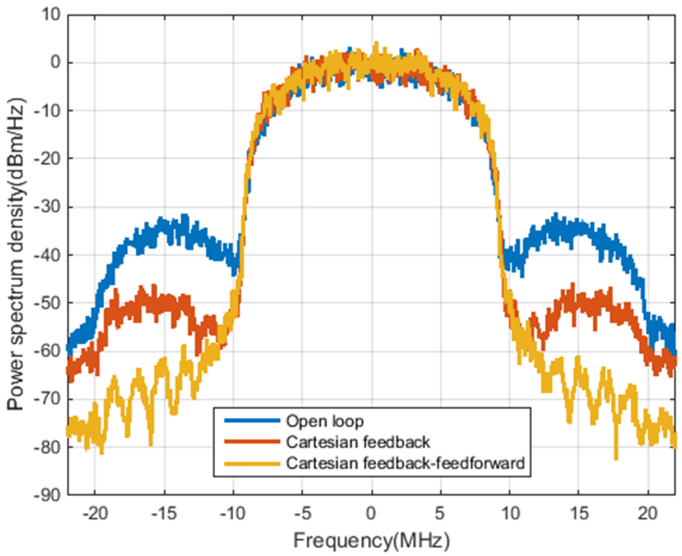

Figure 3.10: Output spectrum of open-loop transmitter, Cartesian feedback transmitter, and Cartesian feedback-feedforward transmitter with no time delay

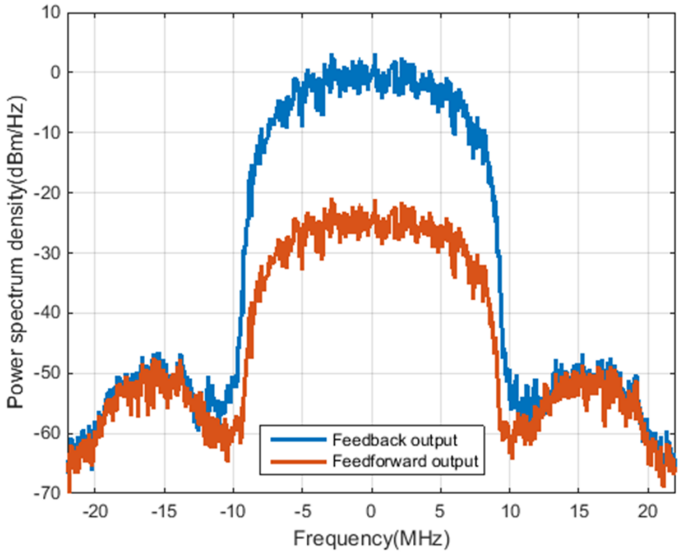

Figure 3.11: Spectrum of feedback output and feedforward output in Cartesian feedback-feedforward transmitter with no delay

X-axis corresponds to the LO frequency of 2.412 GHz and adjacent channel leakage (ACL) is observed at the 16.5 MHz offset [42]. As shown in Fig. 3.10, a transmitter with Cartesian feedback alone achieves 16 dB ACLR improvement compared to the open-loop transmitter. The Cartesian feedback-feedforward transmitter provides an additional 13.3 dB ACLR improvement compared to the Cartesian feedback in this simulation. Fig. 3.11 shows the spectrum of the feedback output and the feedforward output in Fig. 3.9. As expected, the two output spectra are seen to overlap in both adjacent channels. When these two signals are combined at the output, the distortion products of the main amplifier in both output signals are canceled and the total ACLR is significantly improved, as indicated in Fig. 3.10.

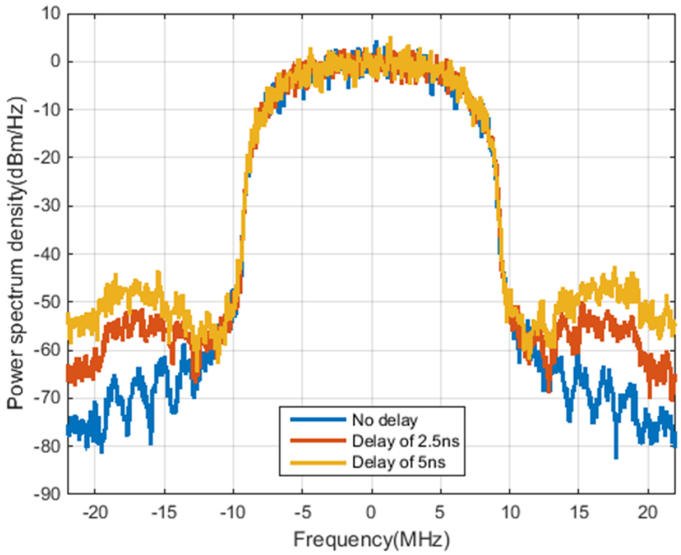

Figure 3.12: Output spectrum of Cartesian feedback-feedforward transmitter using the phase shifter (τ_{ff}) in the feedforward path for $\tau_2 = 0,\ 2.5\,ns$, and $5\,ns$

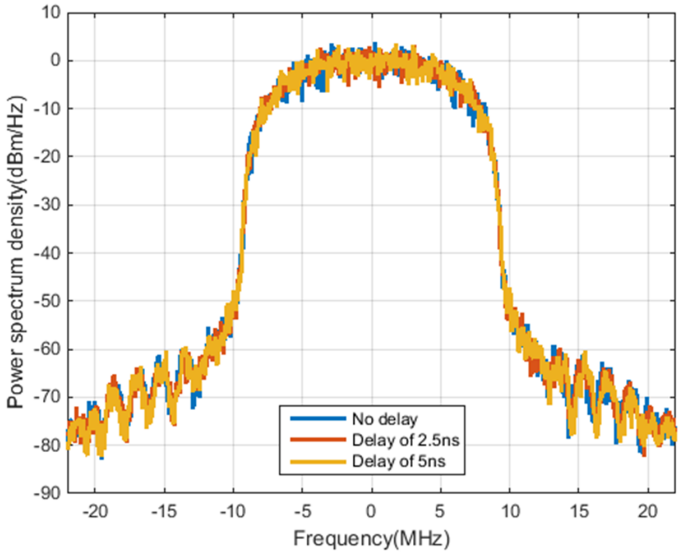

Figure 3.13: Output spectrum of Cartesian feedback feedforward transmitter using the phase shifter (τ_{fb}) after the feedback output for $\tau_2 = 0,\ 2.5\,ns$, and $5\,ns$

Fig. 3.12 and Fig. 3.13 show the output spectrum of the Cartesian feedback-feedforward transmitter when the time delay (τ_2) was included in the feedback path. As discussed in Section 3.3.3, there are two methods to compensate for the feedback time delay. One is to add a phase shifter into the feedforward path. In this scheme, the phase shifter (τ_{ff}) in the feedforward path needs to satisfy $(2\omega_1 - \omega_2)(\tau_2 + \tau_{ff}) \approx 2\pi f_{LO}(\tau_2 + \tau_{ff}) = 2\pi N; N = 0, 1, 2, \cdots$. An LO frequency, $f_{LO} = 2.412$ GHz was employed in this simulation.

Fig. 3.12 is the output spectrum of the transmitter, which adjusts the time delay of the phase shifter in the feedforward path, when the time delay τ_2 is assumed to be 0, 2.5 ns and 5 ns. In Fig. 3.12, the ACLR of

the transmitter with the time delay 5 ns is degraded by 15 dB, compared to the transmitter with no time delay. Therefore, when the phase shifter is employed in the feedforward path, the time delay in the feedback path can limit the achievable feedforward cancellation. Another way of compensating for the effect of the time delay (τ_2), is to apply a delay (τ_{fb}) after the feedback output that satisfies $\tau_{fb} = \tau_2$. Fig. 3.13 represents the output spectrum of the transmitter, which employs a phase shifter after the feedback output to adjust the time delay of the main feedback output signal. Unlike in Fig. 3.12, the output spectrum in Fig. 3.13 is almost unchanged regardless of the feedback time delay and the ACLR difference of the three outputs differs by about 1 dB. Based on this, we can conclude that it is useful to adjust the line delay after the Cartesian feedback loop, shown as τ_{fb}, to enhance the effectiveness of feedforward cancellation for broadband signals, when the feedback path may have a large time delay.

3.5 Conclusion

In this chapter, a Cartesian feedback-feedforward transmitter is proposed. The proposed approach is based on Cartesian feedback architecture but for a given loop bandwidth, it can achieve enhanced linearity performance by using an additional Cartesian feedforward path. The improvement in linearity is analyzed using a Volterra-series based approach, and verified by means of simulations using two-tone and modulated signal tests.

Although Cartesian feedback-feedforward can enhance the linearity

compared to use of Cartesian feedback alone, the linearity improvement provided by feedforward is still limited by the loop characteristics. For this reason, it is crucial to attain sufficient loop gain and bandwidth in the Cartesian loop. If the loop gain is degraded, the error signal that is applied to the input of the feedfoward path is increased, which causes the distortion product of the feedforward path to increase.

The time delay of the Cartesian feedback loop is critical, both for the stability and for the phase alignment. As discussed in Chapter 2, the time delay can degrade the phase margin significantly, which makes it challenging to achieve the required loop bandwidth. In addition, as Section 3.4.2 shows, when the time delay in the feedback is large, the delay adjustment in the feedforward path does not help in enhancing the linearity of Cartesian feedback-feedforward transmitter. For this case, a suitable time delay should be added at the feedback output.

Chapter 4

Transmitter Prototype IC

4.1 Introduction

In the previous chapter, a Cartesian feedback-feedforward transmitter was proposed for improving the linearity of Cartesian feedback. The proposed technique is expected to achieve additional improvement in linearity without increasing the loop bandwidth, which is the most challenging aspect in the design of a Cartesian loop. The proposed design showed significant ACLR improvement in a system simulation with high order modulation.

In this chapter[1], a prototype transmitter IC for Cartesian feedback-feedforward is presented, and the measurement results are also provided [44]. Section 4.2 describes the design of the prototype transmitter IC. After the structure of the prototype IC is illustrated, the functions of the main design blocks are explored. These include an I/Q up-conversion mixer, a driver amplifier, an I/Q down-conversion mixer, an error amplifier, an op-amp, LO circuits and an loop filter.

The proposed Cartesian feedback-feedforward architecture was imple-

[1]This chapter includes material from the publication : Sungmin Ock, Hyejeong Song and Ranjit Gharpurey, "A Cartesian Feedback-Feedfoward Transmitter IC in 130nm CMOS", *IEEE Custom Integrated Circuits Conference*, pp. 1 - 4, 2015, © 2015 IEEE.

mented using the prototype transmitter IC and several discrete components, which is explained in Section 4.3. The test set-up and key linearity results (e.g., ACLR comparison) are discussed in the same section.

4.2 Transmitter IC Implementation

The block diagram of the prototype transmitter is shown in Fig. 4.1. It has two transmit paths consisting of a main signal path and a feedforward path. The main signal path consists of an error amplifier, loop filter, up-conversion I/Q mixer and a PA driver amplifier. The error amplifier combines input quadrature signals and feedback signals with variable gain control. The loop filter is implemented using external resistors and capacitors on the board.

An off-chip PA is assumed in the main signal path and its output is coupled to the feedback path. Three LO signals are separately delivered by the frequency divider for accurate I/Q differential signals and the following LO buffer. Two off-chip phase shifters are assumed for adjusting the phases of the feedback LO signal and the auxiliary LO signal, respectively. The feedforward path is nearly identical except for the loop filter. An off-chip amplifier is also assumed for feedforward cancellation.

4.2.1 Up-Conversion Mixer

Fig. 4.2 shows the schematic of the I/Q up-conversion mixer. The designed mixer uses a transconductance amplifier to convert the input voltage signal, applied from an off-chip low pass filter (LPF), into a current signal

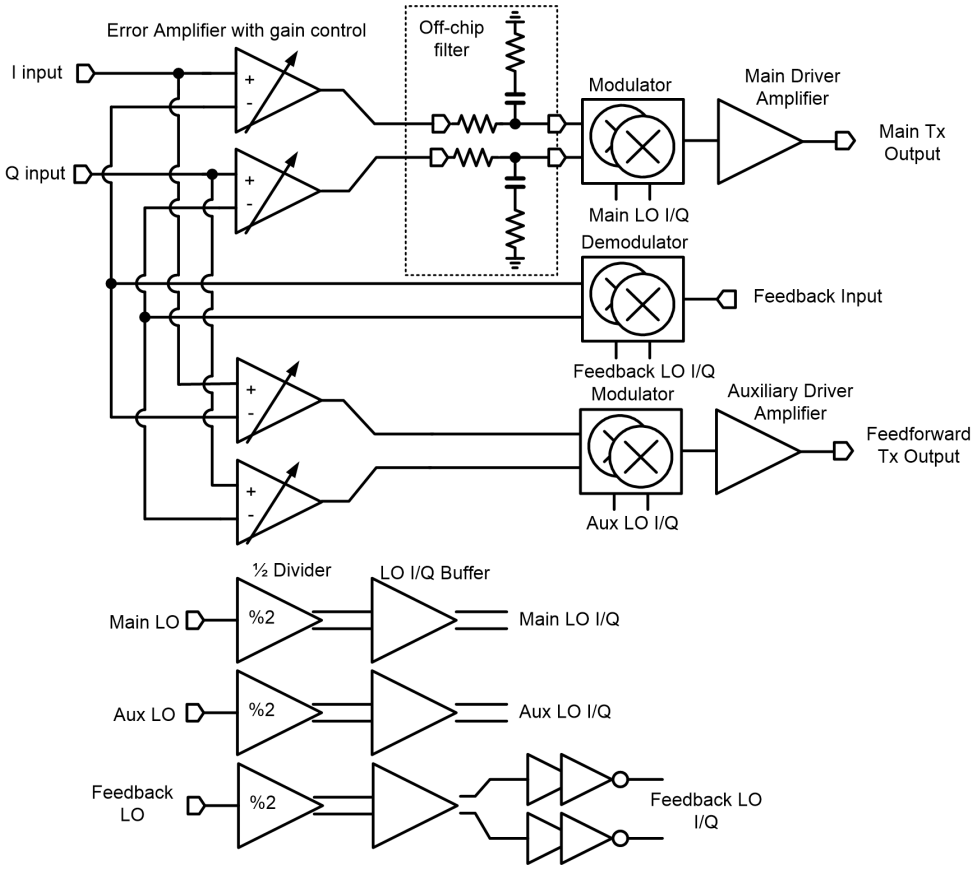

Figure 4.1: Block diagram of prototype transmitter IC with differential signaling

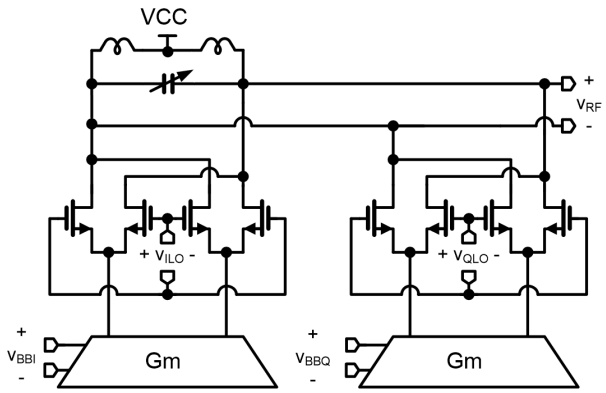

Figure 4.2: Simplified schematic of the up-conversion mixer

which is applied to a Gilbert active mixer [45]. Up-converted I/Q currents are combined at the mixer outputs and converted to voltage by an internal LC tank.

Fig. 4.3 represents the transconductance amplifier in the up-conversion mixer. Input pairs of the transconductance amplifier have source degeneration resistors and op-amps to regulate the source voltages of the pairs, which linearizes voltage to current conversion. Output current mirrors are implemented by cascode stacking with self-biasing for achieving high output impedance. Op-amps and bias currents on the differential pairs could generate substantial DC offset, which could increase I/Q impairment, as discussed in Chapter 2. Additional current sources for offset control are added in parallel with the bias currents.

The internal LC tank at the mixer output is critical not only for achieving a large voltage gain but also for preventing LO harmonic folding at the following driver amplifier [8]. Fig. 4.4 illustrates the harmonic folding phe-

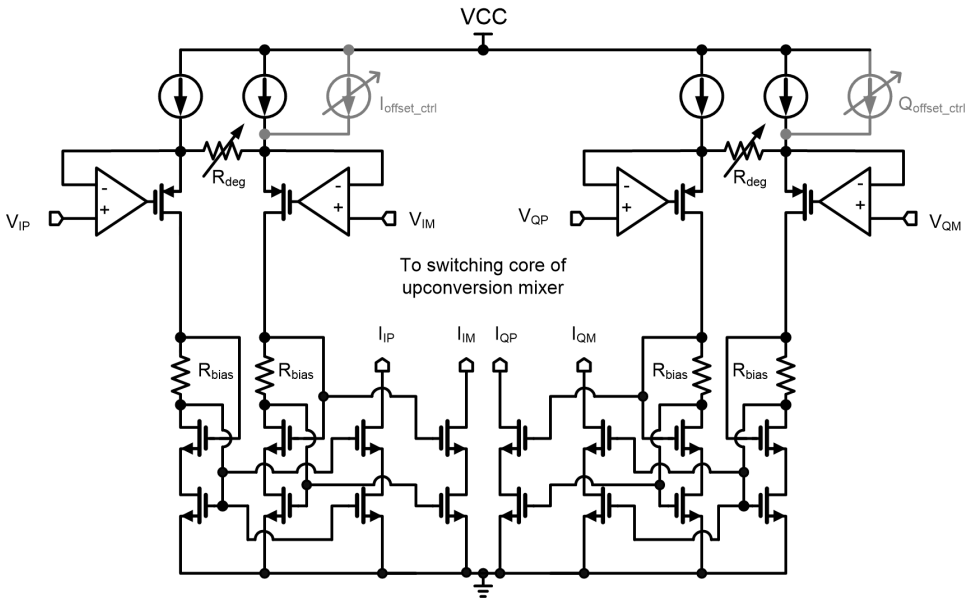

Figure 4.3: Simplified schematic of the input transconductance (gm) cell in an up-conversion mixer

nomenon which increases the IM3 level at the driver amplifier output. When a 3rd order LO harmonic tone is combined with 3rd order distortion of the driver amplifier, the LO harmonic term can generate additional IM3 terms both on the desired band and on the image band, which degrades the linearity of the driver amplifier significantly. Therefore, the mixer output needs to reject the high order LO harmonic tones, which is typically achieved by using an LC tank.

4.2.2 Driver Amplifier

Fig. 4.5 shows a schematic of the two stage PA driver amplifier. The first stage is a pseudo differential amplifier with internal LC tank for the

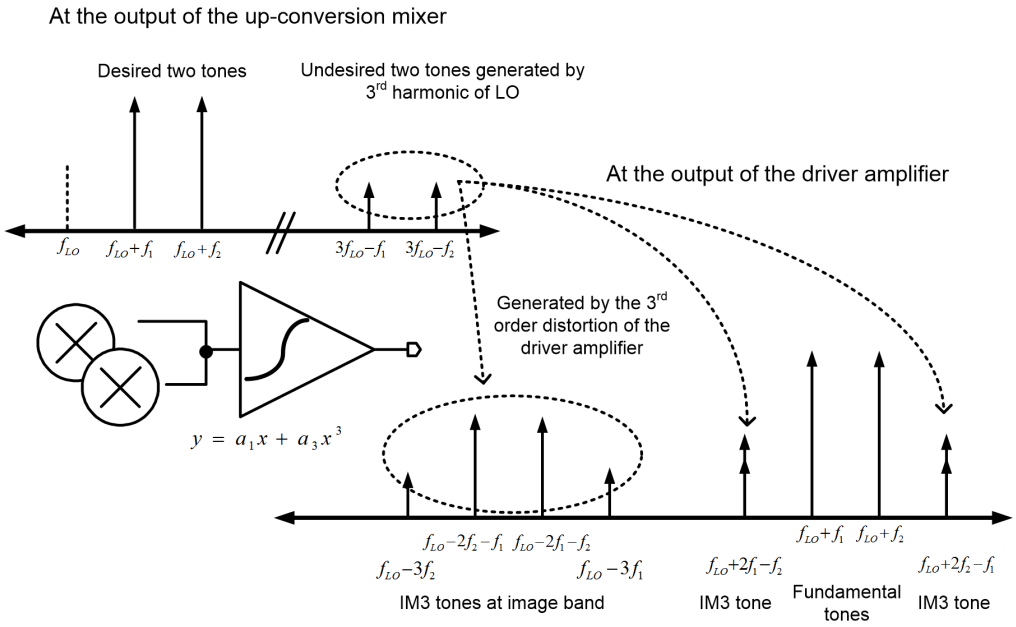

Figure 4.4: LO harmonic folding due to the nonlinearity of the driver amplifier [8, 9]

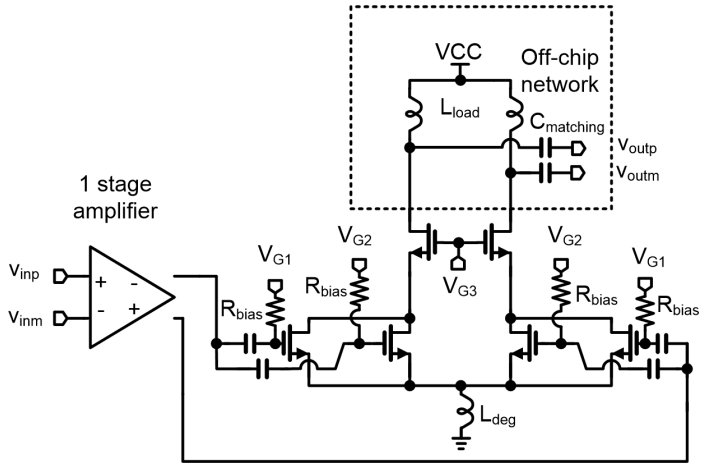

Figure 4.5: Simplified schematic of the driver amplifier

output load. The 2nd stage is a cascode amplifier with open drain outputs, which require careful off-chip output matching. The voltage swing of the 2nd stage output can be huge and the cascode device alleviates the reliability issue.

When the operating mode of an active MOS device transitions from weak inversion to strong inversion, the 3rd order distortion coefficient g_{m3} is modified from a negative to a positive value [46, 47]. Therefore, if two active devices are connected in parallel, with appropriate sizing, the g_{m3} of the two devices can be made equal in magnitude but opposite in polarity, to reduce the total g_{m3}. This is called the derivative superposition method for enhancing the small signal linearity [48, 49]. Fig. 4.6 shows typical g_{m3} plots of the two devices used in derivative superposition. If M1 is biased in the weak inversion region with low V_{GS}, and M2 is biased in the strong inversion region with high V_{GS}, the total third-order distortion coefficient (g_{m3}) can be significantly reduced. This approach is employed for linearizing the driver amplifier (Fig.

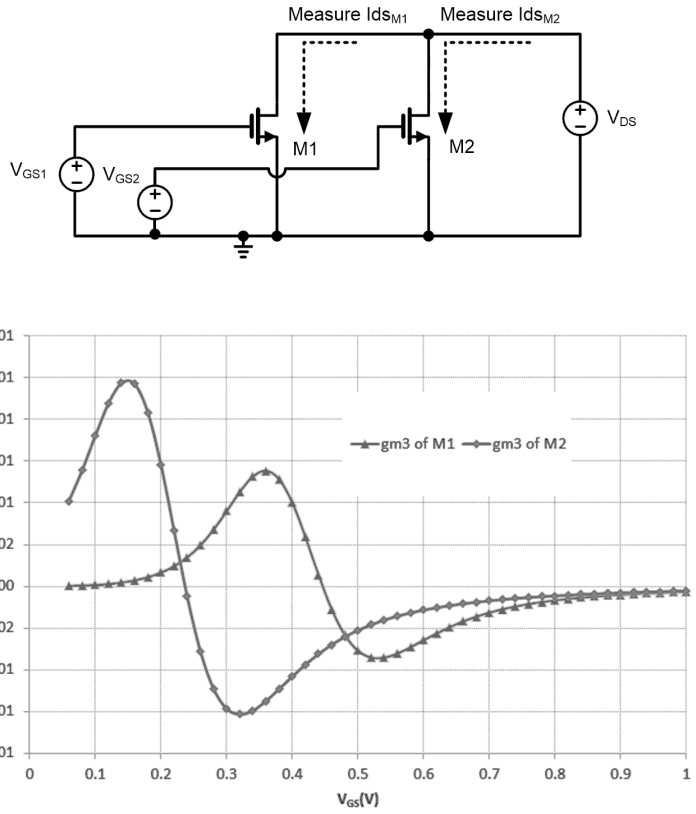

Figure 4.6: The g_{m3} characteristics of two devices in parallel used for derivative superposition

4.5).

4.2.3 Down-Conversion Mixer

Fig. 4.7 shows the schematic of the I/Q down-conversion mixer in the feedback path. As addressed in Chapter 2, the linearity of the feedback path is critical for the Cartesian feedback loop. To achieve high linearity, unlike an I/Q up-conversion mixer using an active switching stage, this I/Q mixer

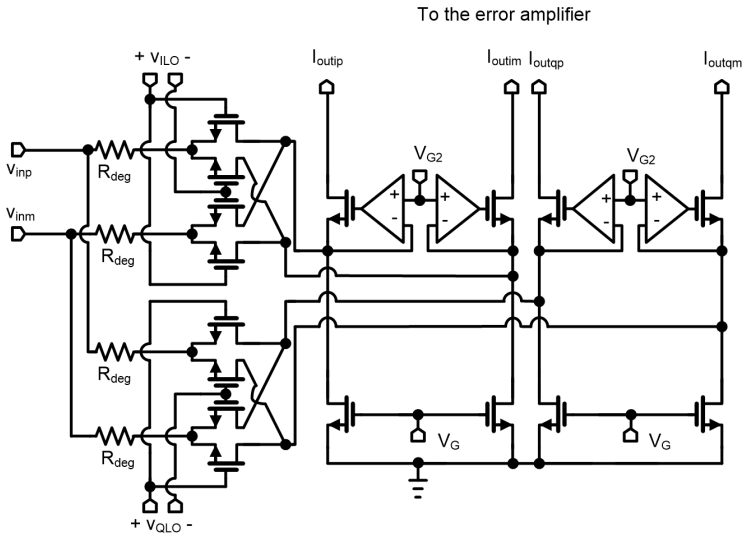

Figure 4.7: Simplified schematic of the I/Q down-conversion mixer in the feedback path

is composed of a passive switching stage and an output buffer [50]. Input series resistors in the mixer (R_{deg} in Fig. 4.7) help to improve input matching and achieve high linearity because they appear in series with the ON state switches, thereby reducing the nonlinearity of the overall on-state resistance.

The output buffer applies the down-converted signal current to the error amplifier. The cascode devices of the buffer are biased by associated op-amps that provide low input impedance for achieving a better virtual ground. When the passive mixer is operated, the input impedance of the output buffer can be observed at the mixer input at RF, with frequency translation. Fig. 4.8 shows impedance transformation in passive mixers [10]. When the buffer has an input impedance of $Z_{BB-IN}(\omega)$ and the I/Q passive mixer has the switch resistance of R_{SW-ON}, the input impedance of the passive mixer can

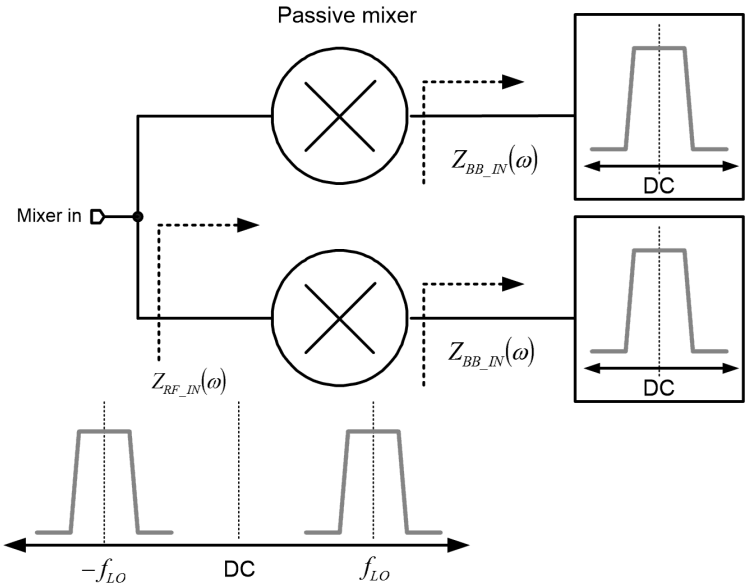

Figure 4.8: Impedance transformation from baseband to RF in a passive mixer [10]

be approximated by

$$\begin{aligned} Z_{RF-IN}(\omega) &\approx R_{SW-ON} + \\ &\frac{2}{\pi^2}\left(Z_{BB-IN}(\omega-\omega_{LO}) + Z_{BB-IN}(\omega+\omega_{LO})\right) \end{aligned} \tag{4.1}$$

Therefore, the baseband impedance is up-converted to $\pm\omega_{LO}$ frequency. If the baseband input impedance is assumed to have a low pass characteristic, the mixer input impedance can have a band pass response at RF.

This input impedance can help to attenuate various interferers in a receiver, and it has been proposed for avoiding a SAW filter in narrow band

receivers [51]. However, in the Cartesian feedback loop, the narrowband impedance response could also reduce the overall loop bandwidth, which should be avoided. In addition, in order to reduce the flicker noise and the DC current mismatch of the output buffer, the output buffer may require the use of large devices with substantial capacitance, which could degrade the pass bandwidth of the effective input impedance.

4.2.4 Error Amplifier

Fig. 4.9 shows a simplified schematic of the error amplifier. The error amplifier is composed of an input transconductance amplifier, a current-mode variable gain amplifier (VGA), and a current-to-voltage converter [52]. The input transconductance stage is similar to that of the up-conversion mixer except for the use of NMOS input pairs. The converted input current and the output current of the feedback mixer are fed to the current-mode VGA with opposite polarity. The current-mode VGA controls the amount of current entering the voltage converter.

4.2.5 Op-Amp

As previously described, the error amplifier, up-conversion mixer, and down-conversion mixer use op-amps to regulate source voltages of input differential pairs and cascode devices, which enable attenuation of the distortion terms generated in them. The op-amps employed need to meet requirements for 1) sufficient loop gain and bandwidth, 2) low DC offset, and 3) low power

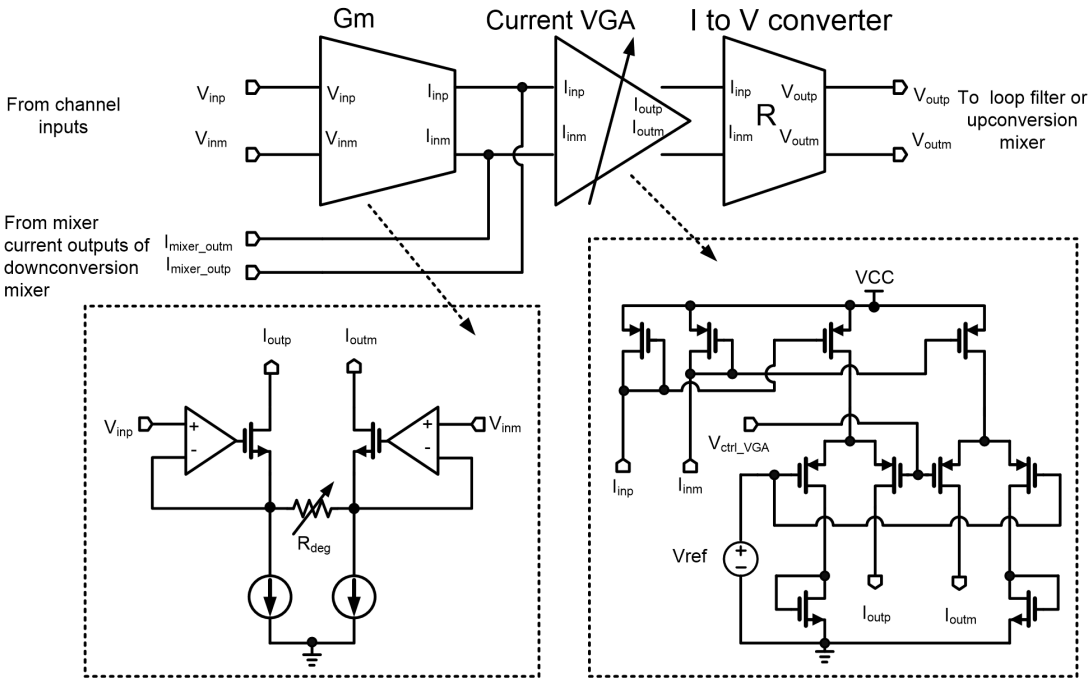

Figure 4.9: Simplified schematic of the error amplifier

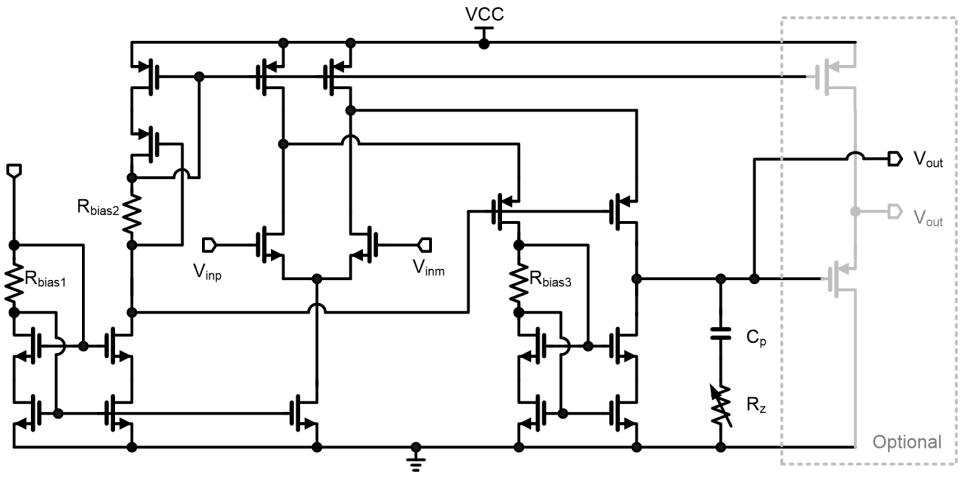

Figure 4.10: Simplified schematic of op-amp

consumption.

Fig. 4.10 is a schematic of an op-amp based on a conventional folded cascode design [53]. For NMOS input pairs, careful device sizing is required, that considers the input capacitance, the transconductance g_m, and the DC offset. Due to the use of a cascode current mirror and low power consumption, the output impedance of the mirror could become large. This could increase DC gain, but would also degrade the stability. To provide the desired stability, suitable output pole and zero, adjusted by C_p and R_z, respectively, are needed. In addition, for the op-amps that need to support high DC voltage at the output, a PMOS output buffer is added to level-shift the output to the required DC bias.

Fig. 4.11 illustrates a typical Bode plot of the op-amp when a load capacitance of 1 pF is assumed. The design has a DC gain of 52 dB and a

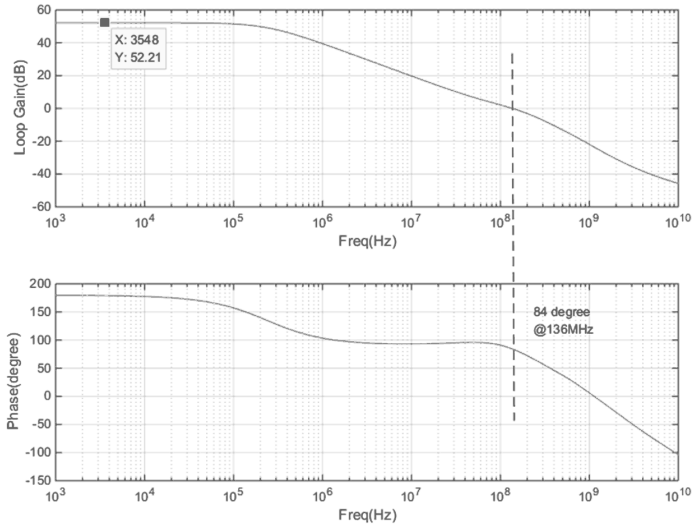

Figure 4.11: Bode plot of the op-amp

unity gain bandwidth of 136 MHz with sufficient phase margin of 84^o, and a gain margin of 23.5 dB, respectively. Each op-amp consumes a DC current of 450 μA, without including the DC current of the PMOS output buffer.

4.2.6 LO Divider and Buffers

The transmitter requires quadrature LO signals for each I/Q mixer but the prototype IC is driven by differential LO signals provided from off-chip baluns and signal generators. If the differential LO signals are well matched in terms of amplitude and phase, polyphase filters are good candidates for generating I/Q signals because they incur no power dissipation and exhibit acceptable phase accuracy [54]. However, due to mismatches caused by the package bonding and balun, the differential LO signals can have substantial

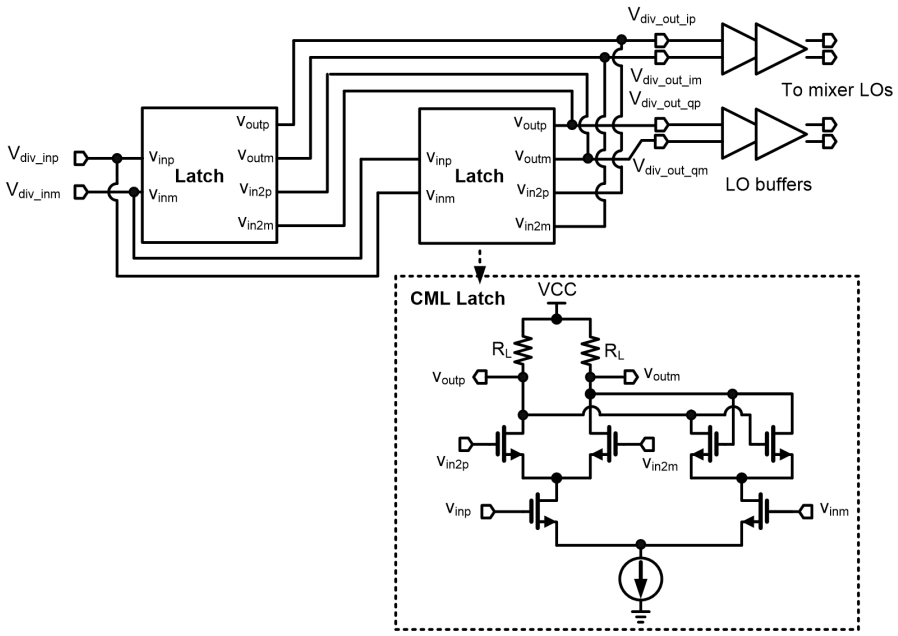

Figure 4.12: Simplified schematic of the LO divider and buffers

imbalance of amplitude and phase. For this reason, a frequency-divider was employed for quadrature signal generation.

Fig. 4.12 displays the designed LO divider and the following buffers. The frequency divider is implemented using two CML based latches with a negative feedback connection [55]. It can provide correct quadrature LO signals delivered to following LO buffers. It should be noted that the load resistance of R_L must be carefully chosen, considering the LO frequency, the effective impedance of cross-coupled pairs, and the DC voltage drop.

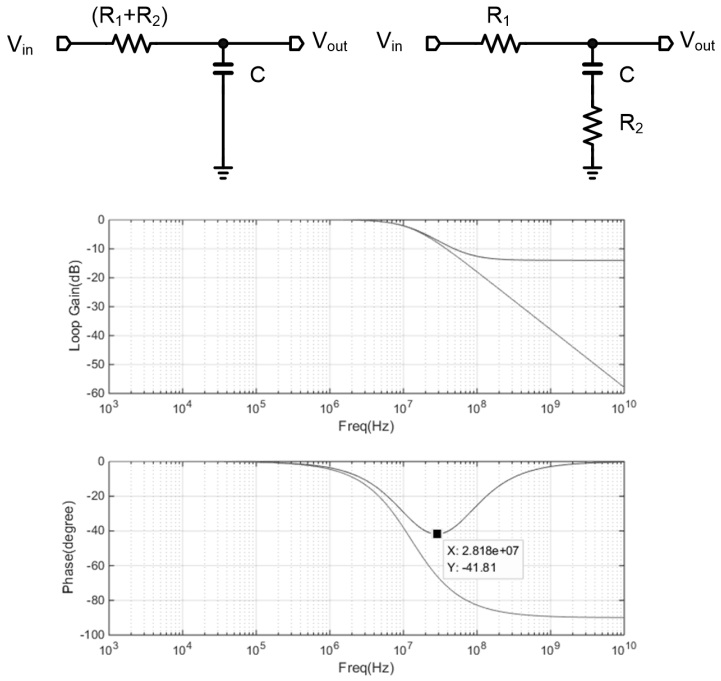

Figure 4.13: Comparison of 1-pole low pass filter and phase lag compensation filter

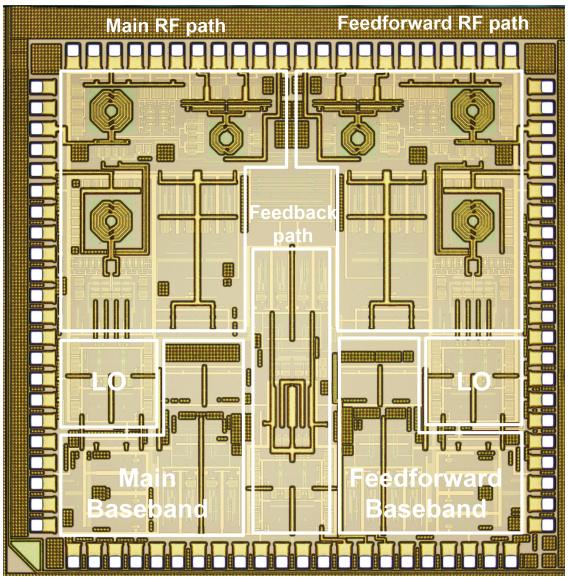

Figure 4.14: Die photo of the prototype transmitter

4.2.7 Loop Filter

The loop filter of the prototype transmitter IC was implemented using off-chip RC components. Fig. 4.13 shows a conventional 1-pole RC filter and the applied phase lag compensation filter [39]. The conventional 1-pole loop filter has the maximum phase lag of 90^o, but in the phase lag compensation filter, the maximum phase lag is determined by the spacing of the dominant pole of $1/\omega\left(R_1+R_2\right)C$ and the zero of $1/\omega R_2 C$. When the zero is getting close to the dominant pole, both the phase lag and the stop band attenuation will be reduced, which requires proper selection of the zero.

4.3 Measurement Setup and Results

4.3.1 Measurement Setup

The prototype transmitter was fabricated in a 0.13 μm CMOS technology and has a die area of 2.4 mm×2.4 mm (Fig. 4.14). The chip is packaged in a 10 mm×10 mm QFN package. The main path and the feedforward path are symmetrically placed in the layout. Table 4.1 shows a performance summary of the prototype IC. The signal path has power dissipation of 81.4 mW and the LO path consumes 51.7 mW.

Table 4.1: Prototype IC performance summary

Technology	0.13 μm CMOS
Die Area	2.4 mm ×2.4 mm
Package Type	10 mm×10 mm QFN package
RF Frequency	2400 MHz
LO Frequency	4800 MHz
Supply Voltage	1.1 V
Power Consumption	Baseband and feedback : 23.1mW
	Main and feedforward RF : 58.3 mW
	LO : 51.7 mW

Fig. 4.15 shows the measurement set-up for the Cartesian feedback-feedforward architecture. The test board is shown in Fig. 4.16. For the main transmit path, two discrete RF amplifiers are cascaded to deliver high power. These cascaded amplifiers have a small-signal gain of 26 dB and an output P1dB of 19 dBm. The feedforward path also uses discrete amplifiers with a total gain of 25 dB and a lower P1dB of 14.5 dBm. For the feedback path, a 20 dB coupler and a variable attenuator with maximum attenuation of 21.5 dB are employed.

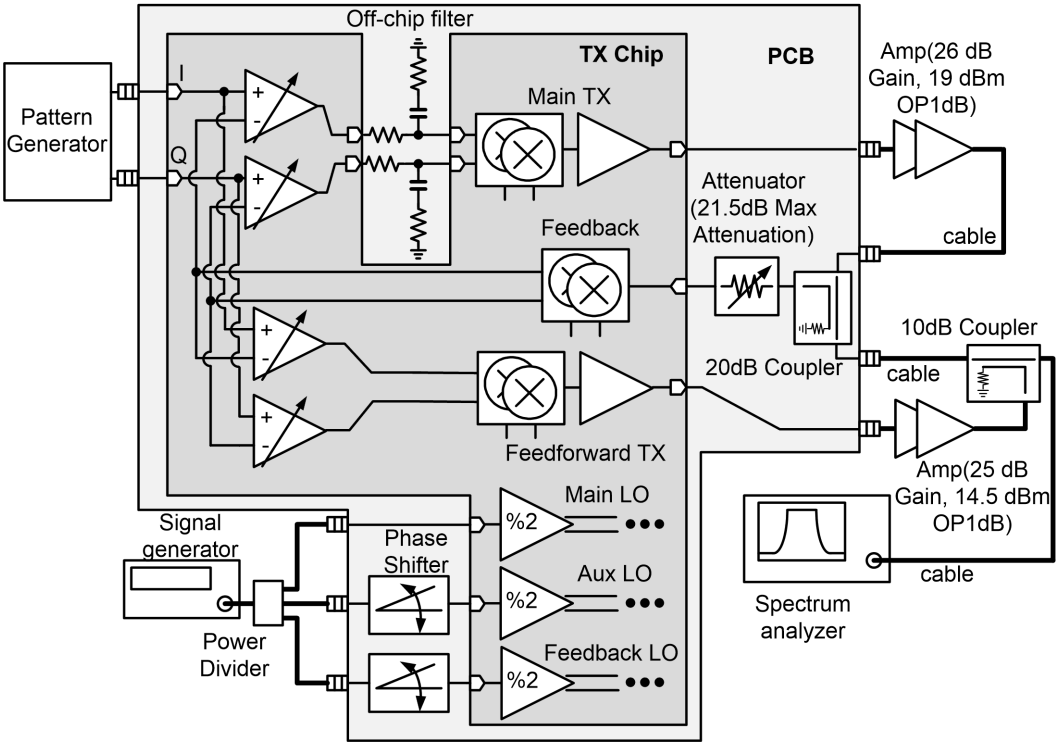

Figure 4.15: Measurement set-up (matching components are not included)

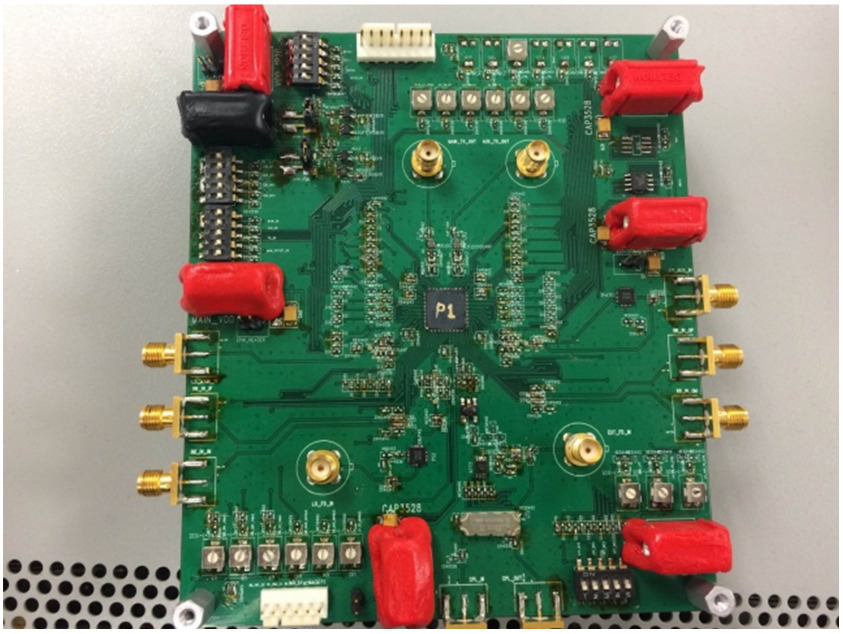

Figure 4.16: Test board

To combine the output of the feedback transmitter and the output of the feedforward path, a 10 dB passive coupler is employed, which attenuates the signal in the feedforward path by this amount. Three LO signals are derived by splitting the signal from an external source using a three-way power divider. Two discrete phase shifters are employed to control the phases of the LO signals in the feedback and auxiliary paths. The RF output frequency is 2.4 GHz. Output spectra of three transmitter structures are measured at the output of the 10 dB coupler. The discrete amplifiers, combined with the external passive components, including combiners and cables, increase the time delay of the Cartesian feedback loop, which limits the achievable bandwidth of the loop.

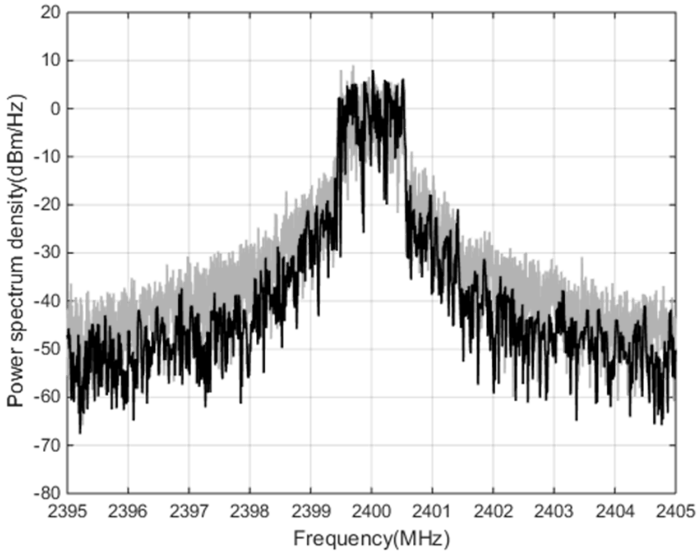

Figure 4.17: Measured output spectrum of open-loop transmitter and Cartesian feedback transmitter using 16-QAM LTE signal with 1.4 MHz bandwidth

4.3.2 Measurement Results

Fig. 4.17 shows the output spectrum of the open-loop transmitter and Cartesian feedback transmitter for a 16-QAM LTE signal with 1.4 MHz bandwidth. Fig. 4.18 shows the output spectrum of the open-loop transmitter and the Cartesian feedback-feedforward transmitter when the same signal is employed. Table 4.2 shows the channel power and ACLR results of three transmitter configurations. The open-loop transmitter has an output power of 17.3 dBm, while the Cartesian feedback and Cartesian feedback-feedforward transmitters have output power levels of 16.7 dBm and 16.6 dBm, respectively.

In the open-loop transmitter, the ACLR of the low-side adjacent channel is 23.8 dBc. The Cartesian feedback transmitter has an ACLR of 29.2

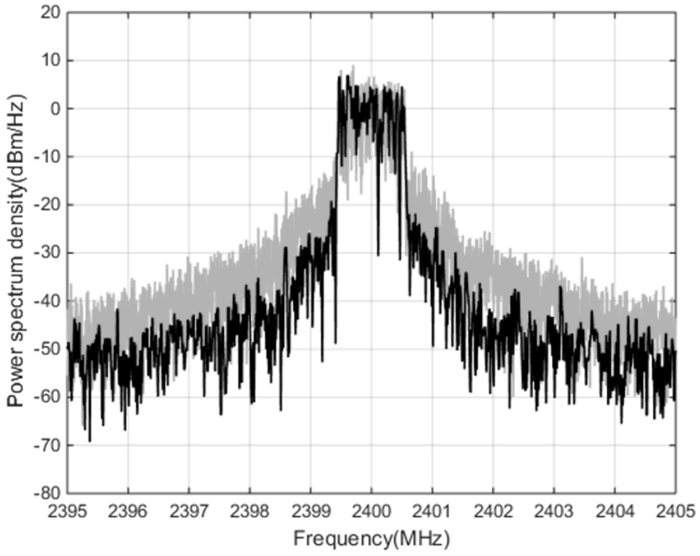

Figure 4.18: Measured output spectrum of open-loop transmitter and Cartesian feedback-feedforward transmitter using 16-QAM LTE signal with 1.4 MHz bandwidth

dBc and the Cartesian feedback-feedforward transmitter has an ACLR of 33.9 dBc. The ACLR of the high-side adjacent channel also has similar results for the three transmitter configurations. If the IM3 relation of two-tone signals is employed to compensate for the difference in the output channel power of the three transmitter configurations, the corrected ACLR of the open-loop transmitter and Cartesian feedback transmitter is approximately 25.2 dBc and 29.4 dBc, respectively, for an output power of 16.6 dBm. Under this assumption, while the Cartesian feedback transmitter achieves an ACLR improvement of 4.2 dB, the Cartesian feedback-feedforward transmitter shows nearly 8.7 dB ACLR improvement, compared to the open-loop configuration.

Table 4.2: Measured channel power and ACLR of three transmitters

Transmitter Architecture	Pout (dBm)	Low-side ACLR (dBc)	High-side ACLR (dBc)
Open-loop transmitter	17.3	23.8	24.1
Cartesian feedback transmitter	16.7	29.2	29.2
Cartesian feedback-feedforward transmitter	16.6	33.9	33.8

Table 4.3 compares this work with other Cartesian feedback transmitters previously reported for linearizing off-chip PAs. Even though the loop bandwidth of this proof-of-concept implementation is limited by the use of off-chip components and cables that were necessitated by the test set-up, it achieves better signal bandwidth with the exception of [5], which employed phase compensation in the loop. It should be noted that the goal of this design is to demonstrate linearity enhancement provided by Cartesian feedforward, when combined with Cartesian feedback. Thus, by combining the approach with techniques such as [5], linearity improvement can be further extended over a wider bandwidth.

4.4 Conclusion

In this chapter, a prototype transmitter IC using 0.13 μm CMOS technology is presented to demonstrate the Cartesian feedback-feedforward archi-

Table 4.3: Comparison with other Cartesian feedback transmitters using an off-chip PA

Reference	Freq. (MHz)	Pout (dBm)	BW (MHz)	ACLR Suppression (dB)
This work	2400	16.6	1.4	8.7
[7]	900	26.6	0.4	15
[5]	2000	15	10	8.2
[6]	2000	20	0.2	18

tecture. The transmitter IC consists of two forward paths, a feedback path, and quadrature LO circuits for all paths. In the forward path, the matching of I/Q channels is highly critical. The DC offset in the error amplifier and the input stage of the up-conversion mixer should also be minimized. In the feedback path, high linearity of the down-conversion mixer needs to be ensured. LO circuits are required to provide balanced quadrature signals for all signal paths.

From measurements, Cartesian feedback-feedforward architecture achieves a linearity improvement of 8.7 dB, compared to an open-loop transmitter configuration, for a 16-QAM LTE signal with 1.4 MHz bandwidth. In this work, achievable bandwidth performance of the transmitter is determined by the Cartesian feedback loop, while feedforward is employed to further enhance linearity over that achieved through the use of feedback alone. As mentioned in Section 4.3, if the proposed architecture is combined with bandwidth enhancement techniques in a Cartesian feedback loop, it could improve the linearity further over a wider signal bandwidth.

Chapter 5

Modified Cartesian Feedback-Feedforward Transmitters

5.1 Introduction

In the previous chapter, a Cartesian feedback-feedforward transmitter was demonstrated that employed a prototype transmitter IC and off-chip components. This combination exhibited significant ACLR improvements when a modulated signal with 1.4 MHz bandwidth was employed. The achievable linearity improvement is primarily governed by the loop gain of the Cartesian feedback. To improve the linearity of Cartesian feedback-feedforward, higher loop gain and wider bandwidth for the Cartesian feedback loop is required.

Although several approaches for increasing Cartesian loop bandwidth have been proposed, it continues to be a challenging problem, especially for linearization of external, off-chip PAs. Thus, methods for improving the linearity of Cartesian feedback-feedforward, without requiring improved loop parameters are highly desirable.

In this chapter, techniques for improving the linearity of Cartesian feedback-feedforward with a given loop bandwidth are explored. Section 5.2 briefly discusses the linearity limitations due to the loop gain and efficiency

requirement. Based on the discussion in Section 5.2, Section 5.3 explores two modified Cartesian feedback-feedforward architectures intended to enhance the linearity further.

5.2 Linearity and Efficiency Limitation

When an off-chip PA is linearized using Cartesian feedback, the feedback loop can have a large time delay that can restrict the loop gain-bandwidth (GBW) severely [5]. If the loop gain is reduced to improve the stability, the linearity improvement of the Cartesian feedback is also degraded. Moreover, the reduced loop gain can increase the error signal of the loop, implying that the Cartesian feedforward would be required to transmit a stronger signal that would lead to larger distortion accordingly.

If the feedforward path is highly linear, the distortion terms generated will be negligible. However the power consumption of the feedforward path should be minimized for overall power efficiency, which can limit the linearity of the feedforward path. For example, the main PA and the auxiliary amplifier are assumed to be Class A amplifiers with a drain power efficiency of 45% at OP1dB. Based on the power consumption of the prototype transmitter IC presented in Table 4.1 of Chapter 4, the main transmit path and the feedforward transmit path are assumed to consume $(23.1\,mW + 58.3\,mW)/2 = 40.7\,mW$ equally. In the open-loop condition, in order to transmit an average power of 23 dBm, the main PA is assumed to have OP1dB of 26 dBm with a 3 dB back-off. Then, the expected power efficiency of the open-loop transmitter

would be $199.5\,mW/\left(884.7\,mW + 40.7\,mW\right) \times 100\,\% = 21.6\,\%$.

With Cartesian feedback-feedforward, we assume that the main PA is required to meet OP1dB of 24 dBm with only 1 dB back-off. If the auxiliary amplifier has an OP1dB of 20 dBm (4 dB lower than OP1dB of the main PA), the overall power efficiency of Cartesian feedback-feedforward can be $199.5\,mW/\left(558.2\,mW + 2 \times 40.7\,mW + 222.2\,mW\right) \times 100\,\% = 23.2\,\%$. In this condition, Cartesian feedback-feedforward can enhance the power efficiency only by 1.6%. The enhancement is limited mainly due to the power dissipation of the feedforward path.

Therefore, it is critical to reduce the power consumption of the feedforward path, for improving the power efficiency with Cartesian feedback-feedforward. In the above example, if the auxiliary amplifier only needs to have an OP1dB of 14 dBm, which is 6 dB lower than OP1dB assumed above, the overall power efficiency could be 28.7 % which would be a significant improvement. However, when the power consumption of the feedforward path is reduced, its overall linearity will be also degraded. This could cause substantial distortion products from the large error signal.

Fig. 5.1 illustrates the block diagram of the architecture employed for system simulation to study the impact of the reduced loop gain and the degraded linearity of the auxiliary amplifier. Most of the blocks and signals are the same as those used in the system simulation shown in Fig. 3.9 of Chapter 3. In the feedback loop, the gain of the main amplifier is reduced from 65 dB to 62 dB which decreases the inband loop gain by 3 dB. Then, the 3 dB

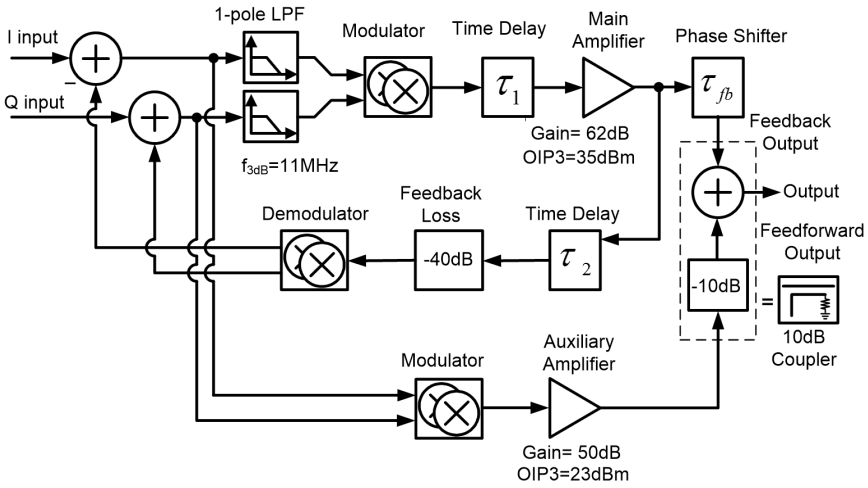

Figure 5.1: Block diagram of Cartesian feedback-feedforward transmitter for system simulation.

frequency of the loop filter is also decreased from 33 MHz to 11 MHz, which diminishes the loop gain in the adjacent bands. In the feedforward path, the OIP3 of the auxiliary amplifier is reduced from 29 dBm to 23 dBm. While the time delay (τ_1) in the main forward path is assumed to be zero, the time delay (τ_2) in the feedback path is assumed to be 2.5 ns. Then, the time delay (τ_{fb}) of the phase shifter at the Cartesian feedback output is set to be 2.5 ns to satisfy $\tau_{fb} = \tau_2$.

Fig. 5.2 shows the output spectrum of the open-loop, Cartesian feedback, and Cartesian feedback-feedforward transmitters. As described in Chapter 3, the center frequency of the X-axis corresponds to 2.412 GHz. The Cartesian feedback transmitter improves ACLR by 9.4 dB, compared to the open-loop transmitter. The Cartesian feedback-feedforward transmitter achieves only 4 dB ACLR improvement over the Cartesian feedback alone. Compared

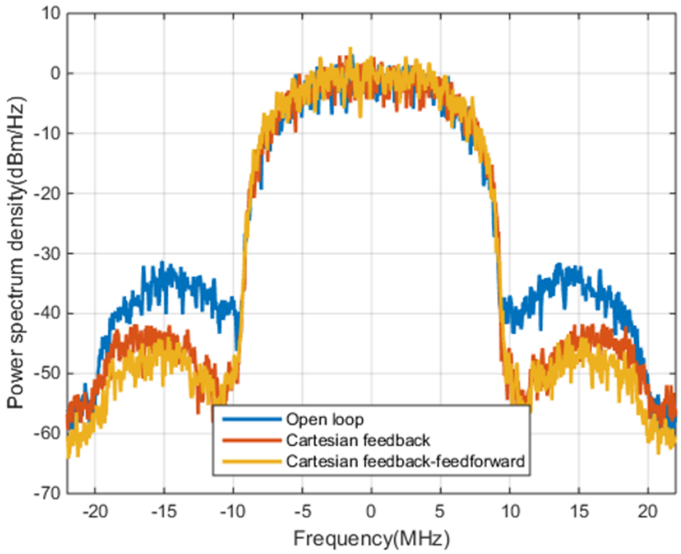

Figure 5.2: Output spectrum of the open-loop transmitter, Cartesian feedback transmitter, and Cartesian feedback-feedforward transmitter

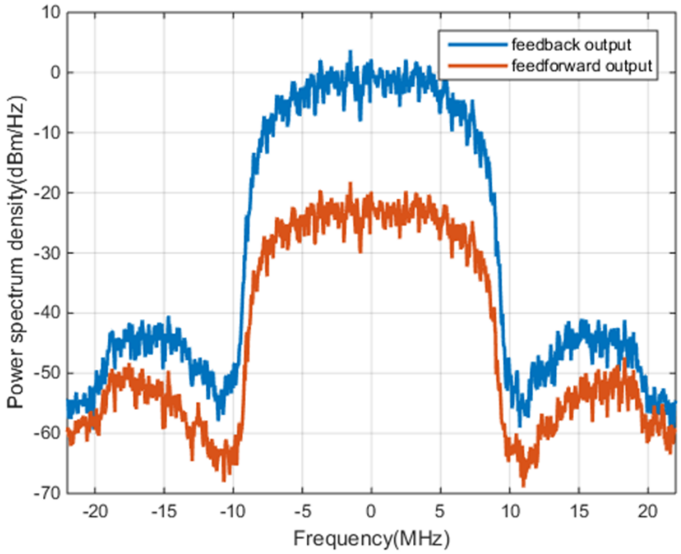

Figure 5.3: Spectrum of feedback output and feedforward output of the Cartesian feedback-feedforward transmitter

with Fig. 3.10 of Chapter 3, the ACLR improvement of both Cartesian feedback transmitter and Cartesian feedback-feedforward transmitter in Fig. 5.2 are significantly degraded due to the smaller loop gain and the relatively poor linearity of an auxiliary amplifier.

Fig. 5.3 exhibits the spectrum of the feedback output and the feedforward output respectively. Compared to Fig. 3.11, the feedforward output signal at the main channel is increased due to the 3 dB reduction of the in-band loop gain. In addition, the feedforward output spectrum typically needs to overlap with the feedback output spectrum on both adjacent channel bands for cancellation, but the feedforward output spectrum in Fig. 5.3 shows smaller ACL than does the feedback output spectrum. This mismatch implies that the distortion products of the feedforward path cannot cancel the distortion signal produced by the Cartesian feedback. This is because the increased error signal and the lower linearity of the auxiliary amplifier generate more distortion products. Therefore, the additional distortion terms of the feedforward chain increase the distortion mismatch between the feedforward and feedback outputs. This deteriorates the improvement provided by feedforward cancellation.

5.3 Modified Cartesian Feedback-Feedforward Transmitters

Two techniques are explored below to enhance the linearity of the Cartesian feedback-feedforward transmitter for a given set of loop parameters.

5.3.1 Cartesian Feedback-Feedforward with Signal-Bleed Path

This technique for RF feedback-feedforward was explored previously in [31, 32] and it can also be applied to Cartesian feedback-feedforward. Fig. 5.4 shows the block diagram of the modified Cartesian feedback-feedforward transmitter with a signal-bleed path. When a proper signal is added to the Cartesian feedback through the bleed path, the error signal does not need to support the entire signal for the forward path, which reduces the error signal.

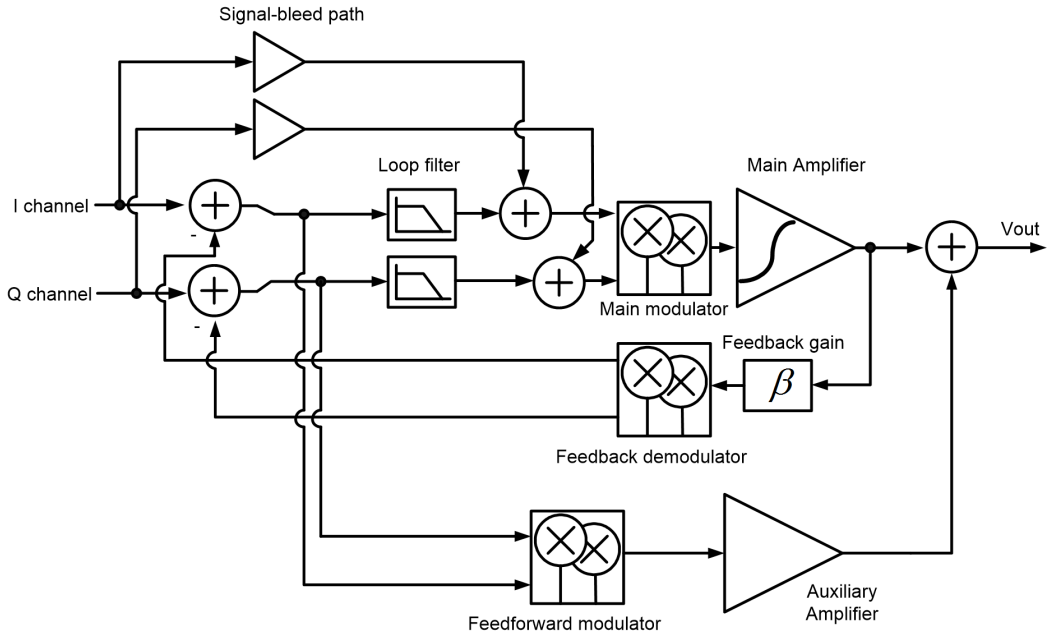

Figure 5.4: Modified Cartesian feedback-feedforward with a signal-bleed path

Fig. 5.5 shows the simplified model of feedback-feedforward system with a signal-bleed path. The model looks similar to Fig. 3.2, but Fig. 5.5 also considers several time delays, corresponding phase shifters, a loop filter, and a signal-bleed path.

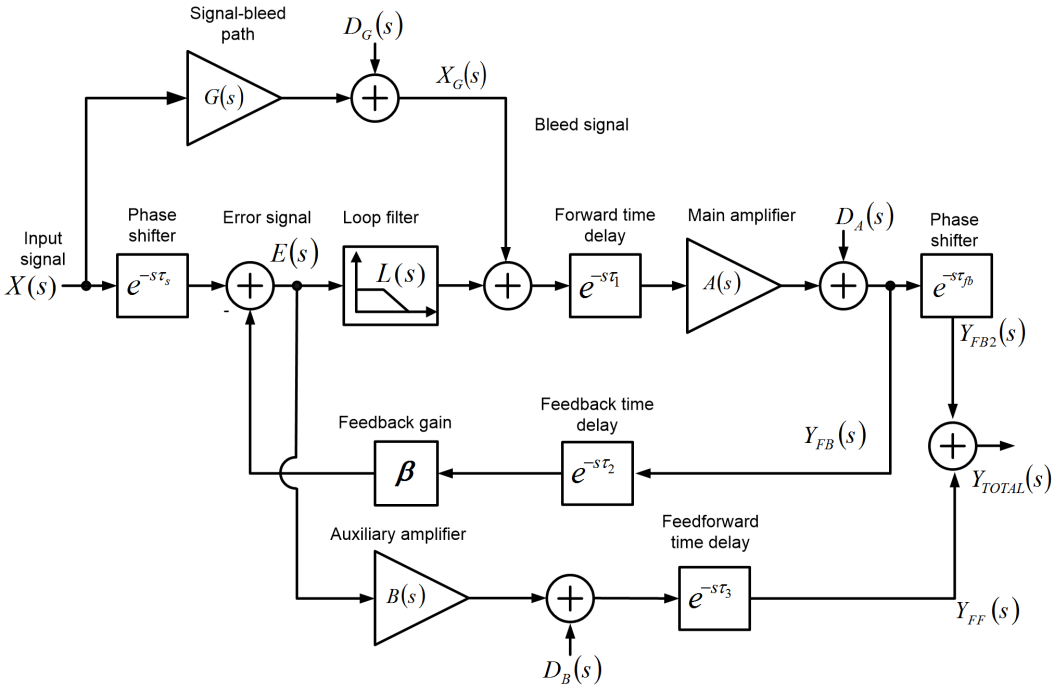

Figure 5.5: Feedback-feedforward model with the signal-bleed path

In Fig. 5.5, $A(s)$ and $B(s)$ represent transfer functions of the main amplifier and the auxiliary feedforward amplifier, respectively. $G(s)$ symbolizes the transfer function of the new signal-bleed path. The distortion products arising from the three paths can be represented as additive errors $D_A(s)$, $D_B(s)$, and $D_G(s)$. Here, β denotes the linear and memoryless feedback gain.

Unlike Fig. 3.2, here, all three paths are assumed to have time delays, that are given by τ_1, τ_2, and τ_3, respectively. Two phase shifters ($e^{-s\tau_s}$ and $e^{-s\tau_{fb}}$) are added at the feedback input and the feedback output, to adjust the overall phase mismatch. The loop filter is separately denoted as $L(s)$.

The feedback output $Y_{FB}(s)$ and the error signal $E(s)$ are given by

$$\begin{aligned} Y_{FB}(s) &= \frac{A(s)\,e^{-s\tau_1}\left[L(s)\,e^{-s\tau_s}+G(s)\right]}{1+L(s)\,A(s)\,\beta e^{-s(\tau_1+\tau_2)}}X(s) \\ &+ \frac{D_A(s)+D_G(s)\,A(s)\,e^{-s\tau_1}}{1+L(s)\,A(s)\,\beta e^{-s(\tau_1+\tau_2)}} \end{aligned} \tag{5.1}$$

$$\begin{aligned} E(s) &= \frac{e^{-s\tau_s}-G(s)\,A(s)\,\beta e^{-s(\tau_1+\tau_2)}}{1+L(s)\,A(s)\,\beta e^{-s(\tau_1+\tau_2)}}X(s) \\ &- \frac{\beta e^{-s\tau_2}\left[D_A(s)+D_G(s)\,A(s)\,e^{-s\tau_1}\right]}{1+L(s)\,A(s)\,\beta e^{-s(\tau_1+\tau_2)}} \end{aligned} \tag{5.2}$$

From Eq. (5.2), if the phase shifter at the feedback input has the time delay of $\tau_s = (\tau_1+\tau_2)$ and the signal-bleed gain $G(s)$ is the inverse

of the loop gain as $G(s) = 1/A(s)\beta$, then the error signal $E(s)$ has only distortion terms and the input signal for the main amplifier $A(s)$ is provided by the signal-bleed path. In addition, typically $A(s)\beta \ll 1$ and $G(s)$ would be provided by the passive type attenuators that can be assumed to have no distortion ($D_G(s) \approx 0$). Therefore, the error signal $E(s)$ can be expressed as

$$E(s) = \frac{-\beta e^{-s\tau_2}}{1 + L(s)A(s)\beta e^{-s(\tau_1+\tau_2)}} D_A(s) \tag{5.3}$$

When the error signal is applied to the input of the feedforward path, the feedforward output $Y_{FF}(s)$, and the phase shifted feedback output $Y_{FB2}(s)$ are given by

$$Y_{FF}(s) = \frac{-B(s)\beta e^{-s(\tau_2+\tau_3)}}{1 + L(s)A(s)\beta e^{-s(\tau_1+\tau_2)}} D_A(s) + D_B(s)e^{-s\tau_3} \tag{5.4}$$

$$\begin{aligned} Y_{FB2}(s) &= \frac{A(s)e^{-s(\tau_1+\tau_{fb})}\left[L(s)e^{-s\tau_s} + G(s)\right]}{1 + L(s)A(s)\beta e^{-s(\tau_1+\tau_2)}} X(s) \\ &+ \frac{D_A(s)e^{-s\tau_{fb}}}{1 + L(s)A(s)\beta e^{-s(\tau_1+\tau_2)}} \end{aligned} \tag{5.5}$$

Then, total output $Y_{TOTAL}(s)$ is given by

$$
\begin{aligned}
Y_{TOTAL}(s) &= Y_{FB2}(s) + Y_{FF}(s) \\
&= \frac{A(s)\, e^{-s\left(\tau_1+\tau_{fb}\right)} \left[L(s)\, e^{-s\tau_s} + G(s)\right]}{1 + L(s)\, A(s)\, \beta e^{-s(\tau_1+\tau_2)}} X(s) \\
&+ \frac{e^{-s\tau_{fb}} - B(s)\, \beta e^{-s(\tau_2+\tau_3)}}{1 + L(s)\, A(s)\, \beta e^{-s(\tau_1+\tau_2)}} D_A(s) \\
&+ D_B(s)\, e^{-s\tau_3}
\end{aligned}
\tag{5.6}
$$

In the total output signal $Y_{TOTAL}(s)$, when the feedforward amplifier $B(s)$ has a gain of $1/\beta$ and the phase shifter at the feedback output has a time delay of $\tau_{fb} = (\tau_2 + \tau_3)$, the distortion term of $D_A(s)$ is canceled and the distortion term of $D_B(s)$ generated by the auxiliary amplifier is the only remaining distortion term. Now the error signal $E(s)$ only contains the distortion output of the main amplifier, while the resulting distortion output of the feedforward amplifier $D_B(s)$ can be made very small. In addition, the total output signal $Y_{TOTAL}(s)$ can be simplified as

$$
\begin{aligned}
Y_{TOTAL}(s) &= \frac{A(s)\, e^{-s(\tau_1+\tau_2+\tau_3)} \left[L(s)\, e^{-s(\tau_1+\tau_2)} + \frac{1}{A(s)\beta}\right]}{1 + L(s)\, A(s)\, \beta e^{-s(\tau_1+\tau_2)}} X(s) \\
&+ D_B(s)\, e^{-s\tau_3}
\end{aligned}
\tag{5.7}
$$

Fig. 5.6 represents the system simulation of the Cartesian feedback-feedforward transmitter with the signal-bleed path. Components and time

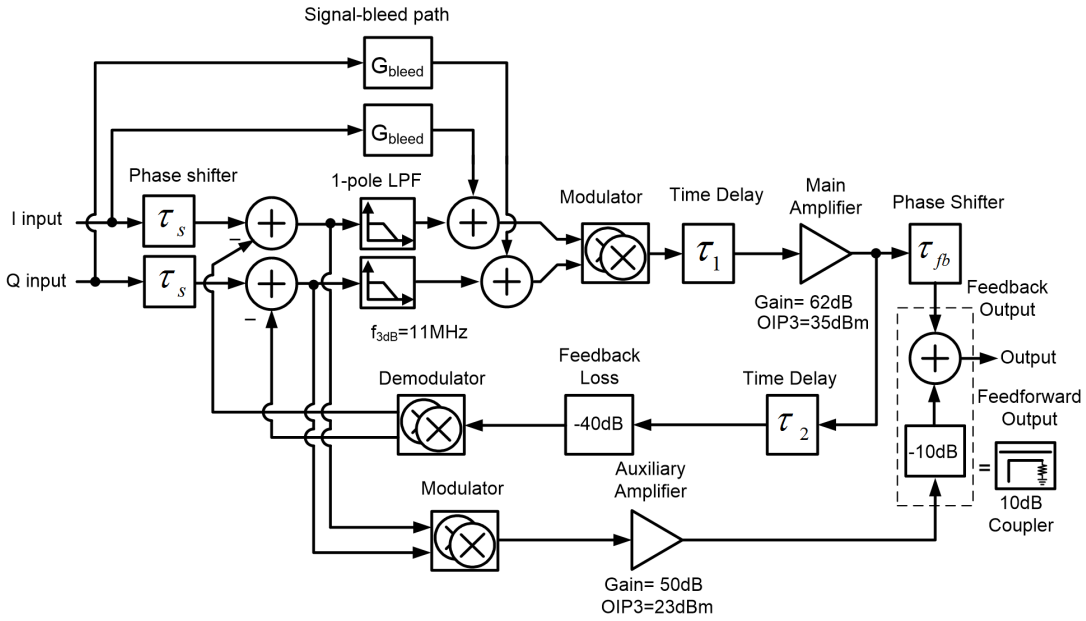

Figure 5.6: Block diagram of Cartesian feedback-feedforward transmitter with the signal-bleed path for system simulation

delays are the same as in the prior simulation shown in Fig. 5.1, except for the addition of the signal-bleed path and the additional phase shifter (τ_s). Based on the above analysis, the equivalent time delay (τ_s) of the phase shifter at the baseband input should be matched to the overall loop delay, $(\tau_1 + \tau_2) = 2.5ns$.

Fig. 5.7 displays the output spectrum of the two Cartesian feedback-feedforward transmitters with and without a signal-bleed path. The proposed architecture with a bleed path achieves a further 16 dB ACLR enhancement, compared with a normal Cartesian feedback-feedforward transmitter. Fig. 5.8 represents output spectrum of the feedback path and the feedforward path, in the Cartesian feedback-feedforward with the signal-bleed path. The feedfor-

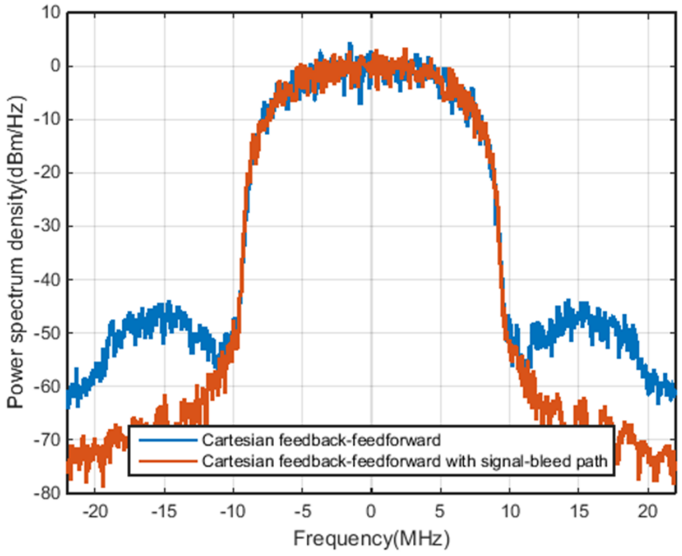

Figure 5.7: Output spectrum of Cartesian feedback-feedforward transmitter with/without the signal-bleed path

ward output spectrum power level in the main channel band can be seen to be as small as that in adjacent channel bands, indicating that the remaining inband signal of the feedforward output would be mostly distortion terms and noise.

Although this approach can greatly improve linearity without the need for enhanced loop bandwidth, it appears to pose an implementation challenge for $G(s)$. From above equations, $G(s)$ needs to equal the inverse of loop gain $1/A(s)\beta$ regardless of its variation. While the feedback gain β is the passive component with small variation, the main amplifier $A(s)$ can vary significantly due to PVT and the output power level. Therefore, in order to make $G(s)$ equal $1/A(s)\beta$ over time, a digitally assisted adaptation mechanism would be

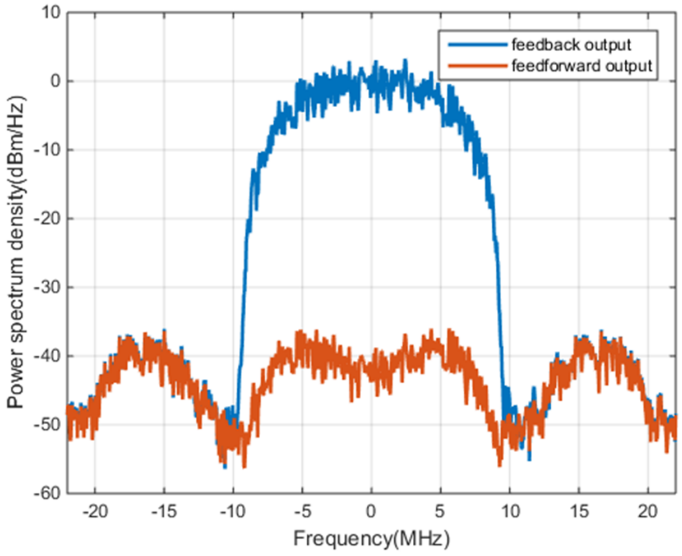

Figure 5.8: Spectrum of feedback output and feedforward output in Cartesian feedback-feedforward transmitter with the signal-bleed path

needed.

Fig. 5.9 illustrates the proposed Cartesian feedback-feedforward architecture with a digital signal-bleed generator. The digital signal-bleed generator detects the error signal and provides a suitable bleed signal into the main forward path. This implementation looks similar to Fig. 2.18 [7], but while the bleed signal in [7] includes a predistortion signal, the bleed signal of the proposed digital signal-bleed generator is the attenuated inband signal, and the distortion signal for compensation is mainly provided by the Cartesian feedforward path.

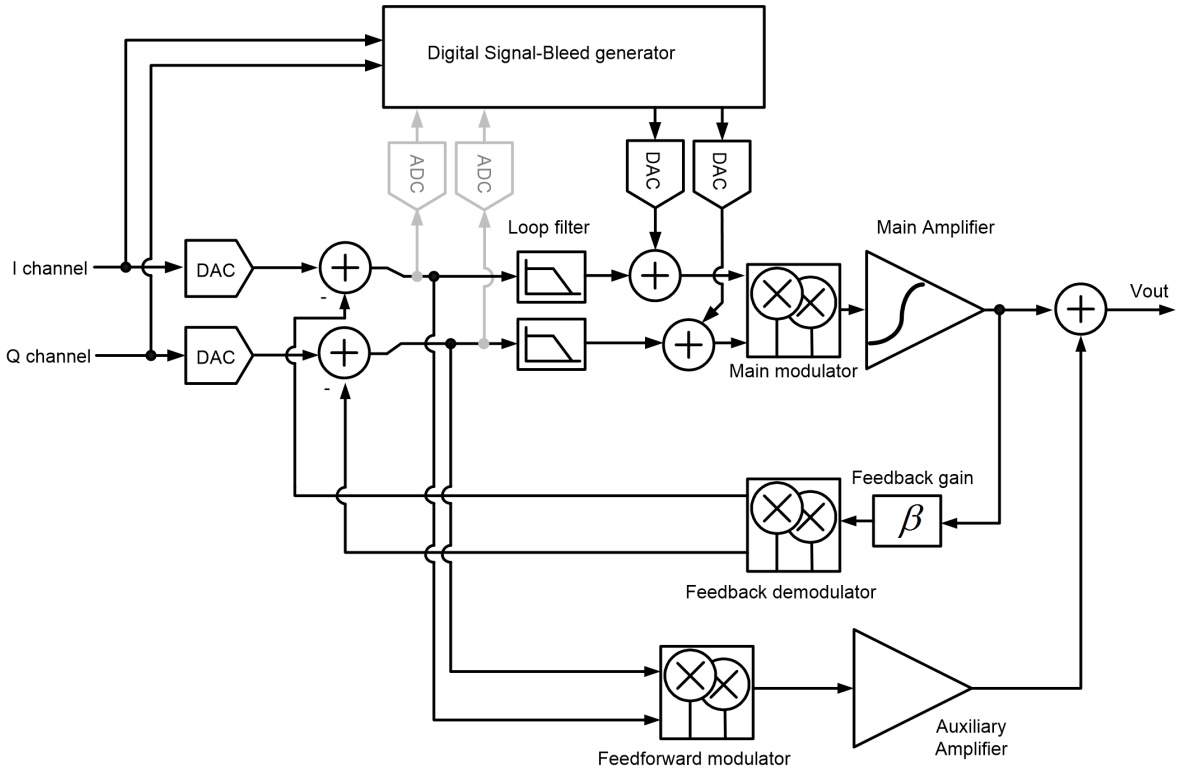

Figure 5.9: Modified Cartesian feedback-feedforward with a digital signal-bleed path

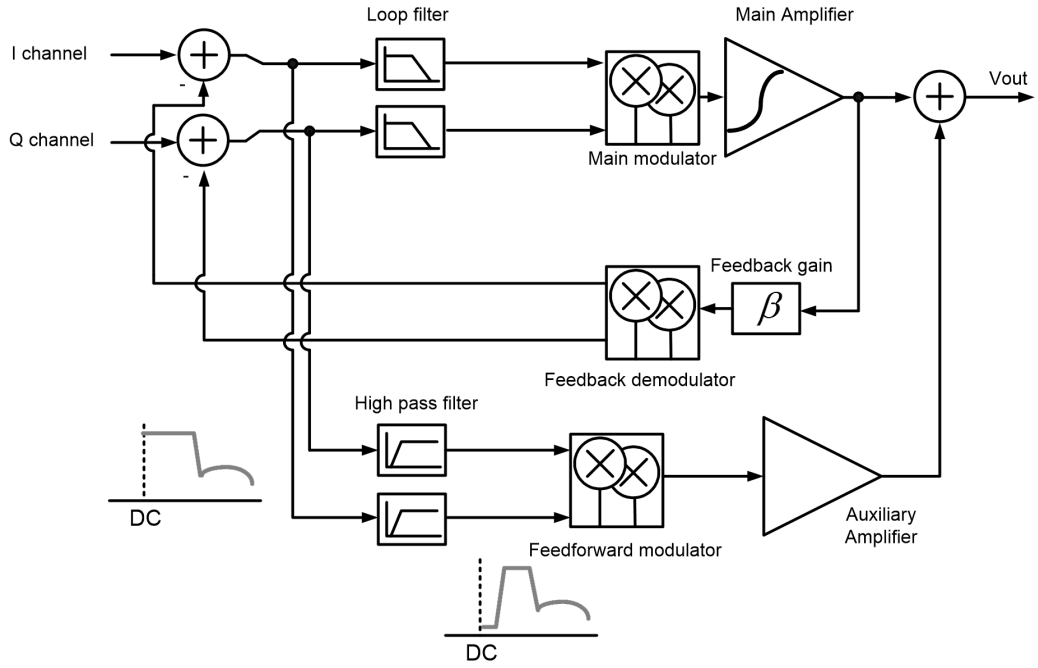

Figure 5.10: Modified Cartesian feedback-feedforward with high pass filters

5.3.2 Cartesian Feedback-Feedforward with High Pass Filters

In the previous section, the signal-bleed path provides the required in-band signal for the Cartesian loop, and the error signal contains only the distortion products and noise. However, in the Cartesian feedback-feedforward transmitter even without the signal-bleed path, if the in-band portion of the error signal is filtered out before the Cartesian feedforward input, the Cartesian feedforward path can transmit a reduced amount of error signal, which could reduce the distortion products generated by the Cartesian feedforward chain.

Fig. 5.10 shows the proposed Cartesian feedback-feedforward transmitter. It includes additional high pass filters at the Cartesian feedforward inputs

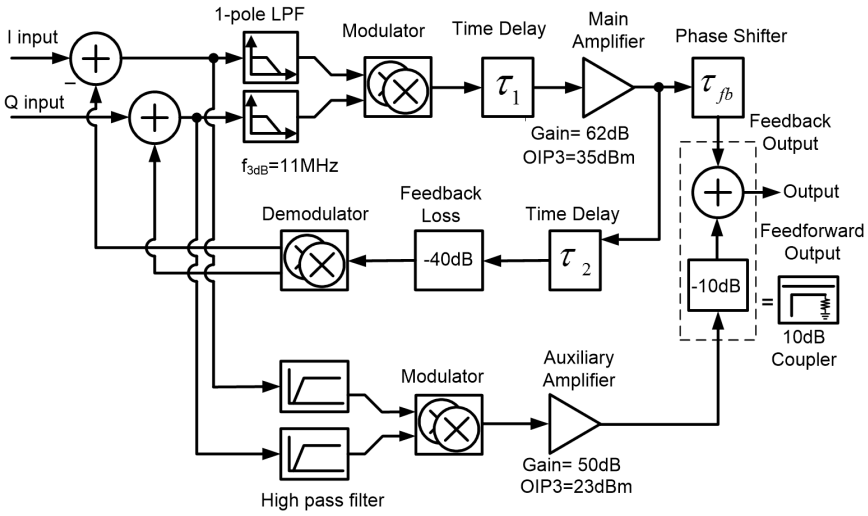

Figure 5.11: Block diagram of the Cartesian feedback-feedforward transmitter with high pass filters for system simulation

that can suppress the error signal in the main channel band, while distortion terms in adjacent channels are allowed through. Unlike the signal-bleed technique, high pass filters would only be able to curtail a certain amount of the error signal near DC. However, this filtering can help to reduce the distortion terms of the Cartesian feedforward path significantly, because most digital modulation signals have substantial power around DC. In addition, while the signal-bleed technique would need real time adjustment due to variation in the PA, this scheme does not need to track real-time variation of the Cartesian loop.

Fig. 5.11 illustrates system simulation blocks of the proposed transmitter with high pass filters. All components and time delays are the same as in Fig. 5.1, except for the high pass filters. A high pass filter is assumed to

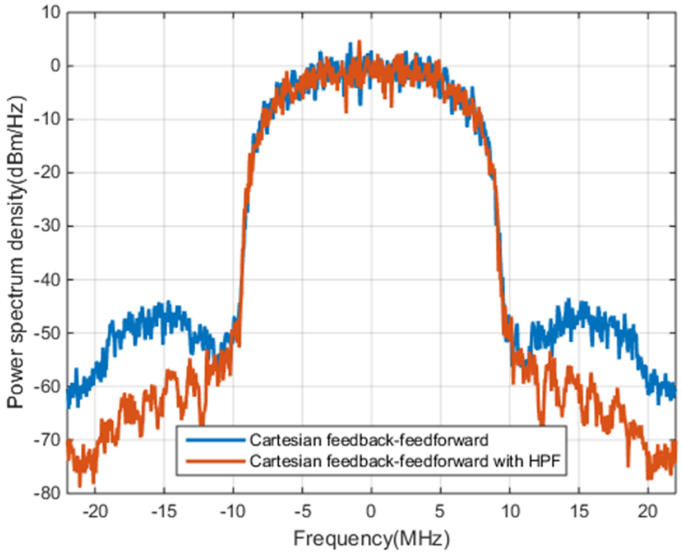

Figure 5.12: Output spectrum of the Cartesian feedback-feedforward transmitter with/without high pass filters in the feedforward path

be a simple biquad filter of the transfer function, as shown in

$$HPF(s) = \frac{\left(\frac{s}{\omega_o}\right)^2}{\left(\frac{s}{\omega_o}\right)^2 + \frac{1}{Q}\left(\frac{s}{\omega_o}\right) + 1} \tag{5.8}$$

where $\omega_o = 2\pi \times 2\,MHz$ and Q=0.5.

Fig. 5.12 represents the output spectrum of two Cartesian feedback-feedforward transmitters with and without high pass filters in the feedforward path. The proposed transmitter with high pass filters achieves an additional 11.3 dB ACLR improvement, compared with the normal Cartesian feedback-feedforward transmitter. Fig. 5.13 shows the output spectrum of the feedback

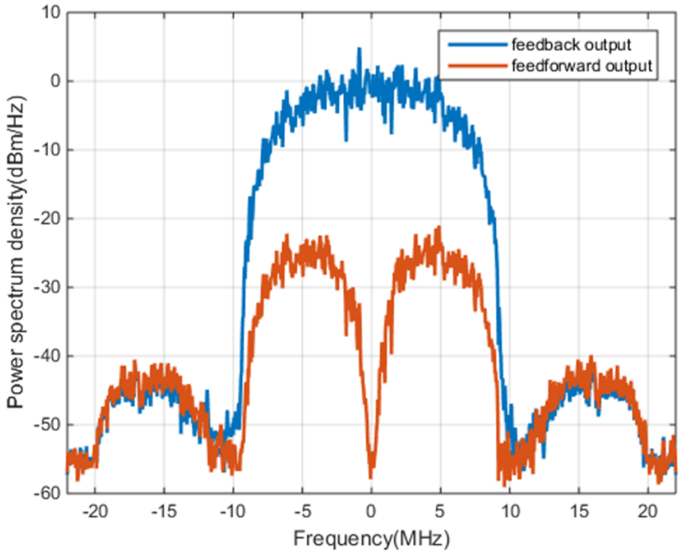

Figure 5.13: Spectrum of feedback output and feedforward output in Cartesian feedback-feedforward transmitter with high pass filters

loop and the feedforward path, in the Cartesian feedback-feedforward transmitter with high pass filters. While both distortion signals in adjacent channels appear similar, the feedforward output signal is filtered out around the center frequency as expected, which can improve the overall linearity, as shown in Fig. 5.12.

5.4 Conclusion

With the Cartesian feedback-feedforward architecture, the Cartesian feedforward chain needs to provide only the distortion products of the Cartesian feedback path for cancellation at the output. However, the error signal of Cartesian feedback includes both in-band signal in the main channel band and

distortion signals in the adjacent channel bands. When the loop gain of the Cartesian feedback is small, this error signal can generate substantial distortion products in the feedforward path due to its non-linearity. In this chapter, two modified architectures were presented to reduce the in-band signal at the feedforward input, without increasing the loop bandwidth. Reduction of the in-band signal helps to curtail creation of further distortion products by the Cartesian feedforward path. For a given overall linearity, the linearity requirement of the Cartesian feedforward path can thus be relaxed. This makes it possible to reduce the power dissipation in the transmitter path, which in turn enhances efficiency.

The first technique employs a signal-bleed path that is applied to the main forward path to remove the desired signal terms in the error signal. If the digital computational power supports real time calibration of the signal-bleed path, this can be a feasible approach for significantly improving the overall linearity for a given loop bandwidth. The second technique is to add high pass filters in the Cartesian feedforward chain, which can also achieve significant improvement of linearity, because high pass filters can partially attenuate the in-band portion of the error signal.

Chapter 6

Conclusion

6.1 Dissertation Summary

Linear, efficient transmitter architectures are essential for enabling future advances in mobile wireless systems with regards to data rates, power efficiency and co-existence. In this dissertation, transmitter architectures for enhancing linearity were explored, and a Cartesian feedback-feedforward transmitter was proposed. It was demonstrated to be a suitable candidate for implementing highly linear wireless transmitters.

In Chapter 2, prior transmitter configurations were surveyed, including feedforward, DPD, and feedback. Feedforward architectures can linearize broadband signals without stability concerns but these involve several implementation challenges due to real time variation of both signal paths, and due to the need for discrete passive components. As CMOS technology has advanced, DPD is becoming increasingly popular in mobile systems. Cartesian feedback and RF feedback, on the other hand, can achieve acceptable linearity improvement without requiring excessive digital computing power. Their performance is primarily limited by the achievable loop bandwidth. It would be challenging to apply a feedback-based architecture to a high-end wireless

transmitter to support a wide signal bandwidth.

In Chapter 3, a Cartesian feedback-feedforward architecture was introduced and analyzed. In the proposed configuration, a Cartesian feedback loop is combined with a Cartesian feedforward path that can achieve additional linearity improvement by canceling the distortion products of the main forward path in the loop. An additive linear model and two-tone analysis using a Volterra series, are used to illustrate the enhancement in linearity enabled by the architecture. The linearity improvement of the proposed architecture, compared to an open-loop transmitter and a Cartesian feedback transmitter, is demonstrated using system simulations with a modulated signal.

In Chapter 4, the prototype transmitter IC that is used to demonstrate the Cartesian feedback-feedforward architecture is described. The transmitter IC was implemented in 130 nm CMOS and consisted of two transmitter paths (the main forward path and Cartesian feedforward path) and a down-converter chain for the feedback path. The Cartesian feedback-feedforward architecture was tested using the prototype IC and several off-chip components. When a high order digitally modulated signal was applied, the test exhibited substantial ACLR improvement.

In Chapter 5, two modified architectures for enhancing the linearity of Cartesian feedback-feedforward transmitter even further were described, along with corresponding system simulations. The first technique that uses a signal-bleed path could be an adequate approach, if an adaptive bleed signal can be generated to take into consideration PVT variations. This would require

the use of an efficient digital signal processor. The second technique using high pass filters could also achieve considerable linearity enhancement while avoiding the requirement for a digital signal processor.

6.2 Future Research

Cartesian feedback-feedforward offers a promising approach for enhancing the linearity of wireless transmitters. However future research is needed to further enhance the robustness and performance of the design.

It is necessary to explore reliable calibration techniques to ensure phase and gain matching of the feedback path in the Cartesian loop and the feedforward path to achieve correct cancellation. Although the feedback path is relatively insensitive to PVT variations, since it uses passive components, the feedforward path is composed of active components that can exhibit substantial variation in performance. Ensuring a constant loop performance requires that these variations be monitored and adjusted regularly.

In the face of restricted loop bandwidth, out-of-band noise emissions of the Cartesian feedback transmitter can increase [56]. Thus approaches that not only cancel in-band and adjacent channel distortion, but also reduce the out-of-band noise would be very useful.

Finally, combinations of the feedback-feedforward approach with digital calibration and pre-distortion can be studied for further enhancement of system linearity and bandwidth.

Bibliography

[1] L. Larson, D. Kimball, and P. M. Asbeck, "Linearity and Efficiency Enhancement Strategies for 4G Wireless Power Amplifier Designs," in *Proc. IEEE CICC*, 2008, pp. 741–748.

[2] P. B. Kenington, *High Linearity RF Amplifier Design*. Artech House, Inc., 2000.

[3] C. Presti, D. Kimball, and P. M. Asbeck, "Closed-Loop Digital Predistortion System With Fast Real-Time Adaptation Applied to a Handset WCDMA PA Module," *IEEE Trans. Micro. Theory and Tech.*, vol. 60, no. 3, pp. 604–618, 2012.

[4] S. Kousai, K. Onizuka, T. Yamaguchi, Y. Kuriyama, and M. Nagaoka, "A 28.3 mW PA-Closed Loop for Linearity and Efficiency Improvement Integrated in a 27.1 dBm WCDMA CMOS Power Amplifier," *IEEE J. Solid-State Circuits*, vol. 47, no. 12, pp. 2964–2973, 2012.

[5] H. Ishihara, M. Hosoya, S. Otaka, and O. Watanabe, "A 10-MHz Signal Bandwidth Cartesian Loop Transmitter Capable of Off-Chip PA Linearization," *IEEE J. Solid-State Circuits*, vol. 45, no. 12, pp. 2785–2793, 2010.

[6] S. Otaka, M. Hosoya, H. Ishihara, T. Hashimoto, and Y. Araki, "0.13 μm CMOS Cartesian Loop Transmitter IC with Fast Calibration and Switching Scheme from Opened to Closed Loop," in *Proc. IEEE ESSCIRC*, 2008, pp. 342–345.

[7] H. H. Boo, S. W. Chung, and J. L. Dawson, "Digitally Assisted Feedforward Compensation of Cartesian-Feedback Power-Amplifier Systems," *IEEE Trans. Circuits Syst. II, Exp. Briefs*, vol. 58, no. 8, pp. 457–461, 2011.

[8] A. Mirzaei, D. Murphy, and H. Darabi, "Analysis of Direct-Conversion IQ Transmitters with 25% Duty-Cycle Passive Mixers," *IEEE Trans. Circuits Syst. I, Reg. Papers*, vol. 58, no. 10, pp. 2318–2331, 2011.

[9] H. Darabi, *Radio Frequency Integrated Circuits and System.* Cambridge University Press, 2015.

[10] A. Mirzaei, H. Darabi, J. C. Leete, X. Chen, K. Juan, and A. Yazdi, "Analysis and Optimization of Current-Driven Passive Mixers in Narrowband Direct-Conversion Receivers," *IEEE J. Solid-State Circuits*, vol. 44, no. 10, pp. 2678–2688, 2009.

[11] ITU, *Mobile-Cellular Subscriptions*, 2015 accessed October 2, 2015, http://www.itu.int/en/ITU-D/Statistics/Pages/stat/default.aspx.

[12] L. R. Kahn, "Single-Sideband Transmission by Envelope Elimination and Restoration," *Proceedings of the IRE*, vol. 40, no. 7, pp. 803–806, 1952.

[13] D. K. Su and W. J. McFarland, "An IC for Linearizing RF Power Amplifiers Using Envelope Elimination and Restoration," *IEEE J. Solid-State Circuits*, vol. 33, no. 12, pp. 2252–2258, 1998.

[14] W. B. Sander, S. V. Schell, and B. L. Sander, "Polar Modulator for Multi-Mode Cell Phones," in *Proc. IEEE CICC*, 2003, pp. 439–445.

[15] M. R. Elliott, T. Montalvo, B. P. Jeffries, F. Murden, J. Strange, A. Hill, S. Nandipaku, and J. Harrebek, "A Polar Modulator Transmitter for GSM/EDGE," *IEEE J. Solid-State Circuits*, vol. 39, no. 12, pp. 2190–2199, 2004.

[16] D. C. Cox, "Linear Amplification with Nonlinear Components," *IEEE Trans. Commun.*, vol. 22, no. 12, pp. 1942–1945, 1974.

[17] S. A. Hetzel, A. Bateman, and J. P. McGeehan, "LINC Transmitter," *Electronics Letters*, vol. 27, no. 10, pp. 844–846, 1991.

[18] X. Zhang, L. E. Larson, P. M. Asbeck, and P. Nanawa, "Gain/Phase Imbalance-Minimization Techniques for LINC Transmitters," *IEEE Trans. Micro. Theory and Tech.*, vol. 49, no. 12, pp. 2507–2516, 2001.

[19] J. Rogers and C. Plett, *Radio Frequency Integrated Circuit Design*. Artech House, 2014.

[20] V. Volterra, *Theory of Functionals and of Integral and Integro-Differential Equations*. Dover, New York, 1959.

[21] S. Narayanan, "Transistor Distortion Analysis Using Volterra Series Representation," *Bell Syst. Tech. J*, vol. 46, no. 3, pp. 991–1024, 1967.

[22] J. Wood, *Behavioral Modeling and Linearization of RF Power Amplifiers*. Artech House, 2014.

[23] J. C. Pedro and N. B. Carvalho, *Intermodulation Distortion in Microwave and Wireless Circuits*. Artech House, 2002.

[24] S. A. Mass, *Nonlinear Microwave Circuits*. Artech House, 1988.

[25] P. Wambacq and W. M. Sansen, *Distortion Analysis of Analog Integrated Circuits*. Kluwer Academic Publishers, 1998.

[26] H. S. Black, "Translating System," Oct. 9 1928, US Patent 1,686,792.

[27] A. A. M. Saleh and J. Salz, "Adaptive Linearization of Power Amplifiers in Digital Radio Systems," *Bell System Technical Journal*, vol. 62, no. 4, pp. 1019–1033, 1983.

[28] Y. Nagata, "Linear Amplification Technique for Digital Mobile Communications," in *Proc. IEEE Veh. Tech. Conf.*, 1989, pp. 159–164.

[29] K.-F. Liang, J.-H. Chen, and Y.-J. E. Chen, "A Quadratic-Interpolated LUT-Based Digital Predistortion Technique for Cellular Power Amplifiers," *IEEE Trans. Circuits Syst. II, Exp. Briefs*, vol. 61, no. 3, pp. 133–137, 2014.

[30] H. S. Black, "Wave Translation System," Dec. 21 1937, US Patent 2,102,671.

[31] M. Faulkner, "Amplifier Linearization Using RF Feedback and Feedforward Techniques," *IEEE Trans. Veh. Tech.*, vol. 47, no. 1, pp. 209–215, 1998.

[32] J. G. McRory and R. H. Johnston, "An RF amplifier for Low Intermodulation Distortion," in *Proc. IEEE MTT-S*, 1994, pp. 1741–1744.

[33] V. Petrovic and C. N. Smith, "Reduction of Intermodulation Distortion by Means of Modulation Feedback," in *IEE Conf. on Radio Spectrum Conservation Techniques*, 1983, pp. 44–49.

[34] M. A. Briffa and M. Faulkner, "Stability Analysis of Cartesian Feedback Linearisation for Amplifiers with Weak Nonlinearities," *IEE Proc. Commun.*, vol. 143, no. 4, pp. 212–218, 1996.

[35] N. Sornin, N. Massei, L. Perraud, and C. Pinatel, "A Robust Cartesian Feedback Loop for a 802.11a/b/g CMOS Transmitter," in *Proc. IEEE RFIC Symp.*, 2004, pp. 145–148.

[36] S. Pipilos, Y. Papananos, N. Naskas, M. Zervakis, J. Jongsma, T. Gschier, N. Wilson, J. Gibbins, B. Carter, and G. Dann, "A Transmitter IC for TETRA Systems Based on a Cartesian Feedback Loop Linearization Technique," *IEEE J. Solid-State Circuits*, vol. 40, no. 3, pp. 707–718, 2005.

[37] L. Perraud, M. Recouly, C. Pinatel, N. Sornin, J.-L. Bonnot, F. Benoist, M. Massei, and O. Gibrat, "A Direct-Conversion CMOS Transceiver for The 802.11 a/b/g WLAN Standard Utilizing a Cartesian Feedback Transmitter," *IEEE J. Solid-State Circuits*, vol. 39, no. 12, pp. 2226–2238, 2004.

[38] J. L. Dawson and T. H. Lee, "Automatic Phase Alignment for a Fully Integrated Cartesian Feedback Power Amplifier System," *IEEE J. Solid-State Circuits*, vol. 38, no. 12, pp. 2269–2279, 2003.

[39] M. Boloorian and J. P. McGeehan, "Phase-Lag Compensated Cartesian Feedback Transmitter," *Electronics Letters*, vol. 32, no. 17, pp. 1547–1548, 1996.

[40] L. Tee, E. Sacchi, R. Bocock, N. Wongkomet, and P. R. Gray, "A Cartesian-Feedback Linearized CMOS RF Transmitter for EDGE Modulation," in *Proc. IEEE Symp. VLSI Circuits*, 2006, pp. 232–233.

[41] S. W. Chung, J. W. Holloway, and J. L. Dawson, "Energy-Efficient Digital Predistortion with Lookup Table Training Using Analog Cartesian Feedback," *IEEE Trans. Microw. Theory and Tech.*, vol. 56, no. 10, pp. 2248–2258, 2008.

[42] S. Ock, J. Ko, and R. Gharpurey, "A Cartesian Feedback Feedforward Transmitter," in *Proc. IEEE ISCAS*, 2011, pp. 209–212.

[43] G. Palumbo and S. Pennisi, "High-Frequency Harmonic Distortion in

Feedback Amplifiers: Analysis and Applications," *IEEE Trans. Circuits Syst. I, Reg. Papers*, vol. 50, no. 3, pp. 328–340, 2003.

[44] S. Ock, H. Song, and R. Gharpurey, "A Cartesian Feedback-Feedfoward Transmitter IC in 130nm CMOS," in *Proc. IEEE CICC*, 2015.

[45] B. Gilbert, "A Precise Four-Quadrant Multiplier with Subnanosecond Response," *IEEE J. Solid-State Circuits*, vol. 3, no. 4, pp. 365–373, 1968.

[46] S. Kang, B. Choi, and B. Kim, "Linearity Analysis of CMOS for RF Application," *IEEE Trans. Micro. Theory and Tech.*, vol. 51, no. 3, pp. 972–977, 2003.

[47] R. Gharpurey, "Linearity Enhancement Techniques in Radio Receiver Front-Ends," *IEEE Trans. Circuits Syst. I, Reg. Papers*, vol. 59, no. 8, pp. 1667–1679, 2012.

[48] D. R. Webster, D. G. Haigh, J. B. Scott, and A. E. Parker, "Derivative Superposition-A Linearisation Technique for Ultra Broadband Systems," in *IEE Colloq. Wideband Circuits, Modelling and Techniques.* IET, 1996, pp. 3/1–3/14.

[49] S. Ock, K. Han, J. R. Lee, and B. Kim, "A Modified Cascode Type Low Noise Amplifier Using Dual Common Source Transistors," in *Proc. IEEE MTT-S*, vol. 3, 2002, pp. 1423–1426.

[50] E. Sacchi, I. Bietti, S. Erba, L. Tee, P. Vilmercati, and R. Castello, "A 15 mW, 70 kHz 1/f Corner Direct Conversion CMOS Receiver," in *Proc. IEEE CICC*, 2003, pp. 459–462.

[51] A. Mirzaei, X. Chen, A. Yazdi, J. Chiu, J. Leete, and H. Darabi, "A Frequency Translation Technique for SAW-Less 3G Receivers," in *Proc. IEEE Symp. VLSI Circuits*, 2009, pp. 280–281.

[52] W. Sansen and R. G. Meyer, "An Integrated Wide-Band Variable-Gain Amplifier with Maximum Dynamic Range," *IEEE J. Solid-State Circuits*, vol. 9, no. 4, pp. 159–166, 1974.

[53] P. E. Allen and D. R. Holberg, *CMOS Analog Integrated Circuit Design*. Oxford University Press, NY, USA, 2002.

[54] F. Behbahani, Y. Kishigami, J. Leete, and A. A. Abidi, "CMOS Mixers and Polyphase Filters for Large Image Rejection," *IEEE J. Solid-State Circuits*, vol. 36, no. 6, pp. 873–887, 2001.

[55] B. Razavi, *RF Microelectronics*. Prentice Hall New Jersey, 2012, vol. 2.

[56] P. B. Kenington, R. J. Wilkinson, and K. J. Parsons, "Noise Performance of a Cartesian Loop Transmitter," *IEEE Trans. Veh. Tech.*, vol. 46, no. 2, pp. 467–476, 1997.

Vita

Sungmin Ock received the B.S. and M.S. degree from Pohang University of Science and Technology (POSTECH), Pohang, Korea, in 1997 and 2000, respectively. Since Fall 2006, he has been working towards the Ph.D. degree in the Department of Electrical and Computer Engineering at the University of Texas at Austin. Currently, he is with Qualcomm, San Diego, CA, prior to which he was with Texas Instruments, Dallas, TX, from 2010 to 2014. From 2000 to 2006, he was in Future Communications IC, Seongnam, Korea, now a part of Silicon Motion, Taiwan. His research interests are in analog and mixed signal integrated circuit design for communications and power management.

Permanent address: sungminock@gmail.com

This dissertation was typeset with LaTeX[†] by the author.

[†]LaTeX is a document preparation system developed by Leslie Lamport as a special version of Donald Knuth's TeX Program.